

I Facoltà di Ingegneria

Corso di Laurea Magistrale in Ingegneria Civile

Experimental and numerical analysis of dam-break waves propagation on vegetated slopes



Relatori:

Prof. Davide Poggi

Prof. Brett F. Sanders

Correlatore:

Ing. Silvia Cordero

Candidato:

Natali Mario

...for my family



Abstract

The main purpose of the analysis is to study the sudden dam-break waves propagation on vegetated slopes looking at a physical model where a uniform canopy is simulated using small and thin metallic pales.

All the analysis aims to the estimation of an expeditious method about the evaluation of the hydraulic hazard regarded to the downside of small reservoirs.

Furthermore two different numerical models related to the same situation are being done and studied.

The models selected for the study are: *parBreZo 8.1.0* which is a two-dimensional (2D) hydrodynamic depth-averaged model and *ANSYS Fluent* that is a three-dimensional (3D) computational fluid dynamics (CFD) .

The software *parBreZo 8.1.0* solves the shallow-water (Saint-Venant) equations, which does not consider the vertical velocities and accelerations, while the three-dimensional *ANSYS Fluent* is based on the Navier-Stokes equations.

The significant results of the analysis, like wave-front velocity and water depth, are being studied looking at the comparison between the usage of the two different numerical models (2D and 3D) and the comparison of them with the experimental data from the physical model.

Keywords: [Dam-Break, Hydraulic, Hydraulic-Modeling, Shallow-Water, Navier-Stokes, Experimental, Numerical]

Contents

1. Introduction	1
2. Literature review	3
2.1. Dam-Break Flows: Acquisition of Experimental Data through an Imaging Technique and 2D Numerical Modeling (Aureli, Maranzoni, Mignosa, Ziveri) [3].....	3
2.2. Experimental study of dam-break flow against an isolated obstacle (S. Soares- Frazão & Y. Zech) [4].....	7
3. Physical model description and experiments	10
3.1. Physical model description	10
3.1.1. Upstream: the tank	13
3.1.2. The sluice gate.....	16
3.1.3. Downstream: the flat horizontal surface	18
3.2. Experiments	21
3.2.1. Smooth horizontal surface.....	22
3.2.2. Vegetated surface	22
4. Analysis of the data from the physical model	24
4.1. Lambert-Beer law review	24
4.2. Water depth detection	25
4.3. Wave-front velocity detection	31
5. Numerical analysis with <i>parBreZo 8.1.0</i>	32
5.1. Software overview	32
5.1.1. Finite volume algorithm.....	32
5.1.2. Modeling of the <i>wetting</i> and <i>drying</i> processes.....	34
5.1.3. Calculation algorithm.....	35
5.1.3.1. Preliminary operations: cells classification and gradients evaluation.....	35
5.1.3.2. Predictor step	37
5.1.3.3. Corrector Step.....	38
5.1.3.4. Godunov solution scheme	39
5.2. How to set up the hydraulic model with <i>parBreZo 8.1.0</i>	39
5.2.1. How to use the software	40
5.2.2. Geometry setup	43
5.2.2.1. Smooth horizontal bed-ground	43
5.2.2.2. Vegetated horizontal bed-ground	44

5.2.3.	Computational parameters of the hydraulic model	46
5.2.3.1.	Smooth horizontal bed-ground	47
5.2.3.2.	Vegetated bed-ground	52
6.	Numerical analysis with ANSYS Fluent	56
6.1.	Software overview [13]	56
6.2.	Geometry setup	57
6.3.	Computational parameters of the hydraulic model.....	61
6.3.1.	Initial Conditions.....	62
6.3.2.	Boundary conditions	62
7.	Results and comparisons	63
7.1.	Numerical results from <i>parBreZo 8.1.0</i>	63
7.1.1.	Smooth horizontal bed-ground.....	64
7.1.1.1.	Water-velocity results and comparison	74
7.1.1.2.	Water depth results and comparison.....	74
7.1.2.	Vegetated horizontal bed-ground.....	80
7.1.2.1.	Water-velocity results and comparison	80
7.1.2.2.	Water depth results and comparison.....	81
7.2.	Fluid vein	85
7.3.	Results from ANSYS Fluent and comparison	87
8.	Future perspectives	90
8.1.	Experimental analysis	90
8.2.	Numerical model with <i>parBreZo 8.1.0</i>	90
8.3.	Numerical model with ANSYS Fluent	91
9.	Conclusions	92
	List of figures.....	94
	Bibliography	97
	Acknowledgements.....	99

1. Introduction

The water has always been one of the most precious resources in the world and the men have always tried to collect and store it developing new techniques and trying to improve these.

Other than use the water as necessary resource for human life the other two main uses are related to agriculture and breeding; going forward through the time with the rapid increase of the population and, as a consequence, of the request of food, is being necessary as much water as possible. Understanding that the only water from the rain, or from natural lakes and rivers, wasn't enough, the population in the world started to develop ideas to store the water and use that whenever it was necessary during the year. The logical consequence of these necessities is represented by the dams which are building barriers across the rivers in order to create artificial reservoirs.

Looking back along the history of the human being the first dam was built around the 4000 B.C. in Egypt; this one was followed by many dams built from the Babylonians that had the purpose of water storage for the improvement of the irrigation system.

Nowadays there are thousands dams placed all over the world and the use of them is not just related to irrigation purpose but this kind of structure has being improved to make possible to use them for Hydroelectric use and furthermore for supply to domestic and industrial water requests.

Technically a dam could be characterized looking at the capacity in terms of volume storage, at the amount of electricity that is able to produce or at the height of the structure; in particular is defined *big dam* a dam with a height of 15 meters or higher from lowest foundation to crest or a dam between 5 meters and 15 meters which contains more than 3 million cubic meters. [14] Otherwise the dam could be defined as a *small dam*.

However the most dangerous aspect regarded to the dams is represented by their collapse; the main types of collapse are: piping, overtopping, substructure failure or as an earthquake's consequence; furthermore the dam's failure type is strictly related to its structure type (Earth dams or Concrete dams).

The failure, or a partial break, of a dam would have incredibly tragic consequences because a significant amount of water will be released causing fast floods of the whole downside area, and obviously being dangerous for people's life.

This dangerous side of the dams is the reason why these kind of structures need a lot of attention and need to be safeguarded.

The size of the dam is strictly linked to the increase of the hazard, so while the big dams are the most dangerous, the failure of the small ones is more frequent [1]. According to a Chinese study [2] more than 900 dams collapsed and the 66% of these were earth dams.

The dam break is a topic that collect a great attention from the scientific community and has been widely studied in the past years; the phenomenon usually is studied with a sudden release of the water behind a wall, where the breach is simulated with a sluice gate. The main hydraulics quantities, linked to this problem, that should be analyzed are mostly the water velocity and the water depth; these two points of interest have a really important role into an hazard analysis associated to this kind of structure.

Most of the small dams are built with irrigation purpose and then on the downside of them is frequent to see a dense vegetation made from orchards. The two quantities already mentioned, water velocity and water depth, are influenced from the presence of the plants. The analysis that is presented here has the objective to study this influence looking at a physical model that will be presented thereafter and also a validation of two different numerical models: one bi-dimensional hydraulic model based on the solution of the Shallow Water Equations and a three-dimensional model that solving the Mass Conservation equation and The Momentum Conservation Equation does not ignore the equation's terms along the vertical direction.

This thesis is only a part of a project that Professor Davide Poggi and Eng. Silvia Cordero are conducting, at the Turin Polytechnic, with the main goal to formulate a simplified expeditious method regarded to the estimation of the flood hazard consequent to the collapse of small dams of little reservoirs with irrigation purpose. Furthermore the analysis which is presented here is related to two different study cases in order to study the wave propagation on a smooth bed-ground or in a situation with a bed-ground that is highly vegetated; the presence of the vegetation in the physical model has been simulated with thin metallic rods.

2. Literature review

The study of the dam break wave propagation has been widely studied during the years trying to find solutions and improvements due to minimize the risks related to the dams. These studies are being made using many different techniques and several kind of experimental setups with the objective to analyze the wave propagation subsequently the sudden opening of a sluice gate which represents the dam collapse; regarding to the sluice gate the several experiments from literature are characterized from diversified kind of opening systems or even more with different shapes of the breach.

However in the literature is difficult to find a description of physical experiments related to the simulation of a bi-dimensional flow in a highly vegetated surface.

2.1. Dam-Break Flows: Acquisition of Experimental Data through an Imaging Technique and 2D Numerical Modeling (Aureli, Maranzoni, Mignosa, Ziveri) [3]

In this paper is presented a two-dimensional numerical analysis of a total amount of four tests related to rapidly varying flow induced by the sudden removal of a sluice gate. The data acquisition was made using an image processing technique using a coloring agent that was added to the water; furthermore the bottom of the facility was backlighted.

Taking pictures of the water on the facility was possible to convert the gray tone of the pixels of the image to water depth; for this operation transfer functions have been used after a calibration process.

Additionally the tests were simulated using a 2D MUSCL-Hancock finite volume numerical model, based on the classical shallow water approximations.

The experimental setup of this experiment is shown in the following pictures.

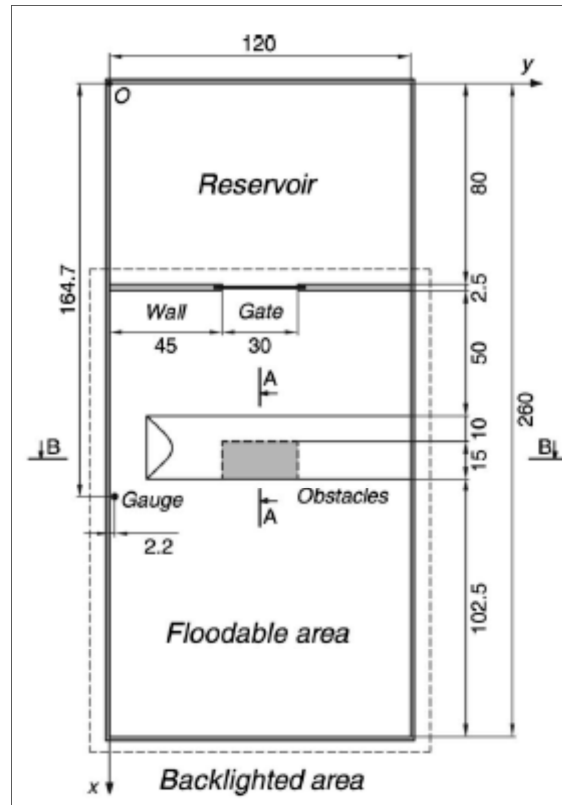


Figure 1: View from above of the experimental setup (Aureli, Maranzoni, Mignosa, Ziveri)

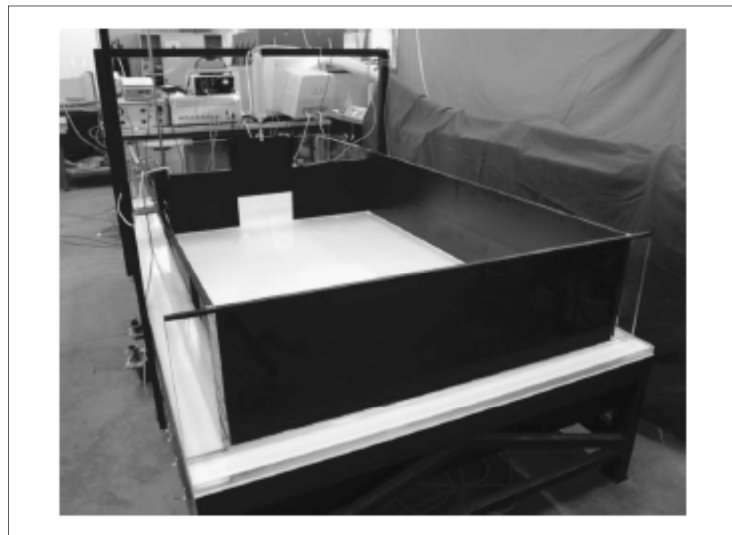


Figure 2: Another view of the experimental facility (Aureli, Maranzoni, Mignosa, Ziveri).

The experimental facility was set up at the Laboratory of Hydraulics in Parma University. This facility is composed from a rectangular tank which is divided into two parts : the first one (smaller) works as a reservoir and the second one (larger) was designed to receive the water wave after the instantaneous opening of the sluice gate that is placed in the middle of the wall which divides the two parts.

The system that moves the sluice gate in this facility is a pneumatic piston.

The third test was performed by placing an obstacle into the floodable area.

The measuring technique as already stated before is an imaging technique which allow to reconstruct the water depth: the water was uniformly mixed with methylene and the bottom of the floodable area was backlighted; then digital images of the flooding were taken with an high framerate.

The initial upstream water level was set up at 0.15 meters and in the downside the surface was completely dry in all the tests less than the fourth one where the downstream water level was 0.01 meters.

The same situation was modeled through a finite volume numerical model (Aureli et al.2006) that solves the 2D shallow water problem using their integral form (Toro 2001). The computational domain was described using discretization with square-cells of 5 mm sides length, while the Manning coefficient that was chosen was set for the bottom at $0.007 \text{ s m}^{-1/3}$.

The results of this analysis are focused in the comparison between the imaging technique and the numerical model. Just an abstract of the results from the analysis that was made from Aureli, Maranzoni, Mignosa, Ziveri are reported below.

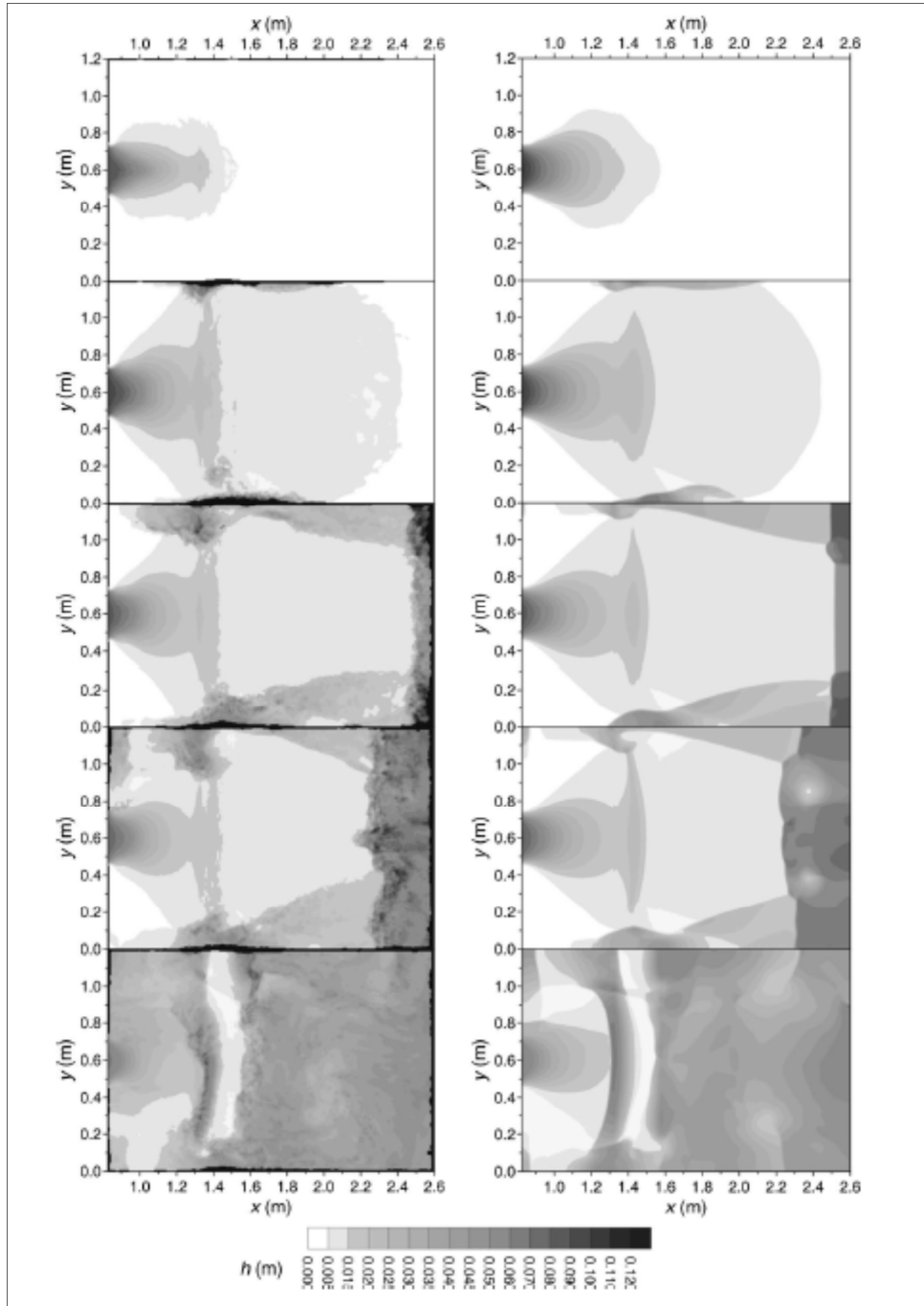


Figure 3: Experimental (left) and numerical (right) water depths for Test 3 at $t=0.46$ s, $t=1.16$ s, $t=1.86$ s, $t=2.58$ s, and $t=4.77$ s (Aureli, Maranzoni, Mignosa, Ziveri).

As a conclusion of their study the two techniques show evident differences especially in the initially stages, but the 2D adopted numerical model is capable to predict and reproduce the main characteristics of the flow fields that they were analyzing.

If the objective is to evaluate the maximum water depth, maximum water velocity and arrival time of the wave-front, then the 2D shallow water approach is a good compromise between the great effort of a physical analysis and the quality of the results that are required.

2.2. Experimental study of dam-break flow against an isolated obstacle (S. Soares-Frazão & Y. Zech) [4]

The main objective of this analysis is to study the influence of an obstacle on a dam-break wave propagation and provide data about that; to make it possible an experimental setup has been set up, and this one consists in a channel with a rectangular shape obstacle placed immediately downstream from the dam.

The water depth evolution during the time has been measured and recorded at five different locations where gauges has been placed, while the surface velocity field was detected using an imaging techniques.

The flow may be significantly be affected by the presence of such natural or artificial obstacle.

All the facility was made at the Civil Engineering Laboratory of the Université catholique de Louvain (UCL) in Belgium.

The channel length is about 36 meters with a rectangular cross section except close to the bed where this section assumes a trapezoidal shape. A gate separates the reservoir that is the upstream part of the channel, and the rest of the channel which simulates the valley.

The channel bed-ground does not have any slope, so it is an horizontal surface; a Manning friction of $0.010 \text{ s m}^{-1/3}$ has been assigned to the bed-ground.

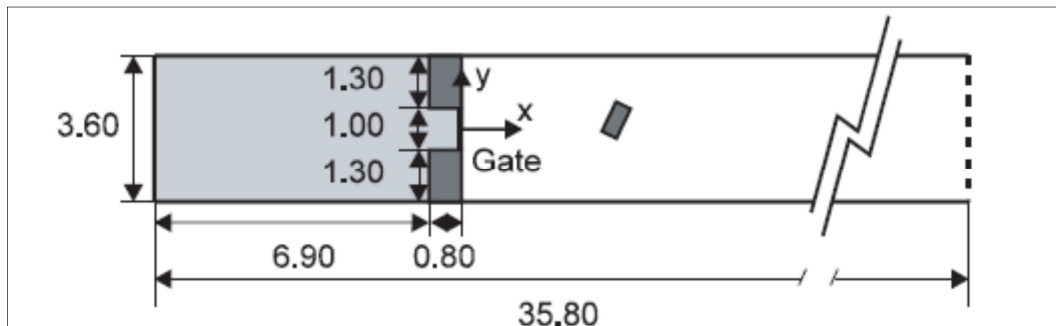


Figure 4: Experimental facility geometry (S.Soares-Frazaao & Y.Zech).

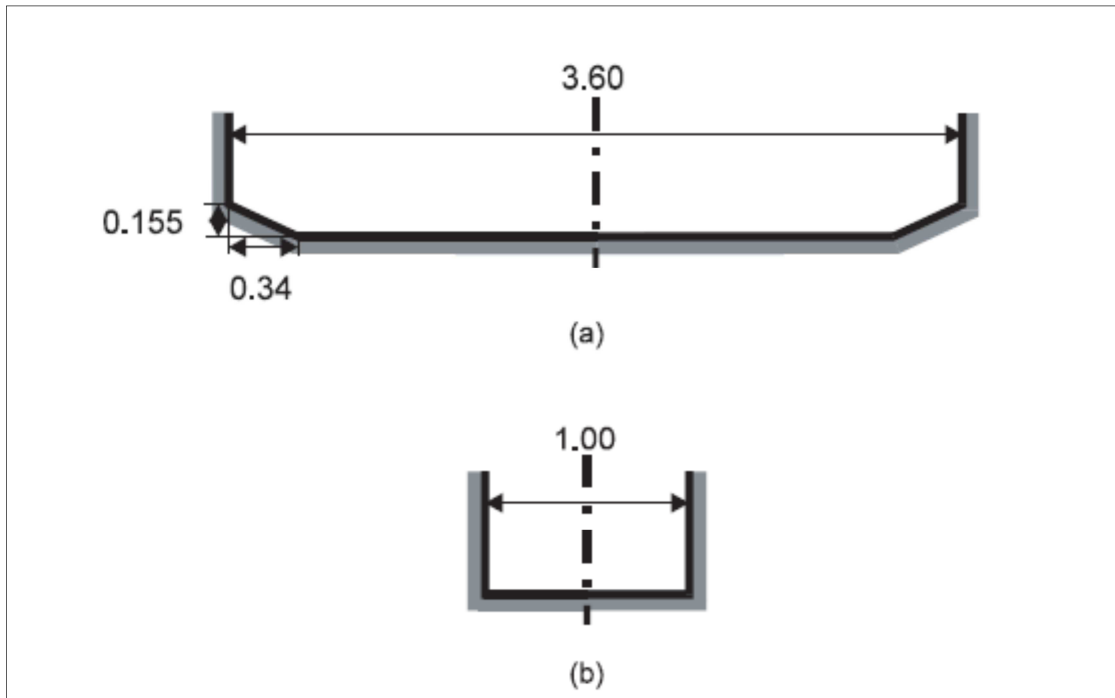


Figure 5: Experimental facility cross-sections: (a) Channel, (b) Gate (S.Soares-Frazaõ & Y.Zech).

The water depth in the upstream reservoir is 0.40 meters while a thin strate of 0.02 meters of water was set up as initial condition.

The simulation of an instantaneous collapse was made pulling up the sluice gate in a time of 0.23 seconds that satisfies the criteria that allow to to define if the opening is sudden or not.

As already state before the water depth evolution was measured using resistive gauges and the velocity is being measured with Acoustic Doppler Velocimeters (ADV). Furthermore alternative measurements of the velocity were took using an imaging techniques. The experiments was runned many times and it showed a pretty good repeatability.

In order to have a complete surface velocity field an high resolution digital camera was placed above the channel to capture the flow; indeed the camera has the capability to take 38 frames per seconds. To catch the water velocity a certain amount of tracers was mixed in the water.

Figure 6 that is shown below is just an abstract of that results achieved by S. Soares-Fra \tilde{z} o & Y. Zech during their analysis.

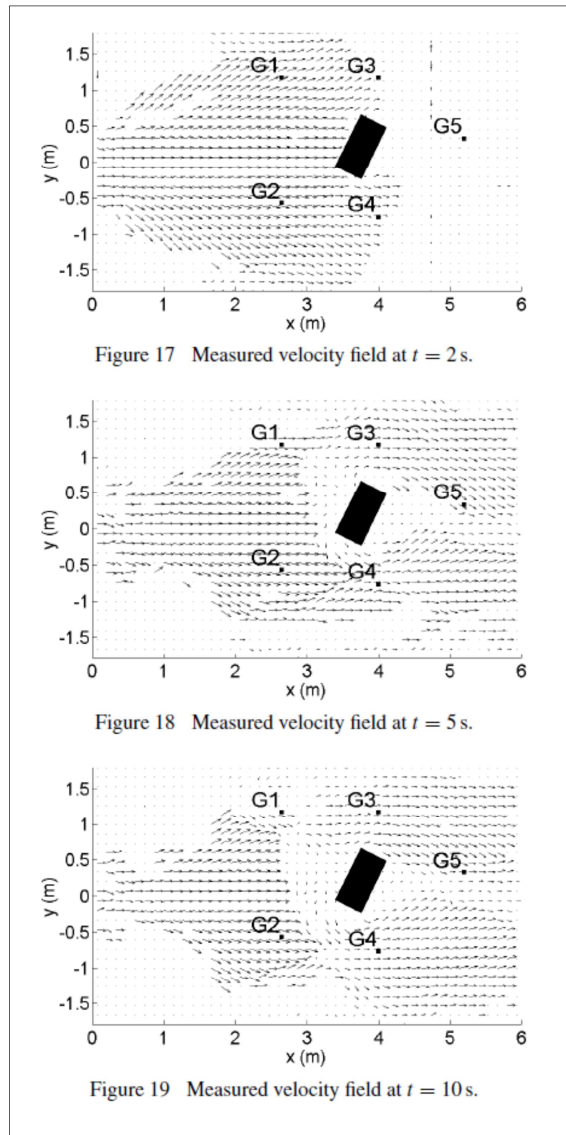


Figure 6: Results from the imaging techniques during different time steps (S. Soares-Fra \tilde{z} o & Y. Zech).

In the results shown in Figure 6 is clearly visible the bi-dimensional character of the spreading of the front wave, especially looking at the first time step which is before the impact with the obstacle.

During this experimental study was shown how the data from the imaging process is useful as an integration of the common data that might be possible to collect from this kind of facilities.

3. Physical model description and experiments

3.1. Physical model description

A part of the results that are illustrated in this thesis are taken from a physical model that has been set up into the *Giorgio Bidone* Laboratory at the Turin Polytechnic.

The facility aims to represent the dam-break wave propagation in particular cases related to small reservoirs with irrigation purpose; in fact the physical model has been built according to the Froude Number similitude and with a geometry scale approximately of 1/30. Indeed:

$$\lambda = \frac{L_{model}}{L_{real}} \cong \frac{1}{30}$$

Where :

- L_{model} = Length in the physical model;
- L_{real} = Length in the reality;

Anyway is important to clarify that the facility is not referred to a precise real case but is something that aims to give a general and adaptable representation of these kind of situations.

In Fig.7 that is shown thereafter is possible to see a global view of that model.

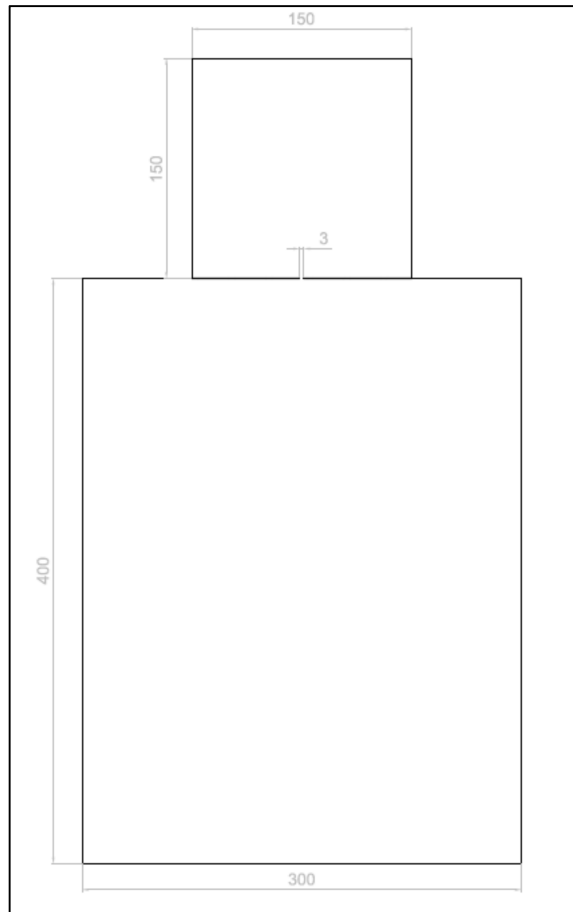


Figure 7: Geometry overview of the whole facility that has been set up at the Giorgio Bidone Laboratory at Turin Polytechnic (dimensions are stated in centimeters).

Another real pictures of the model are shown below; in these images the facility is shown from the upstream.

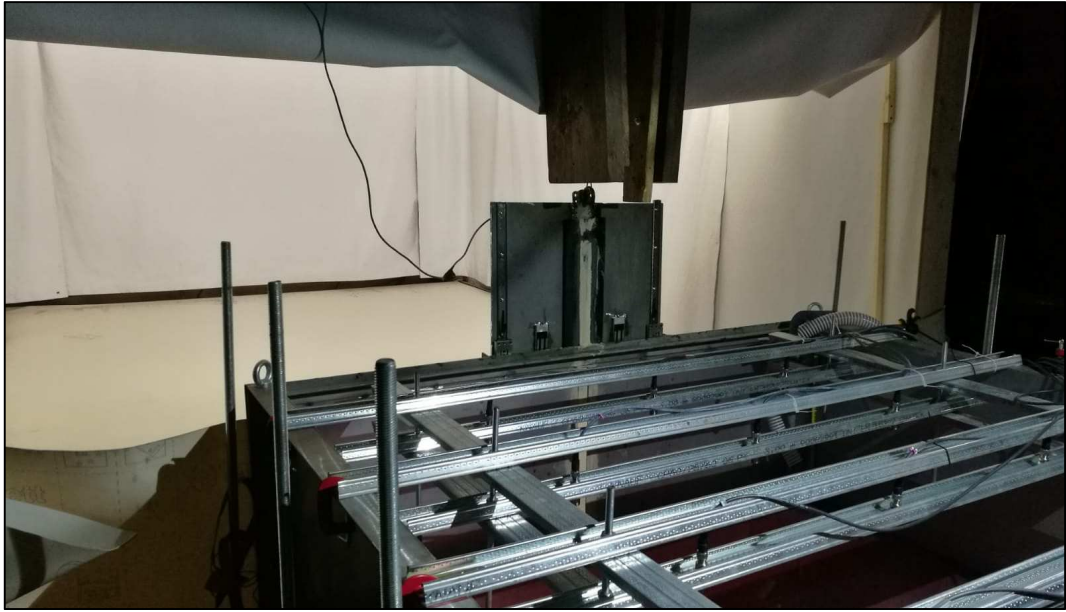


Figure 8: Picture took from upstream of the physical model.

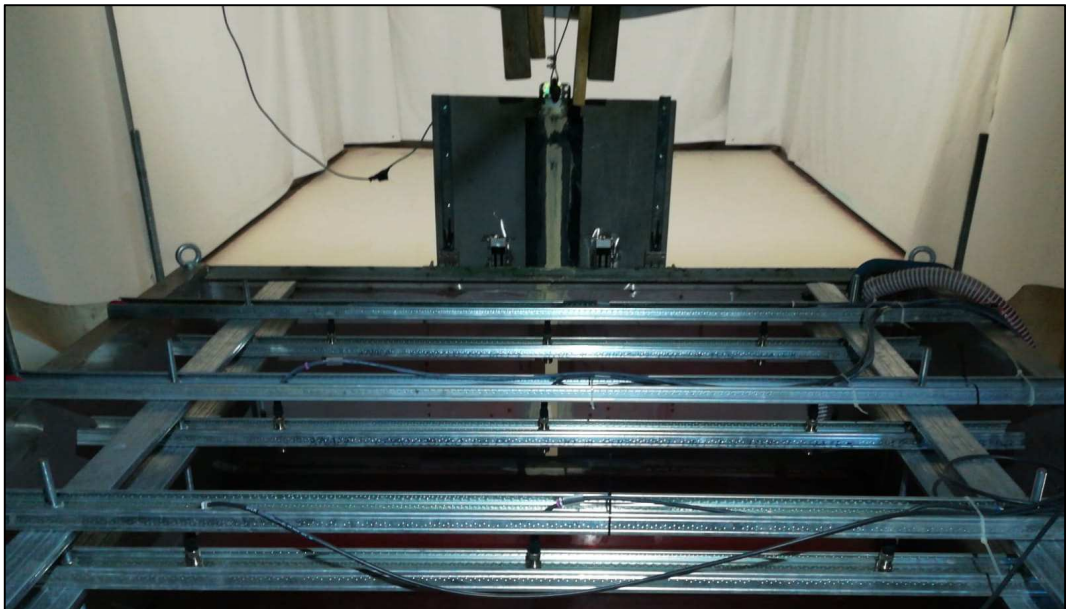


Figure 9: Picture took from upstream of the physical model.

The water that was used from all the experiments has been mixed with a coloring agent which makes the water kind of red color.

This operation was done to increase the quality of the imaging techniques that will be shown in the next chapters of this thesis.

3.1.1. Upstream: the tank

As is possible to see from figures 7, 8 and 9 on the upside of the physical model has been placed a metallic tank.

It has a square geometry and each one of its side is long 150 centimeters.

Regarding the experiments that will be analyzed in this thesis the water depth into the tank has been set as initial condition to $h_0 = 30$ centimeters.

The water depth measurement is made with a system of twelve ultrasonic probes that has been set on the top of the tank with a metallic frame.

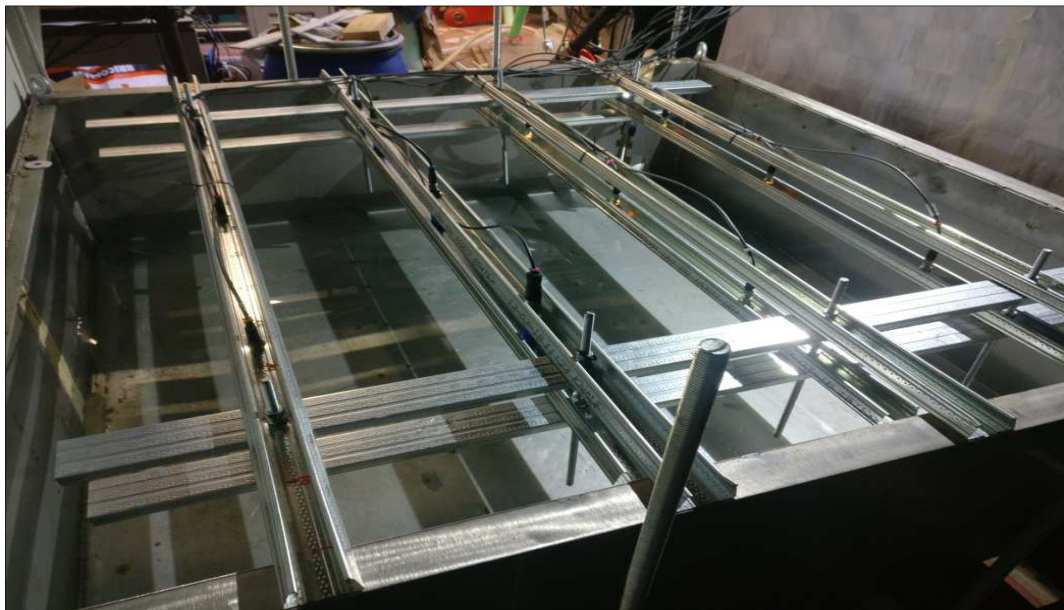


Figure 10: System of ultrasonic probes set on a metallic frame that was placed above the tank.

The model of the ultrasonic probes used is *BUS_18M1-07/035 Balluff*.



Figure 11: Extract from the ultrasonic probes' manual (Balluff) .

This model is able to take 80 measurements for each second ($frequency = 80 Hz$).

The monitoring of the measurements taken from the probes has been made with the software *LabVIEW*.

The signal that the probes are able to take is a potential difference that has been transformed to a water depth value through a calibration process; this process consists simply in the recording of the value of the signal (in potential difference) when the value of water depth into the tank is known.

Doing this operation for a certain number of values of water depth between 0 centimeters and 30 centimeters was possible deduce a relationship between water depth and potential difference; this analytical relationship was wrote for all the probes and then was possible measure the water level into the tank during the whole duration of the experiment.

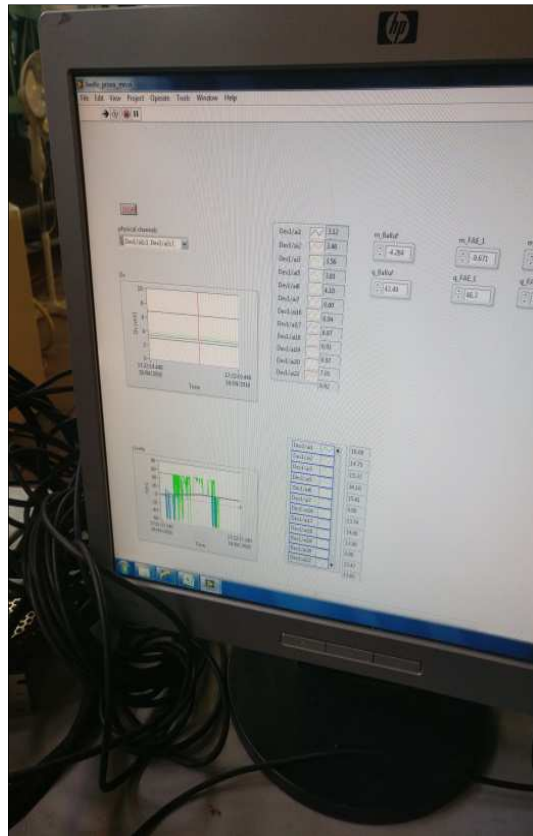


Figure 12: Image of the working station that was used for the monitoring of the probes' measurements with LabVIEW .

After that the all facility regarded to the probes has been set properly the consequence was the capability of measure the water depth evolution into the tank during the time. To make it possible the data measured by the probes are being processed with Matlab; A three-dimensional reconstruction of the water surface into the tank is shown in the figure below.

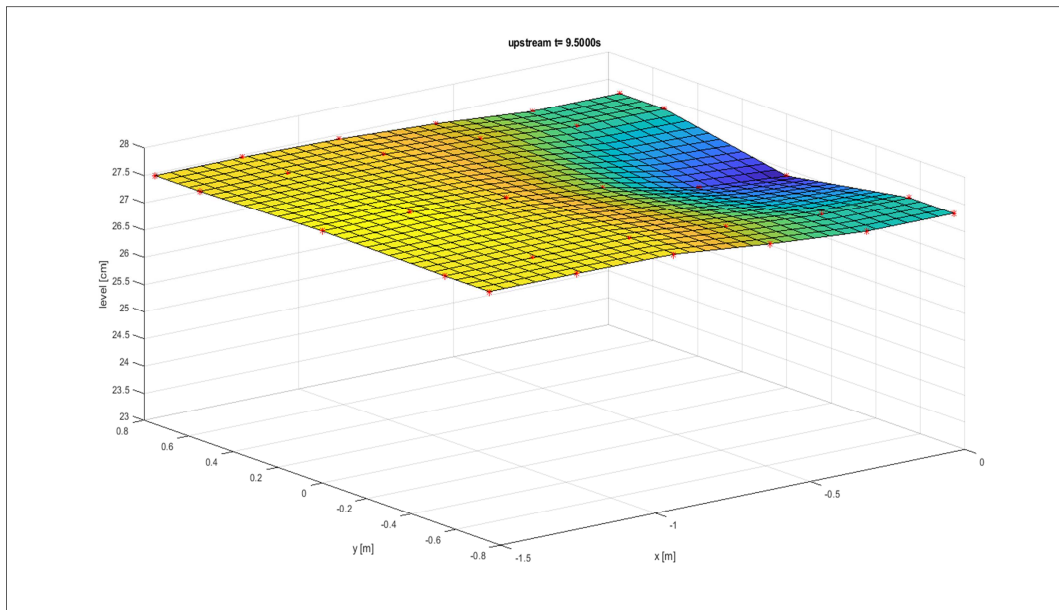


Figure 13: Three-dimensional reconstruction of the water surface into the tank in a sample time step during the experiment.

Having the complete knowledge of the water surface into the tank is possible to calculate how much volume has been released from the tank in every moment during the experiment.

In particular the volume is calculated looking at the lowering of the water surface into the tank; that surface is schematized as a flat plan with an elevation equal to the average value measured by the probes in each time step. This type of approach has been chosen because considered more robust.

3.1.2. The sluice gate

As is shown in Fig.8 and Fig.9 between the tank and the flat horizontal surface, which is in the downside, has been set up a metallic sluice gate that aims to simulate the sudden collapse of the dam with the creation of the breach.

The breach that is considered in the experiments that are presented in this thesis is characterized from a width of 3 centimeters and it has a rectangular shape.

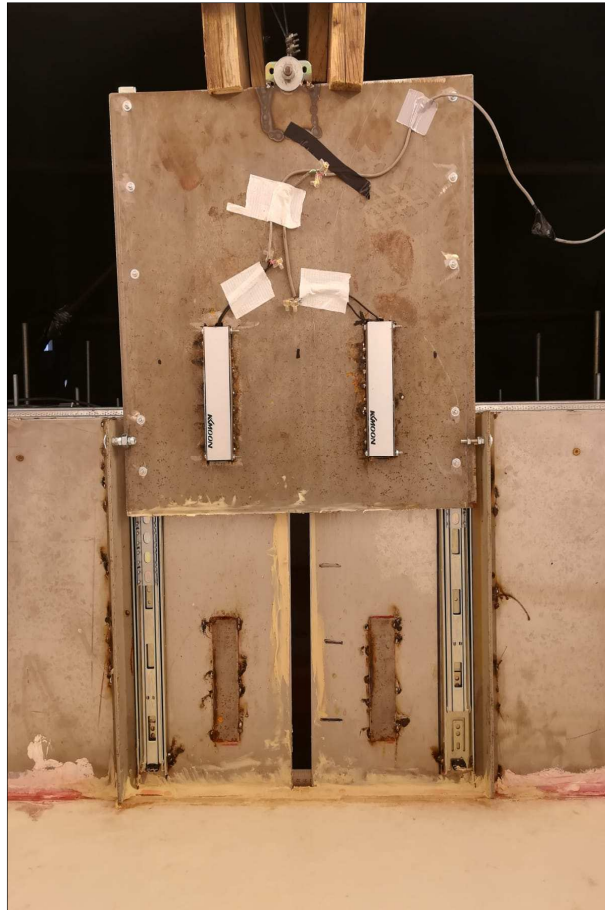


Figure 14: Three-dimensional reconstruction of the water surface into the tank in a sample time step during the experiment.

In order to considerate the gate opening as an instantaneous opening it needs to be pulled up as fast as possible; the system that has been adopted in this facility is described in the following lines: the cofferdam is equipped with two magnets (they are visible in Figure 14) that make possible to keep the gate closed before the instantaneous opening. Furthermore the sluice gate is connected with a system of cables and pulleys to an heavy metallic block that is as well connected to another magnet that is on the top of the facility; when the electricity to this system is removed all the magnets stop working and then the heavy block is free to fall down from the starting position to his ending position (close to the ground) and at the same time the cofferdam is free to being pulled up and leave the breach available for the fluid flow from the tank.

After that the sluice gate has been opened it dissipates all his energy in a wooden dissipation block that is placed upper to the gate.

The opening time of the sluice gate of the facility that is described in this thesis is:

$$t_{opening} = 0.095 \text{ seconds}$$

This time can be compared with the criterion of Vischer and Hager (1998) which state that a dam break can be considered instantaneous if the opening time satisfies the following relationship:

$$t_{opening} \leq 1.25 \sqrt{\frac{h_0}{g}} = 0.21 \text{ seconds}$$

Another criterion was established by Lauber and Hager (1998):

$$t_{opening} \leq \sqrt{\frac{2 h_0}{g}} = 0.25 \text{ seconds}$$

The two criteria stated above are satisfied and so the gate opening could be considered as an instantaneous dam-break.

3.1.3. Downstream: the flat horizontal surface

In the downstream of the facility there is a flat surface that for the experiments presented here has been kept horizontal.

The dimensions of this part of the model are shown in Figure 7; it has a rectangular geometry with two sides respectively of 3 meters and 4 meters.

The core material is wood but all the surface is being coated with a plastic thin layer to make it waterproof. In particular the material is vinyl chloride.

In order to estimate the roughness of this surface a survey with a roughness measuring instrument has been done. Further information regarding to this process are reported in the thesis of D'Oria Anna Dina (Turin Polytechnic April 2019).

As a result of this analysis the Manning value associated to this surface is $n_{model} = 0.0093 \frac{s}{m^{\frac{1}{3}}}$.

Remembering what stated at point 3.1. of this document, the physical model under discussion is a model with Froude Number constant, then in this case the scaling factor for

the Manning coefficient is $\lambda_{Manning} = \lambda^{1/6}$. So passing from the model to the reality the Manning coefficient is:

$$n_{real} = \frac{n_{model}}{\lambda^{1/6}} = 0.016 \frac{s}{m^{3/2}}$$

Above the flat surface two different cameras have been set up.

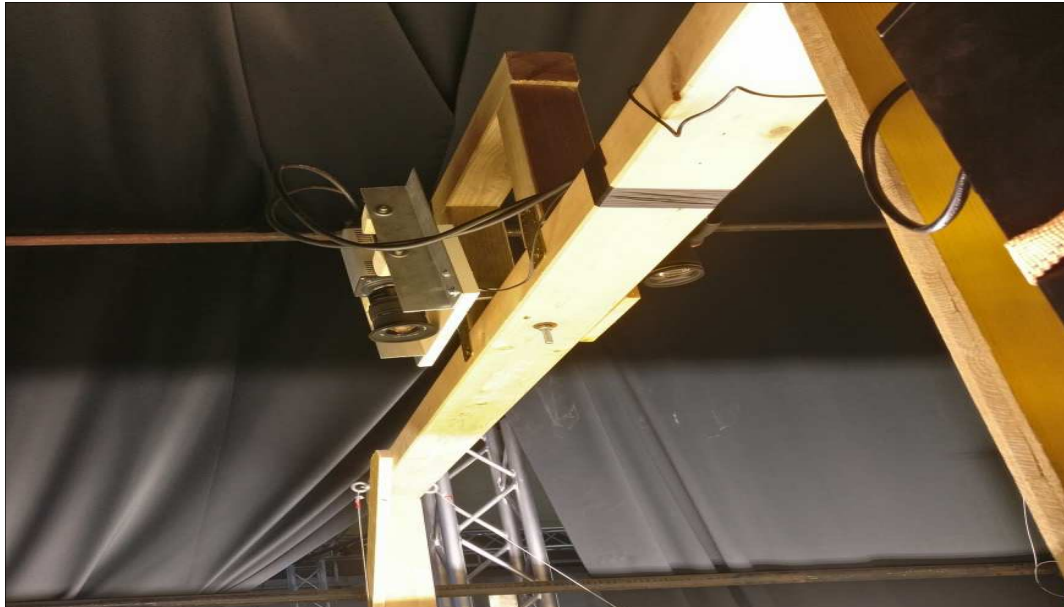


Figure 15: View of the two cameras that are placed above of the flat horizontal surface.

The two cameras are:

- Nikon D810: that was used to take colored pictures only with the scope of a better representation;
- Zyla sCMOS: the pictures taken from this camera are the picture that will be used for the imaging techniques that will be presented in the next chapter. These pictures are in a grayscale and the resolution of each one of those is 2160 x 2560 pixel. The framerate of the camera is set to **41.3** frame per second.



Figure 16: Picture extracted from the Zyla sCMOS manual.

Moreover a lightening system has been set in order to have the right light condition for the image processing techniques.

Two lines of lights are being set close to the sides of the facility; these lights are oriented in order to illuminate a reflective surface that is in the top of the model. Therefore the light reaches indirectly the flat surface.

Elsewhere the facility's boundaries are covered with a plastic reflective coating in order to not dissipate the light that come from the lightening system.

Just to be clear the figure shown below is a sample picture that represents the view from the camera (Zyla) while the surface is completely dry.



Figure 17: Sample picture taken with Zyla from where the camera is placed; in this figure the surface is completely dry.

When during the experiments the water reaches the end of the surface, there is a system of pumps that collect all of it into another external tank; in this way the water is not disperse and it is available for the other experiments.

Obviously the dimension of the pictures from the camera are given in pixel; in order to transform that in a metric output the Camera Calibrator Matlab's tool has been used.

3.2. Experiments

In order to reach the goal of this thesis the experiments are being made with two different situations:

- Dam-break wave propagation with a smooth horizontal surface as a bed-ground;
- Dam-break wave propagation with a vegetated horizontal surface as a bed-grund;

With the experimental setup that has been described in the previous subchapters is possible to represent and analyze the two study cases.

3.2.1. Smooth horizontal surface

With regard to this study case the necessary facility has been already described at point 3.1. of this document.

Below is shown a sample slideshow of the images that are used within the imaging techniques that will be showed in the next chapter.

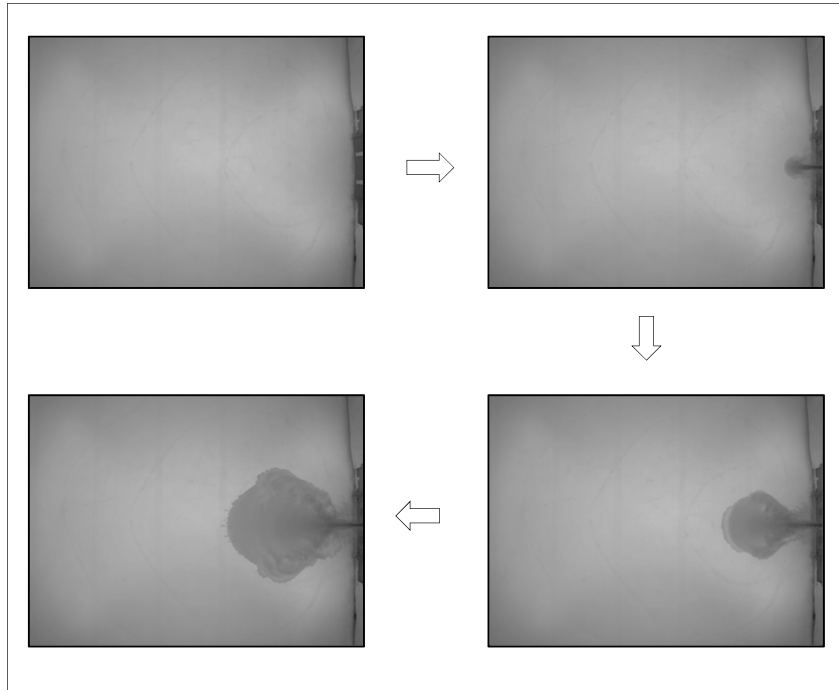


Figure 18: Sample slideshow taken from the Zyla camera during an experiment with smooth and horizontal surface.

The analysis of this kind of experiment will be illustrate in the next chapters.

3.2.2. Vegetated surface

To analyze this type of situation the physical model described at point 3.1. has been equipped with PVC panels placed on the flat horizontal surface described at point 3.1.3. . In this panels small and thin metallic rods have been fixed in order to simulate the influence of the vegetation like an orchard.

The diameter of the rods is about 4 millimeters and their height is about 5 centimeters, while the distance between one rod and another one is 5 centimeters along the X direction

and Y direction where the two axis are oriented with an angle of 45° in respect of the breach's direction.

Below is shown a sample slideshow of the experiment considering this situation.

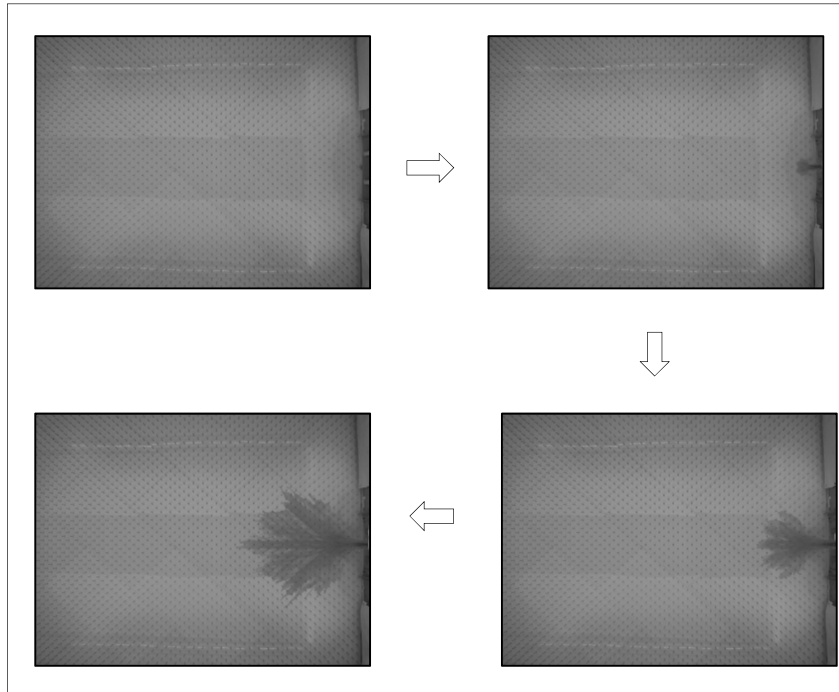


Figure 19: Sample slideshow taken from the Zyla camera during an experiment with vegetated surface.

The analysis related to this situation will be illustrated in the next chapters.

4. Analysis of the data from the physical model

The main purpose of the usage of the physical model is to be able to extract information regarded to:

- Water depth in the whole horizontal surface;
- An estimation of the water velocity looking at the wave-front evolution during the experiment.

Is being possible to use the high framerate of the camera to analyze quite well the wave-front propagation; while in order to achieve the information about the water depth, the Lambert-Beer law has been applied to both the study cases:

- Smooth horizontal surface;
- Vegetated surface.

4.1. Lambert-Beer law review

The Lambert-Beer law is an empirical relationship between the amount of light absorbed from an object and the chemical nature of that one; furthermore the law considers the concentration and the thickness of the object traversed from the light.

The law is based on the Lambert's enunciated (1760) which states that the absorbance of a solution is directly proportional to its thickness. Many years later August Beer improved the law discovering that the absorbance is proportional to the concentration of the absorbent specie within the sample.

The modern version of the law is a combination of those two mentioned before; in fact the law represents a relationship between the concentration of the absorbent specie within the solution and the length of the optical path into the material.

The analytical form of the law is:

$$\ln\left(\frac{I}{I_0}\right) = -k(\lambda) h \quad (4.1)$$

Where:

- I = local intensity;
- I_0 = initial intensity of the radiation;
- h = length of the path of the radiation through the solution;
- $k(\lambda)$ = constant value that is function of the wavelength of the radiation.

4.2. Water depth detection

An imaging technique has been applied in order to calculate the water depth values during the experiments; this technique is based on the Lambert-Beer law that has been readapted in order to fit with the study cases presented previously.

The starting data for the law's application is represented by the images taken during the experiments made at the laboratory (chapter 3.2.).

Furthermore several measurements with the spectrometer were made; those measurements were taken when a certain water depth value (constant on the whole bed-ground surface) was set up.

As a consequence of this process it has been possible to have the spectrums correspondent to different water depth values.

The same operations and measurements were done using even an aquarium filled with the same colored water used during the experiments with the physical model.

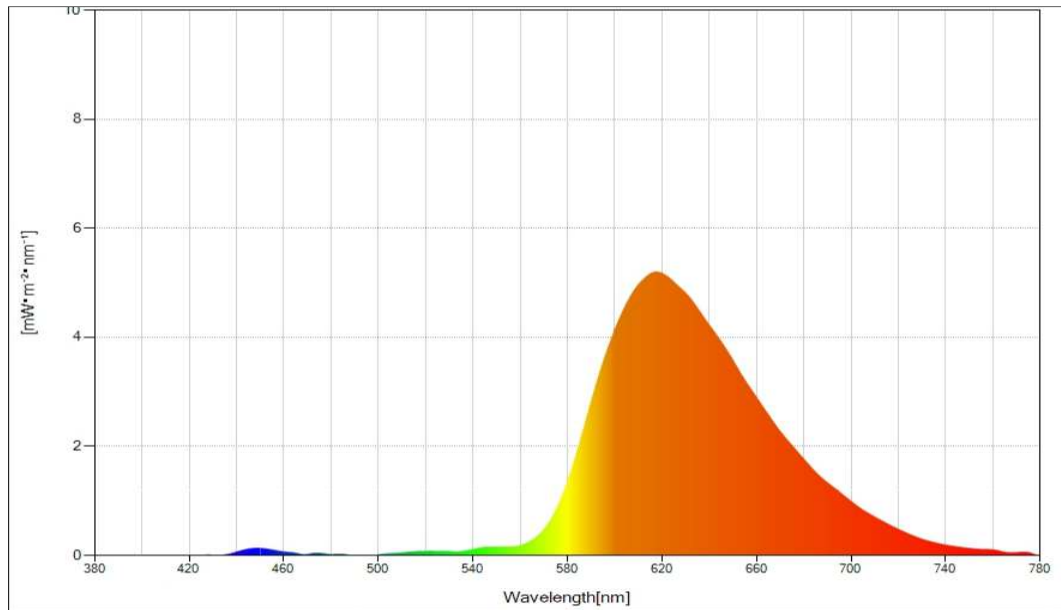


Figure 20: Example of a spectrum measured by the spectrometer.

To analyze the study cases presented in this thesis the Lambert-Beer law (4.1) could be rewrote as follow:

$$\frac{I}{I_0} = e^{-k(\lambda)h} \quad (4.2)$$

$$k(\lambda) = -\left(\frac{\ln\left(\frac{I}{I_0}\right)}{h}\right) \quad (4.3)$$

Where:

- λ = is the wavelength of the light's radiation measured with the spectrometer;
- I = it is the value of the integral of the spectrum referred to the generic image during the experiments;
- I_0 = it is the value of the integral of the spectrum referred to the image of background (flat surface without water);
- $k(\lambda)$ = is the value calculated from the equation (4.3).
- h = as already stated is the water depth value.

Then focusing the attention on the aquarium was possible to plot the graph shown below.

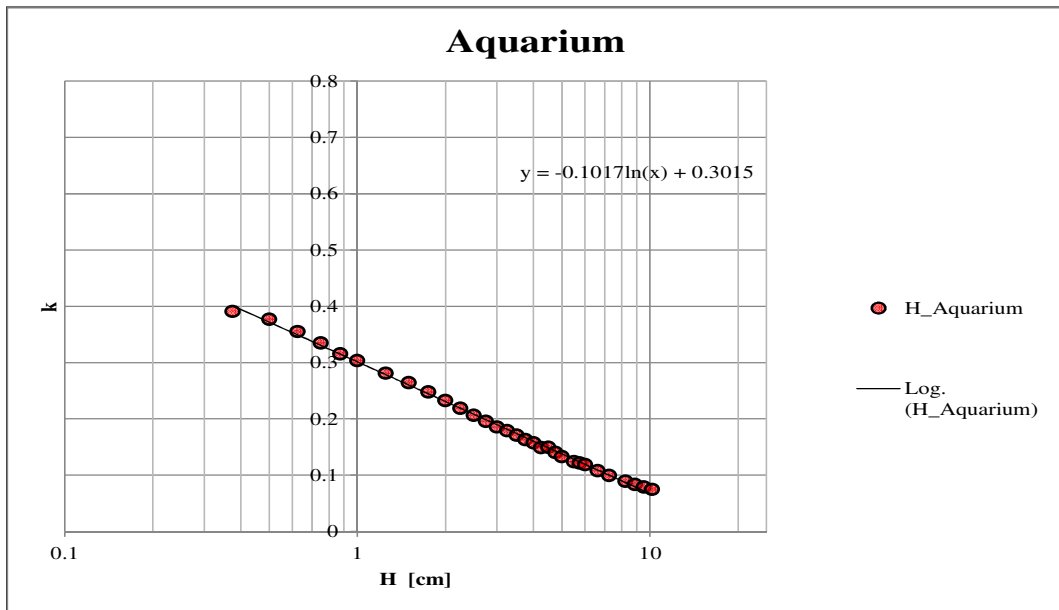


Figure 21: Relationship between the constant K and the water depth values (Aquarium).

It is possible to notice that the relationship is almost linear using a logarithmic scale of the x-axis; the pattern could be described with the following equation:

$$k(\lambda) = a \ln(h) + b = -0.1017 \ln(h) + 0.3015 \quad (4.4)$$

Continuing the analysis looking at the measurements done on the flat surface of the physical model has been possible to build the same type of graph made for the aquarium:

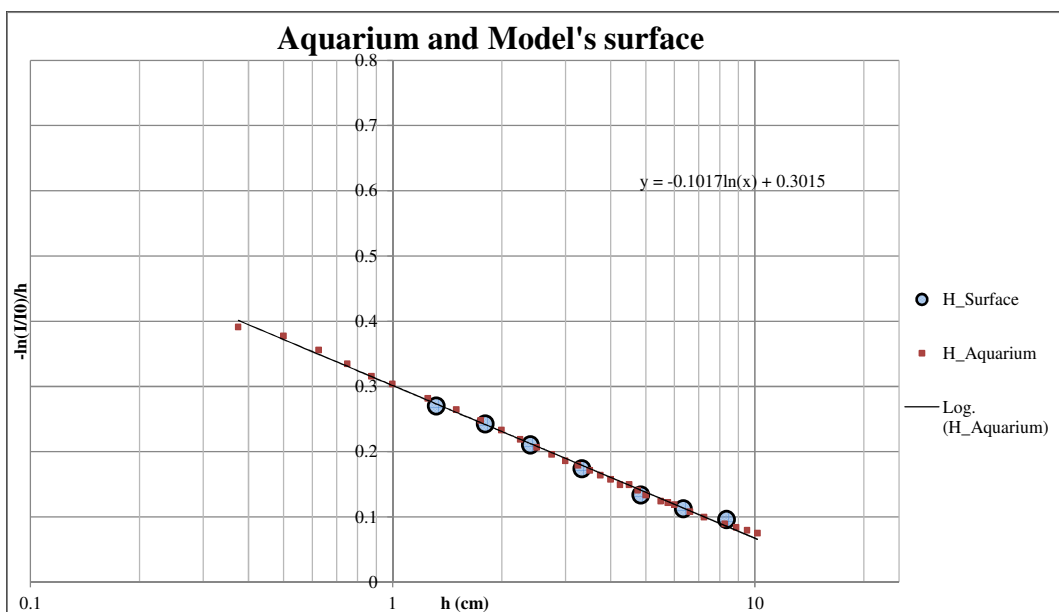


Figure 22: Relationship between the constant K and the water depth values (Aquarium and Model's surface).

It is important to notice that the y-axis' label is $-\left(\frac{\ln\left(\frac{I}{I_0}\right)}{h}\right)$ that is the way how to calculate the value of the constant $k(\lambda)$, as already stated in equation (4.3). Those values were calculated using the images taken during the spectrometer's measurements with a known water depth value.

With the objective to fit those values with the equation calculated for the aquarium it was necessary to apply a corrector coefficient to the values of water depth measured on the flat surface; this coefficient is equal to 1.5.

It is necessary to apply this coefficient because of the conditions change passing from the aquarium to the physical model; in fact the light in the aquarium comes from the bottom and also the water in the model is in movement.

The next step consists in find a relationship between the ratio $\frac{I}{I_0}$ (that is what is known in every instant during the experiments) and the water depth (h) in order to make possible to apply the Lambert-Beer law to this situation.

Combining the equations (4.2) and (4.4) the relationship becomes:

$$\frac{I}{I_0} = e^{-[a \ln(h)+b]h} = e^{-[-0.1017 \ln(h)+0.3015]h} \quad (4.5)$$

In the following graph are shown:

- The studied relationship extracted from the experimental data taken with the spectrometer in the aquarium;
- The same relationship but calculated using the equation (4.5) ;
- The same curve but calculated referring to the measurements taken with the spectrometer on the flat surface of the physical model.

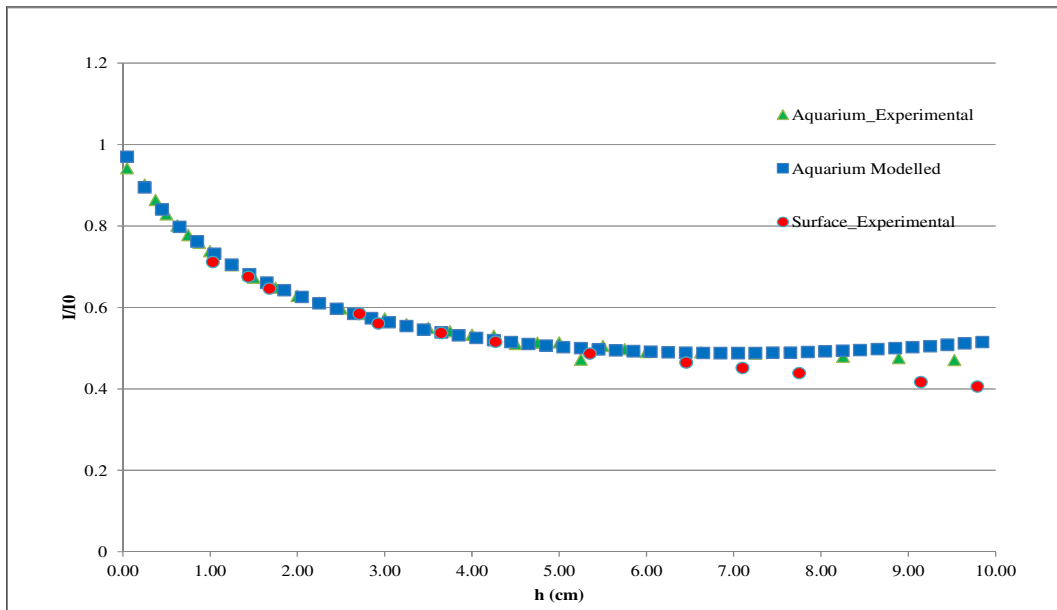


Figure 23: Relationship between I/I_0 and water depth for the three different situations that were analyzed.

It is important to point out that to make possible to have the match between the analytical model calculated for the aquarium and the one calculated for the physical model is necessary to multiply the considered image to a corrector factor estimated equal to **2.4**.

Summarizing the procedure during a generic experiment:

- a) Calculate the ratio $\frac{I}{I_0}$ for each pixel of each image taken during the experiment;
- b) Multiply that ratio for the corrector factor 2.4;
- c) Calculate the value of the water depth from the equation (4.5).

All the results achieved with the procedure described in this chapter are shown in the following chapters.

Just to give an example of what are the results in terms of water depth for a sample frame during an experiment the following figures are shown.

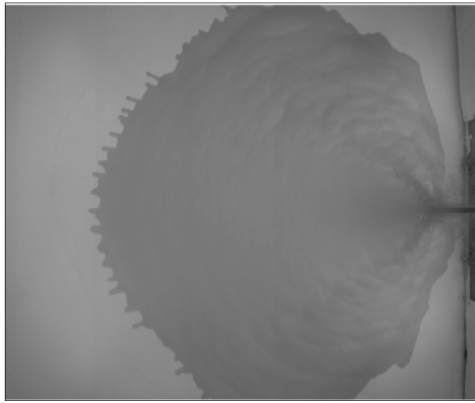


Figure 27: Sample frame taken by Zyla during an experiment with smooth horizontal surface.

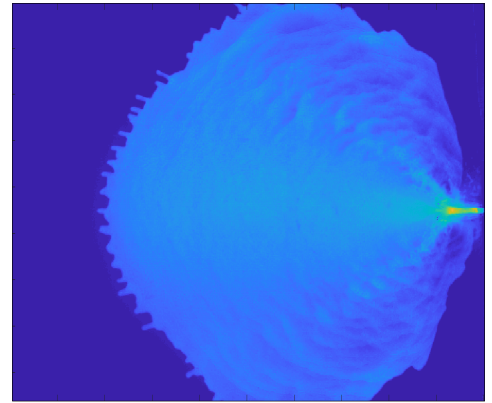
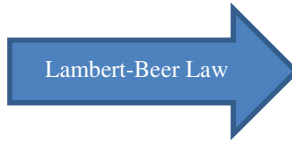


Figure 27: Reconstruction of the water depth's field associated to the frame. The water depth value is known in every pixel of the image.



Figure 27: Sample frame taken by Zyla during an experiment with smooth horizontal surface.

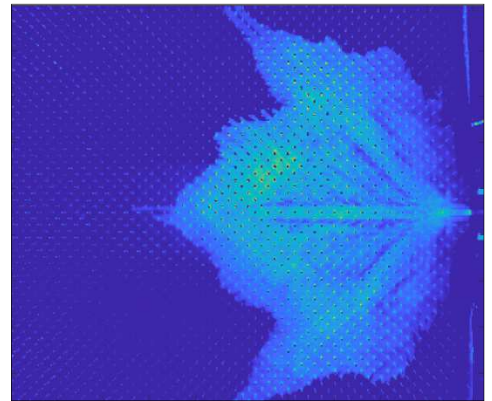


Figure 27: Reconstruction of the water depth's field associated to the frame. The water depth value is known in every pixel of the image.

4.3. Wave-front velocity detection

The detection of the wave-front during the dam-break's experiments is definitely easier than the water depth calculation described in the previous subchapter.

In fact having the images of the experiments is possible to analyze them and applying opportune thresholds, in terms of gray intensity, to the images is possible to obtain the edges of the wave during the whole duration of the experiments.

Below are shown some examples of the results of this process while all the significant results of this analysis are shown in the next chapters.

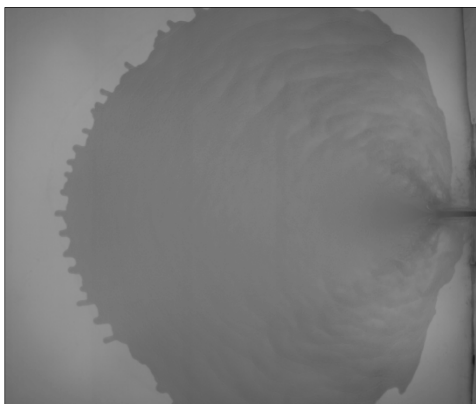


Figure 29: Sample frame taken by Zyla during an experiment with smooth horizontal surface.

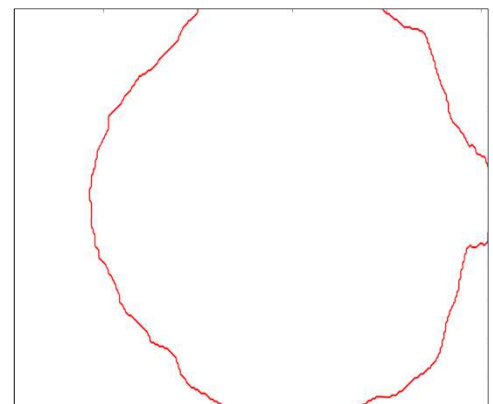


Figure 29: Wave's edges representation.

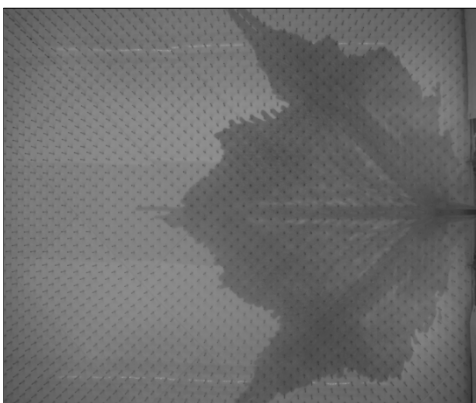


Figure 31: Sample frame taken by Zyla during an experiment with vegetated horizontal surface.

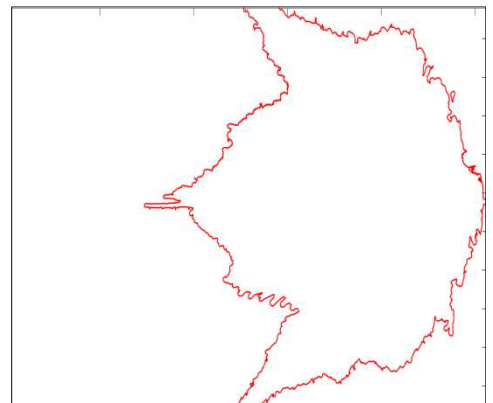


Figure 31: Wave's edges representation.

With the knowledge of how the wave evolves during the experiment is possible to calculate an estimation of the wave's average velocity. Results will be showed in the following chapters.

5. Numerical analysis with *parBreZo* 8.1.0

This part of the thesis has been developed by the author during a period of three months spent at the *University of California Irvine (UCI)*.

This time has been useful to learn how to use the software with the precious supervision of Professor *Brett F.Sanders* which is the software's creator.

The building of an hydraulic numerical model of the facility described widely in the previous chapters aims to:

- Verify how much the physical model is coherent with the equations that govern this numerical model;
- Make the analysis faster with the possibility to try many different configurations of the vegetation without changing the physical model;

5.1. Software overview

BreZo solves the shallow-water equations using a Godunov-type finite volume algorithm that has been optimized for wetting and drying applications involving natural topography and runs on an unstructured grid of triangular cells. There are several versions of BreZo as a result of an ongoing research process [5].

The version that has been used in the numerical model presented here is the *parBreZo 8.1.0* which differently from the previous releases offer to the users the possibility of solve the numerical model using all the available processors in parallel.

5.1.1. Finite volume algorithm

The solution through the finite volume algorithm is based on a discretization in an integral form of the equations which governs the phenomenon: the De Saint Venant Equation:

$$\frac{\partial}{\partial t} \int_{\Omega} U \, d\Omega + \oint_{\partial\Omega} (F \, dx - G \, dy) = \int_{\Omega} S \, d\Omega \quad (5.1)$$

Where:

- Ω is the bi-dimensional domain where the calculation is done (in this particular situation it is the triangular cell) bounded by the border $\delta\Omega$;

- U, F, G, S represent the arrays that are defined with the expression (5.2) stated below, where u and v are the velocity components averaged along the vertical direction, z_b is the channel's slope, c_D is the term that represents the channel's roughness as a function of the Manning Coefficient ($c_D = g n^2 h^{\frac{1}{3}}$).

$$U = \begin{pmatrix} h \\ uh \\ vh \end{pmatrix} \quad (5.2. a)$$

$$F = \begin{pmatrix} uh \\ u^2 h + \frac{1}{2} g h^2 \\ uvh \end{pmatrix} \quad (5.2. b)$$

$$G = \begin{pmatrix} vh \\ uvh \\ v^2 h + \frac{1}{2} g h^2 \end{pmatrix} \quad (5.2. c)$$

$$S = \begin{pmatrix} -gh \left(\frac{\partial z_b}{\partial x} \right) - c_D u \sqrt{u^2 + v^2} \\ -gh \left(\frac{\partial z_b}{\partial y} \right) - c_D v \sqrt{u^2 + v^2} \end{pmatrix} \quad (5.2. d)$$

Regarding the spatial discretization of the bi-dimensional domain Ω , the discrete solution of the De Saint Venant equations in integral form uses a cell grid where the cells have a triangular shape; so we can define the number of nodes N_n , cells N_c and faces N_f . The topography of the geometry could be defined associating an elevation value to every node of the grid.

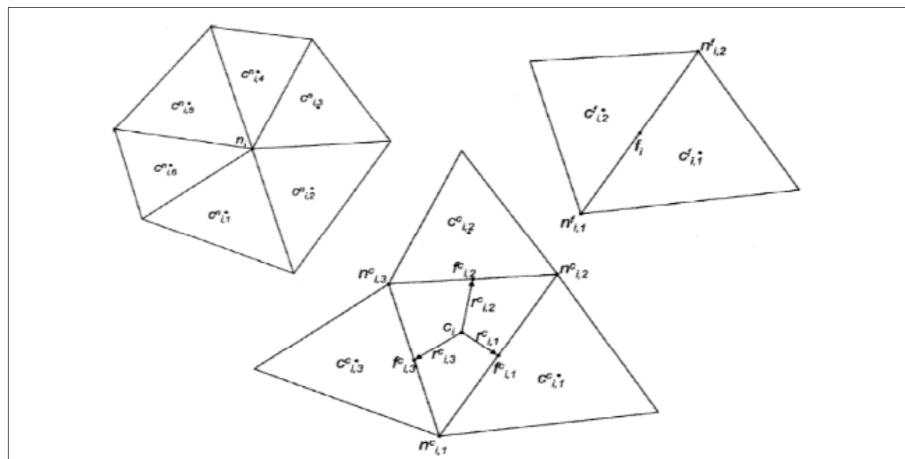


Figure 32: Example of computational cells and relative parameters.

5.1.2. Modeling of the *wetting* and *drying* processes

One of the main benefits of the usage of the finite volume algorithm is that it gives the possibility of a good modeling of the wetting and drying phases; the meaning of these two words is the description of the phenomenon when the water gets into areas(cells) that previously were completely dry.

Regarding this aspect the finite element methods give as a results the generation of spurious oscillations of the water depth while the finite volume algorithm constitutes a significant improvement even if it is not the best and definitive solution.

An accurate and reliable procedure regarding this aspect has been presented by Sanders and Begnudelli in the 2006. [7]

As already mentioned before the whole method is based on the usage of a triangular unstructured cells grid, and what is important is to find a relationship between the water depth and the water volume of the wet cells.

Usually the finite volumes schemes assume that the water surface elevation of the cell has to be calculated in the center of the same cell.

But if one cell is not totally wet the procedure aforementioned does not work properly; just to be clear if the water surface elevation is lower than the cell's center elevation then that cell will be considered as a dry cell.

With the objective of the improvement of the description of those cells that are partially wet was introduced a distinction between the water surface elevation and the water depth calculated in the centroid of the cell.

Indeed the average water depth of each cell is calculated evaluating the ratio between the fluid volume V and the cell's area, while the water surface elevation η is given from the elevation in the wet part of the cell. Then the consequence is that the relationship $\eta = h + z_c$ would be right only for those cells that are completely wet.

Hence when a cell is partially wet, the correlation between h and η is given by some relationships which are called VFRs (*Volume/Free surface relationships*); those represent a correlation between the water surface elevation and the volume.

Considering a cell where its vertexes' coordinates are (x_1, y_1, z_1) , (x_2, y_2, z_2) , (x_3, y_3, z_3) and with the hypothesis that $z_1 \leq z_2 \leq z_3$ the VFR equation that correlates h and η and the number of vertexes submerged is:

- if $\eta \leq z_1$ the cell is completely dry and then $h = 0$;
- if $z_1 < \eta \leq z_2$ the VFR equation is:

$$h = \frac{V}{A} = \frac{(\eta - z_1)^2}{3(z_2 - z_1)(z_3 - z_1)} \quad (5.3. a)$$

- if $z_2 < \eta \leq z_3$ the VFR equation is:

$$h = \frac{V}{A} = \frac{\eta^2 + \eta z_3 - 3\eta z_1 - z_3 z_2 + z_1 z_2 + z_1^2}{3(z_3 - z_1)} \quad (5.3. b)$$

- if $z_3 < \eta$ then $\eta = h + z_c$ where $z_c = \frac{z_1 + z_2 + z_3}{3}$

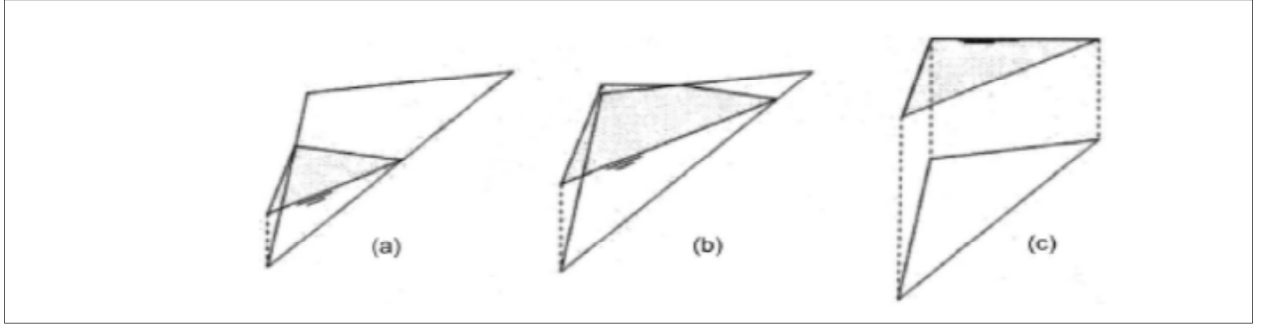


Figure 33: Volume into the computational cell; (a) $z_1 < \eta \leq z_2$ (b) $z_2 < \eta \leq z_3$ (c) $z_3 < \eta$.

5.1.3. Calculation algorithm

In this numeric solution the calculation of the fluxes is done using the approximated solution presented by Roe for the Riemann condition while for the calculation of the equation of mass conservation it uses the upwind monotone scheme MUSCL achieving a second order approximation spatially. [10]

In order to optimize the temporal evaluation of the variables the predictor-corrector (Hancock) is been adopted.

5.1.3.1. Preliminary operations: cells classification and gradients evaluation

The first step of the algorithm is the finding of the cells which are totally wet, partially wet or dry.

As already aforementioned, a cell has to be considered totally wet if all its vertexes are submerged; in this situation for every time step the solution the continuity equation and the momentum equation are solved, otherwise only the continuity equation will be solved.

The submerged nodes are characterized by a water depth of $h_n > \delta^W$ (δ^W is the threshold value that is $10^{-6} m$).

The value of the water depth calculated in correspondence of the node is evaluated subtracting the node's elevation from the average value of the water surface elevation considering all the cells adjacent to that node.

The analytical form of this calculation is stated below:

$$\eta_i^n = \frac{1}{M_i^w} \sum_{c_i, k^n \in C_i^n} \eta_{c_i, k^n} \quad (5.4)$$

Where C_i^n represents set of wet cells that surround the node and M_i^w is the number of those cells.

Then the water depth in correspondence of that node is evaluated with the following expression:

$$h_i^n = \max(\eta_i^n - z_{b1}, 0) \quad (5.5)$$

The next step is represented by the gradients evaluation: the gradients of the main variables u , v and η are calculated for each cell, independently from how much water they contain, using a method that allow to exclude the starting solutions that could be not physically based.

Considering a point within the domain, the components $\delta_x q$, $\delta_y q$ of the gradient of a generic dependent variable q are evaluated as a first try using the values q_1, q_2, q_3 of that variable in correspondence of the three vertexes of coordinates (x_1, y_1) , (x_2, y_2) , (x_3, y_3) using the formula:

$$\begin{pmatrix} \delta_x q \\ \delta_y q \end{pmatrix} = J \begin{pmatrix} q_2 - q_1 \\ q_3 - q_1 \end{pmatrix} \quad (5.6)$$

Where J is the right element of the Jacobian matrix:

$$J = \frac{1}{(x_2 - x_1)(y_3 - y_1) - (x_3 - x_1)(y_2 - y_1)} \begin{pmatrix} y_3 - y_1 & -y_2 + y_1 \\ -x_3 + x_1 & x_2 - x_1 \end{pmatrix} \quad (5.7)$$

Each one of the elements of J is a function of the coordinates of the grid's point, then in order to minimize the computational effort this matrix is calculated during a *preprocessing* phase.

The effective components $\overline{\delta_x q}$ and $\overline{\delta_y q}$ are obtained multiplying $\delta_x q$ and $\delta_y q$ for the *scalar limiting function* Φ .

5.1.3.2. Predictor step

Knowing the values of the variables at the time t , what the predictor step does is to evaluate the solution at time $t+\Delta t / 2$. If the cell considered is dry the usage of the predictor step is simply the transcription of the solution of the previous time-step. Otherwise if the cell is classified as a wet cell the predictor step consists in the solving of the De Saint Venant equations without considering the fluxes.

The following equations aim to upload the solution regarded to a cell at the time step p .

$$\begin{cases} \eta_i^p = \eta_i - \frac{\Delta t}{2} (u \overline{\delta_x h} + h \overline{\delta_x u} + v \overline{\delta_y h} + h \overline{\delta_y v})_i \\ u_i^p = u_i - \frac{\Delta t}{2} (u \overline{\delta_x u} + g \overline{\delta_x \eta} + v \overline{\delta_y u} + c_D h^{-1} u^p \sqrt{u^2 + v^2})_i \\ v_i^p = v_i - \frac{\Delta t}{2} (v \overline{\delta_x v} + g \overline{\delta_y \eta} + v \overline{\delta_y v} + c_D h^{-1} v^p \sqrt{u^2 + v^2})_i \end{cases} \quad (5.8)$$

The entity of the fluxes is determined using the predictor step using the Roe method (1981).

Furthermore the evaluation of the variables η, u, v (that will be stated generally as q) in correspondence of the middle point of each face of the cell is calculated with the following relationships.

$$q_L = q_{C_{i,1}} + r_{C_{i,1},f_{i,1}}^C (\overline{\nabla q})_{i,1} \quad (5.9.a)$$

$$q_R = q_{C_{i,2}} + r_{C_{i,2},f_{i,1}}^C (\overline{\nabla q})_{i,2} \quad (5.9.b)$$

The symbols q_L and q_R represents the values of the variables calculated for the right and left edges of the cell.

The water depth in each one of the edges is obtained subtracting from the values η_L, η_R , the elevation of the middle point of the cell's face: if the values that are obtained are negatives values these are forced to be zeros.

The fluxes through every faces is given by the sum of the Roe flux and a correction value.

$$F = F_{Roe} + F_{Corr} \quad (5.10)$$

$$F_{Roe} = \begin{pmatrix} h\hat{u} \\ hu\hat{u} + \frac{1}{2}gh^2r_x^f \\ hv\hat{u} + \frac{1}{2}gh^2r_y^f \end{pmatrix} \quad (5.11)$$

Where:

- \hat{u} is the velocity component perpendicular at the face of the cell;
- r_x e r_y are the components of the r array evaluated along the x and y directions;

Hence the definition of the corrector factor is stated below:

$$F_{Corr} = \begin{pmatrix} 0 \\ \frac{1}{12} g(\Delta_t h)^2 r_x^f \\ \frac{1}{12} g(\Delta_t h)^2 r_y^f \end{pmatrix} \quad (5.12)$$

5.1.3.3. Corrector Step

The corrector step completes the calculation of the variables at the time $t+\Delta t$.

Explaining briefly how it works, its duty is to calculate the Shallow Water equations if the cell is classified as a wet cell or only the continuity equation if the cell is dry.

Cause the system is clearly explicit is necessary to evaluate the stability of the system using the Courant-Friedrichs-L Levy (CFL) criterion; this one is a condition that is necessary for the convergence of some hyperbolic equations. [11]

Then it is necessary that the chosen time-step is lower than a certain value of time.

For unidimensional analysis the CFL criterion is:

$$Cr = \frac{u \Delta t}{\Delta x} < K \quad (5.13)$$

Where u is the velocity, Δt is the time step and Δx is the spatial dimension regarded to the geometry; so K is a constant derived from the equation stated above.

The Cr abbreviation indicates the Courant number.

If the study case is related to a bi-dimensional grid, then the Courant number is:

$$Cr = \frac{u_x \Delta t}{\Delta x} + \frac{u_y \Delta t}{\Delta y} \quad (5.14)$$

If the grid is made with triangular cells than:

$$Cr = \Delta_{tmax_{i=1..N_c}} \left\{ \frac{3 \max_{(k=1,2,3)} |\lambda_{f_{i,k}} l_{f_{i,k}}|}{A_i} \right\} \leq 1 \quad i = 1, \dots, N_c \quad (5.15)$$

$\lambda_{f_{i,k}}$ is the component of celerity that is perpendicular at the face k of the cell i.

5.1.3.4. Godunov solution scheme

The numerical solutions presented by Sergei K. Godunov in the 1959 are based in the solution of the Riemann problem.[9]

In a generic case of the solution of an hyperbolic system the Riemann problem needs to solve the initial condition:

$$U_t + F(U)_x = 0 \quad (5.16)$$

Where:

$$U(x, 0) = \begin{cases} U_l & x < 0 \\ U_r & x > 0 \end{cases} \quad (5.17)$$

5.2. How to set up the hydraulic model with parBreZo

8.1.0.

As aforementioned the software that has been used in this analysis presented here is *parBreZo 8.1.0*.

This version of the software was made available for this study directly from Professor Brett F.Sanders. Differently from the version that is available online for free download this one has not any limitation in terms of number of cells.

5.2.1. How to use the software

This software is not equipped with a graphic interface available for the user but it needs to be used through the command prompt of the computer.

The first step that must be done is to create a working directory; into this one is necessary to set the following elements:

- The executable file of the code (for example *parBreZo.exe*) which contains different fortran routines that make the software works;
- The project directory which needs to be called as '*nameoftheproject.1*';
- The *brezo.start* file which is just the file that contains the name of the project directory that we want to execute.

Into the project directory is necessary to put several files that will be listed in the following lines:

- ***Nameoftheproject.poly***

This file is a simple text file where is possible to set up the geometry of the study case; indeed is possible to set all the vertexes that are required to build the geometry, like the points which represents the borders of the domain or others that are used to define areas where a refinement of the mesh is needed.[6]

Suddenly after the definition of the vertexes is necessary to give to the software how this points are connected between each other; then is necessary to define the number of edges and which are the nodes connected by that edge.

Furthermore into the *.poly* file is possible to indicate the number, position and details regarded to the eventual holes present within the domain.

In the last lines of this file is possible to set the maximum dimension of each element of the mesh looking if the cell is or not inside any area where a mesh refinement is needed.

When the *poly* file is ready it is used as an input file for a two-dimensional mesh generator called Triangle [12] that was created by Jonathan Richard Shewchuk (University of California at Berkeley); even this tool has to be executed from the command prompt and is also possible to set up the minimum angle of each triangle. During this analysis the value of 30° has been used as minimum angle opening for each triangle of the mesh.

Using the *Triangle.exe* tool with the *poly* file related to the project that has to be run some other files will be created:

- ***Nameoftheproject.node***: it represents a file with information regarded to each node of the whole mesh, as their coordinates, attributes and boundary marker (if is a node close to the boundaries of the domain or not).

- *Nameoftheproject.edge*: this file contains information about the connections between all the nodes of the mesh.
- *Nameoftheproject.neigh*: in this file are reported the neighbors for each one of the triangles of the mesh.
- *Nameoftheproject.ele*: inside of this file there is a list of all the elements of the mesh (tringles) and which are the nodes that are a part of that triangle.

Further information and description related to the usage of Triangle could be found at <http://www.cs.cmu.edu/afs/cs/Web/People/quake/triangle.html> .

- *Nameoftheproject.input*

This file is used to select all the computational parameters that will be necessary during the calculations.

Some of the parameters that could be managed with this file are listed below:

- Coordinate system: is possible to choose between SI, US or GEO;
- Maximum Computational Interval and Courant number;
- Start date of the simulation stated as *year, mon, day, hour, min, sec*;
- Stop date of the simulation stated as *year, mon, day, hour, min, sec*;
- Initial condition options: is possible to select between a cold start with a constant eta (bed elevation + water depth) or water depth. So is possible to manage the initial condition even with a proper file that is described thereafter;
- Animation options: in this section is possible to choose between the Matlab or Tecplot animation format; also for the Tecplot output format is available the possibility to have an output file for each time step of the simulation; is even possible to select if the output has to be calculated in correspondence of the cell center or in every node;
- Time interval for the animation: in correspondence of these intervals the results will be recorded as output files;

- Friction option: this section is dedicated to the choice of the friction, this one could be described selecting between: Manning, Chezy, Darcy-Weisbach or frictionless;

Furthermore there are other options regarded to monitoring cross sections within the geometry, source points, sewer options and even the possibility to use the porosity method. Anyways these last options are not particularly useful regarding to the analysis reported in this document.

- ***Nameoftheproject.bc***

This file is used to set the boundary conditions of our domain; in fact is necessary to assign a boundary condition ID that will be paired with the boundary condition type (specified eta, specified flow, dry, soft wall).

In order to be clear, the boundary condition ID is the number that has to be write into the poly file in correspondence of the right edge.

Moreover the boundary condition would be applied in a constant way or with an harmonic path.

- ***Nameoftheproject.ic***

The initial conditions file is a simple way to indicate the value of a variable (water depth, eta, velocity) into a subdomain that needs to be created as a separate geometry but using a coherent coordinates system with the main geometry's files.

In order to assign the elevation of each cell of the entire domain a fortran code was made available, its name is *makepltfile.f90* . Inside of this code is possible to amend the right part that is dedicated to the elevation assignment.

To obtain the executable file needed is necessary to compile the fortran code using a fortarn compiler; what this executable file does is to create new geometry files which contain the information about the elevation; those files change their names with the addition of a '.1' string (for example: *nameoftheproject.node* → *nameoftheproject.1.node*).

5.2.2. Geometry setup

In order to build the geometry the two-dimensional mesh generator *Triangle* was used [12]; as described at point 5.2.1. what we have to define is the poly file which works as an input file for the tool.

The two study cases that are presented in this thesis are:

- Smooth horizontal bed-ground;
- Vegetated horizontal bed-ground;

For each one of the study cases a different geometry has been built.

5.2.2.1. Smooth horizontal bed-ground

In relationship of this situation, after that several simulations were done the definitive choice was to divide the mesh in three different main zones where a different cell-size has been used.

The details regarding the numerical value of the cell-size in the different areas is reported and widely described in the next subchapter.

The three main different zones are:

- *Zone A*: it is the part of the geometry that is inside of the tank; within this area is possible to use a coarser resolution than the rest of the geometry;
- *Zone B*: in order to obtain a detailed representation of the first part of the propagation is necessary to use a fine resolution in the area that is close to the breach. This zone is wide 1 meter and its height is about 50 centimeters.
- *Zone C*: in the rest of the flat horizontal surface in the downstream the cell size will be coarser than *Zone B* but finer than *Zone A*.

A graphic scheme of this subdivision is shown in the following figure.

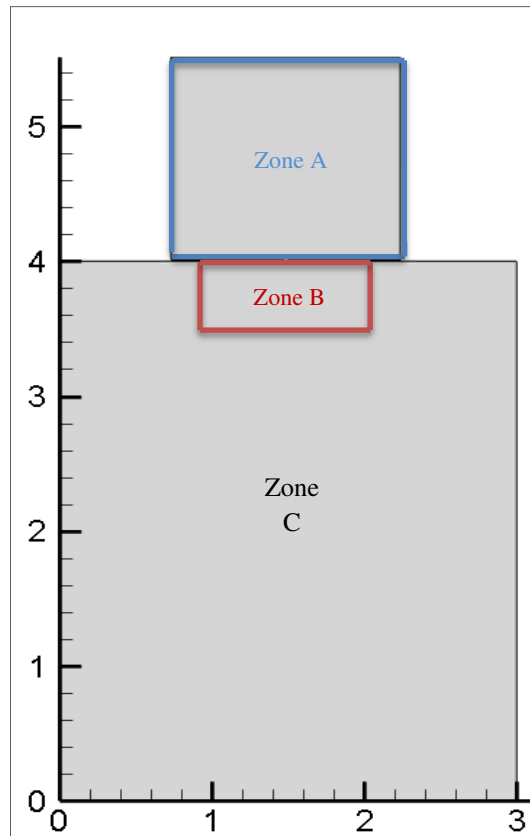


Figure 34: Subdivision of the whole geometry in three different zones where a different mesh resolution has been used.

5.2.2.2. Vegetated horizontal bed-ground

As already stated in the previous chapters the vegetation in the physical model has been simulated with small and thin metallic rods with a diameter of 6 millimeters; furthermore the distance between one rod and another one is 5 centimeters in both directions, x and y where the two axis are oriented with an angle of 45° in respect of the breach's direction.

To simulate the presence of the rods on the flat horizontal surface in the software parBreZo was necessary to create holes into the mesh in correspondence of every rod.

However because is not possible to insert circles in the geometry trough the poly file was necessary to schematize them as decagonal holes into the mesh.

In order to represent those holes was necessary to amend the poly file including for each one of the rods:

- 11 new vertexes where 10 are the external vertexes and the other one is the center of the decagon (this last one must be stated as hole into the .poly file);
- 10 new edges to represent the external sides of each decagon.

Consequentially the poly file regarded to this situation is obviously a bigger file cause the large amount of points.

Even in this study case the subdivision in three different zones were done (Figure 34). In the following figure the view of some of the rods is shown.

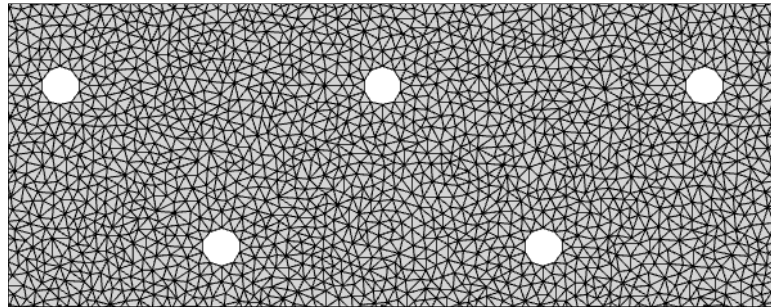


Figure 35: Representation of some of the decagonal holes (image from Tecplot).

5.2.3. Computational parameters of the hydraulic model

The parameters needed to set up properly the hydraulic model are mainly:

- Simulation time;
- Computational interval / Courant Number;
- Roughness information: Manning coefficient of the bed-ground;
- Cell-size of the different zones;

For every simulation presented hereafter, all those parameters have been estimated as a result of a sensitivity analysis that was done once several simulations were accomplished. All this process had the objective to estimate the best values of those parameters in order to match as much as possible the results from the numerical model with the results of the physical model (Chapter 4).

This sensitivity analysis was pursued with the attention mainly in the Manning coefficient, breach schematization and mesh's dimensions; anyway looking at the results of many different simulation was noticed that the most influential parameters were the Manning coefficient and the mesh's dimension. Then fixing the cell-size of the different zones of the geometry all the investigation has been reduced to a *one-way problem* with the finding of the right Manning coefficient that makes it possible to have the best correspondence between the wave-front from numerical and experimental results.

Furthermore in order to study correctly these study cases it is necessary to set:

- Initial conditions;
- Boundary conditions;

For the two study cases presented here these conditions are the same.

- **Initial conditions:**

In order to set the initial conditions in the BreZo model is required to amend the *nameoftheproject.ic* file, that has been described at point 5.2.1.; in particular an initial value of `eta_ic` (bed-ground elevation + water depth) has been set equal to 30 centimeters into the tank.

- **Boundary conditions:**

To make the solution of the model possible is necessary to specify a boundary condition; this one could be stated inside the *nameoftheproject.bc*. In particular in this project a *dry* condition has been set, in order to represent a free outlet from the domain.

As already previously stated, the boundary conditions and even the initial conditions are the same for all the BreZo models presented thereafter in this document.

5.2.3.1. Smooth horizontal bed-ground

In order to analyze the influence of the no slip condition, applied to the tank's walls, two different geometries were developed; both of these are related to the case of smooth horizontal bed-ground.

a. Model A:

This geometry has been built following the path showed at point 5.2.2.1. and the elevation of the whole surface is set to zero; then it is a two-dimensional domain, where only the water depth is evaluated along the Z direction.

The main parameters of the hydraulic model are stated in table 1:

<i>Computational parameters Model A</i>		
Simulation Time	Courant Number	Manning Coefficient
[s]	[-]	[s m ^{-1/3}]
2	0.8	0.0084

Table 1: Computational parameters of Hydraulic model A related to smooth horizontal bed-ground.

Regarding to the cell-size of the mesh it is necessary to remember the subdivision of the whole domain in three different zones (Figure 34 Chapter 5.2.2.1.).

The maximum cell-size is reported in the following table.

<i>Mesh's dimensions Model A</i>		
Zone A	Zone B	Zone C
[cm ²]	[cm ²]	[cm ²]
0.5	0.1	0.2

Table 2: Mesh's dimensions related to the geometry of Model A.

The total amount of cells is **1'060'921**.

With the objective to make the explanation clearer the following images show the different cell-size of the three zones.

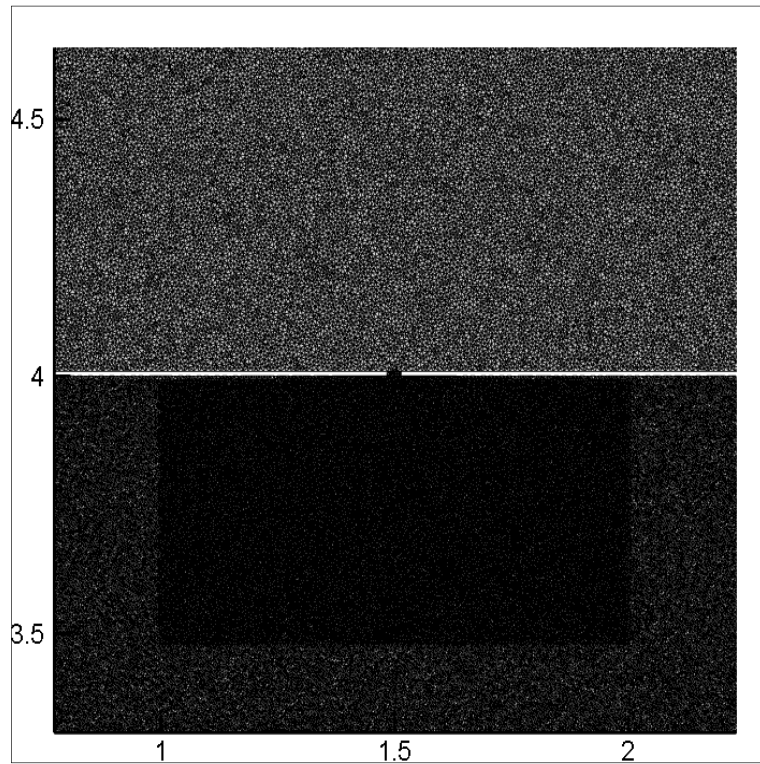


Figure 36: Zoomed view of the three different mesh's zones resolution(Tecplot).

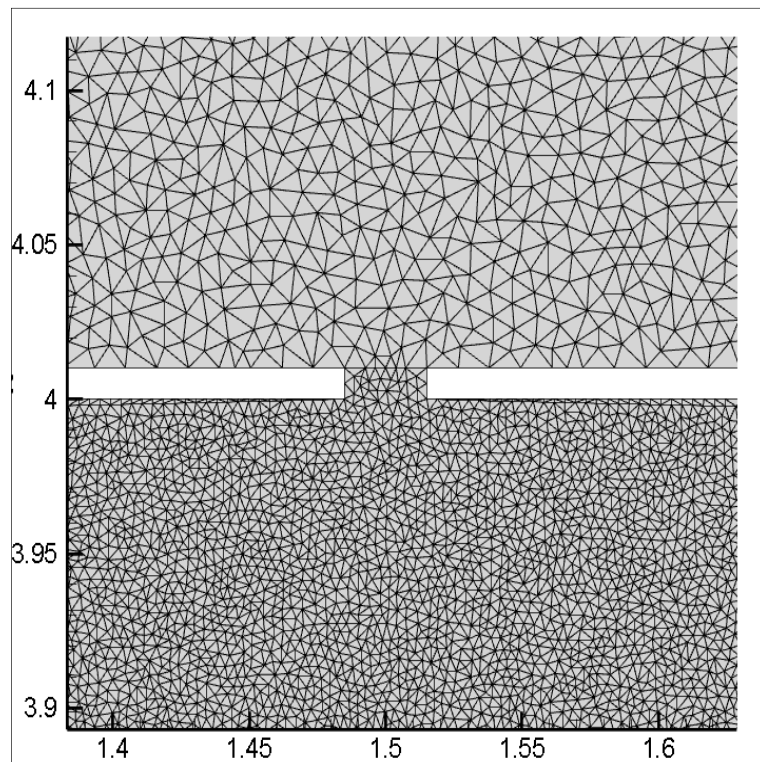


Figure 37: Zoomed view of mesh in the area close to the breach(Tecplot).

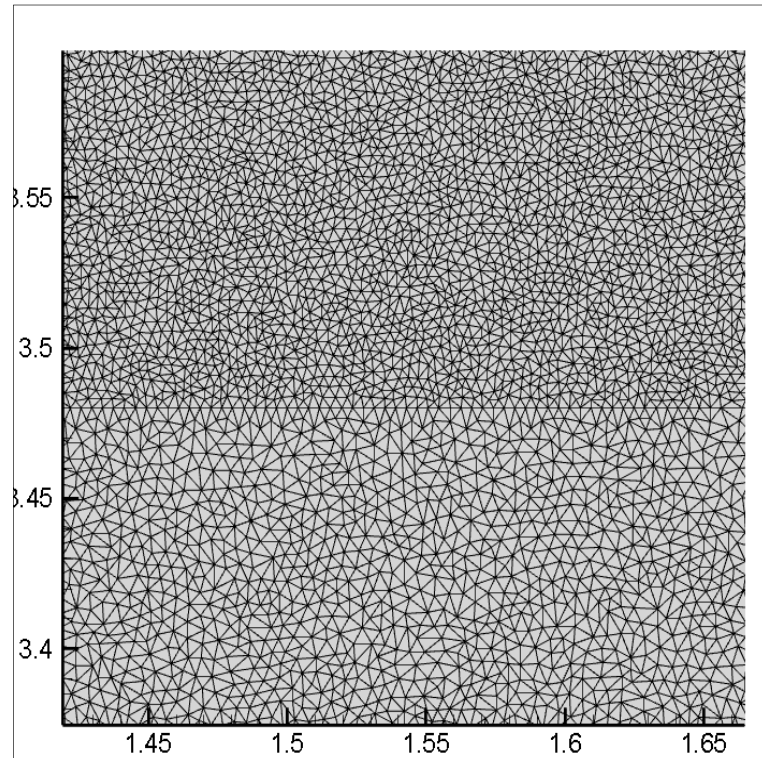


Figure 38: Zoomed view of the mesh interface between Zone B and C (Tecplot).

Knowing the mesh of the geometry and, following the criterion described at point 5.1.3. , the *computational interval* is about:

$$\Delta t \cong 0.25 \times 10^{-4} \text{ seconds}$$

b. Model B:

The difference between the *Model A* and the *Model B* is that in this last one an elevation has been set to the borders of the tank in order to create a real three-dimensional geometry.

As stated during the experimental setup description, the tank's walls height is about 50 centimeters; then an elevation equal to that value was assigned to the tank's walls.

This procedure aims to investigate in a better way how the no slip condition influence the flow from the tank. In fact giving an elevation to the tank the Manning coefficient works even in the tank's walls reducing the transversal velocity along them.

The main parameters of the hydraulic model are stated in table 3:

<i>Computational parameters Model B</i>		
Simulation Time	Courant Number	Manning Coefficient
[s]	[-]	[s m ^{-1/3}]
2	0.8	0.0084

Table 3: Computational parameters of Hydraulic model B related to smooth horizontal bed-ground.

The maximum cell-size is reported in the following table.

<i>Mesh's dimensions Model B</i>		
Zone A	Zone B	Zone C
[mm ²]	[cm ²]	[cm ²]
7.0	0.1	0.2

Table 4: Mesh's dimensions related to the geometry of Model B

Considering the dimensions stated in Table 4 the total amount of cells is **1'603'910**.

Related to the cell-size of the Zone A it is required to point out that this kind of much finer dimension was necessary to avoid instability problems of the code in the vertical cells of the tank's walls; indeed those cell are really tight triangles with a significant height.

In this situation is possible to see the geometry as a three-dimensional representation.

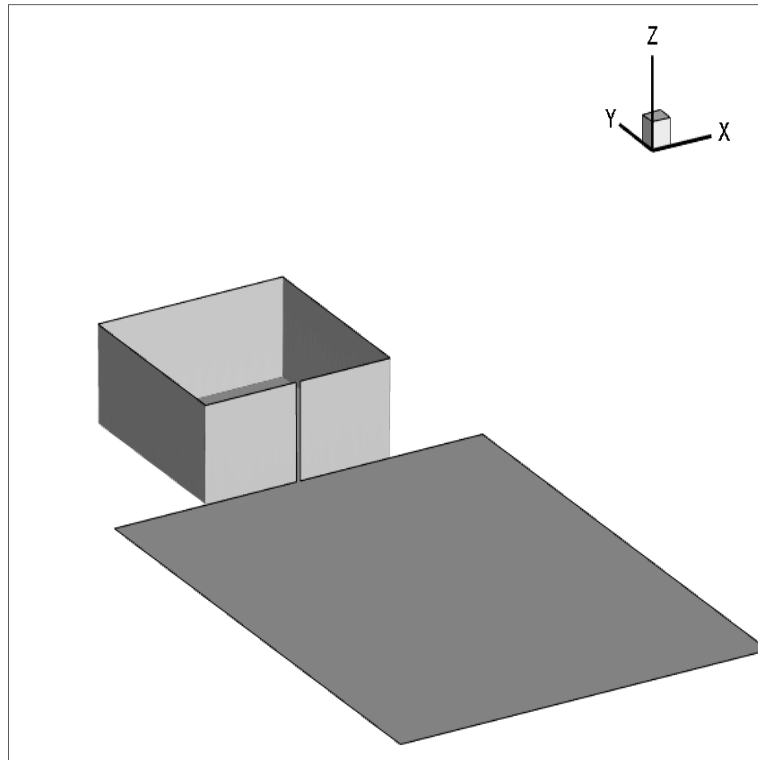


Figure 39: Three-dimensional view of the model from downstream(Tecplot).

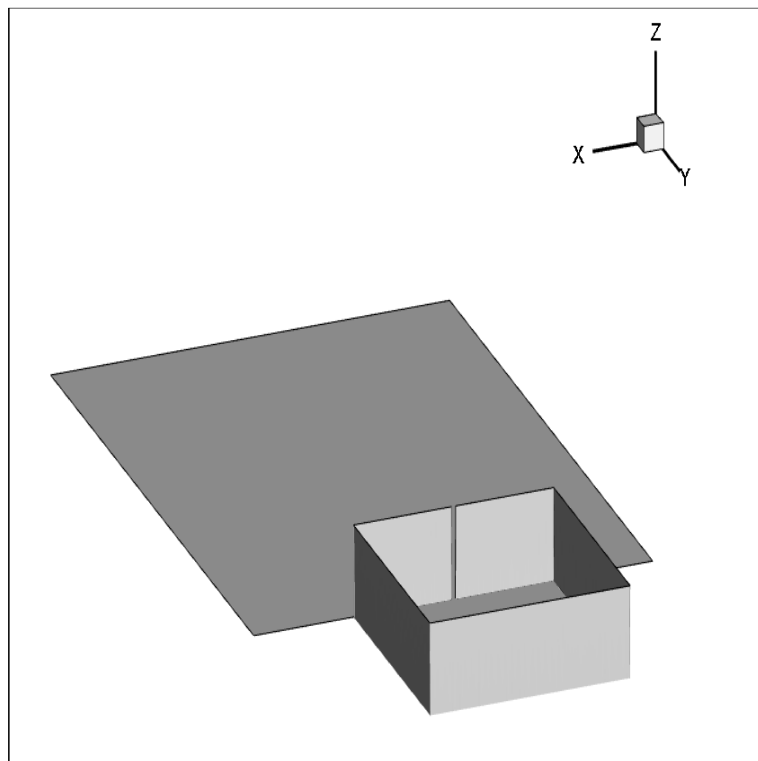


Figure 40: Three-dimensional view of the model from upstream(Tecplot).

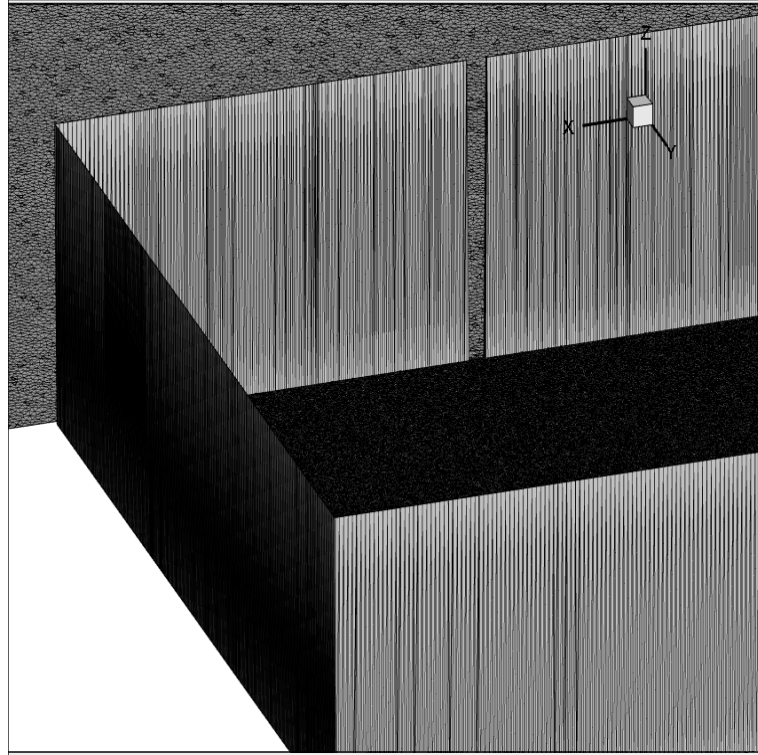


Figure 41: Three-dimensional detail of the tank and the breach(Tecplot).

With this geometry and following the criterion described at point 5.1.3. , the *computational interval* is about:

$$\Delta t \cong 0.15 \times 10^{-4} \text{ seconds}$$

5.2.3.2. Vegetated bed-ground

As described at point 5.2.2. in this situation the 6 millimeters diameters rods are simulated trough decagonal holes; as a consequence of those such small holes in the mesh is obviously necessary to use a finer mesh's resolution.

The main parameters of the hydraulic model are stated in table 5:

<i>Computational parameters Vegetated bed-ground</i>		
Simulation Time	Courant Number	Manning Coefficient
[s]	[-]	[s m ^{-1/3}]
2	0.4	0.003

Table 5: Computational parameters of Hydraulic model of vegetated bed-ground.

Has been necessary to use a lower value of the Courant Number in order to avoid instability issues in the model.

Regarding the Manning coefficient: it was chosen as a result of the sensitivity analysis mentioned at the beginning of point 5.2.3.; in this study case the value of the coefficient is much lower than the usual values associated to the real materials.

The value used in the BreZo model is significantly lower than the real value of the Manning related to the surface discussed at point 3.1.3. of this document. The reason why is because what the numerical model aims is to match the results of the physical model; furthermore in this study case the vegetation has been set and it has a significant contribution in terms of resistance, even because in the software the role of the surface tension in each rod is not considered.

Another reason why the Manning coefficient is different from the situation with smooth bed-ground is given by the fact that the rods, as already stated before, are fixed on PVC panels.

Regarding to the cell-size of the mesh it is necessary to remember the subdivision of the whole domain in three different zones (Figure 22 Chapter 5.2.2.1.).

The maximum cell-size is reported in the following table.

<i>Mesh's dimensions Vegetated bed-ground</i>		
Zone A	Zone B	Zone C
[cm²]	[mm²]	[mm²]
8.0	5.0	10.0

Table 6: Mesh's dimensions related to the geometry of the Vegetated bed-ground model

The total amount of cells is **1'964'446**.

As shown in the table above is possible to notice that a coarser resolution has been used into the tank (Zone A) with the objective to reduce as much as possible the duration of the simulation.

With the objective to make the representation as much clear as possible several pictures are shown below.

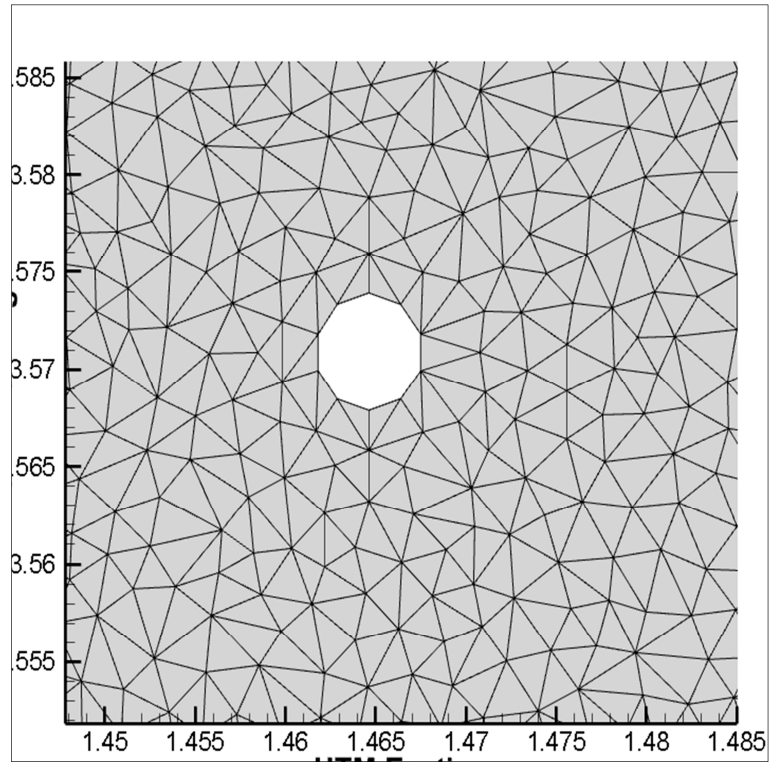


Figure 42: Detail of the rod schematization as a decagonal hole and the mesh around it (Tecplot).

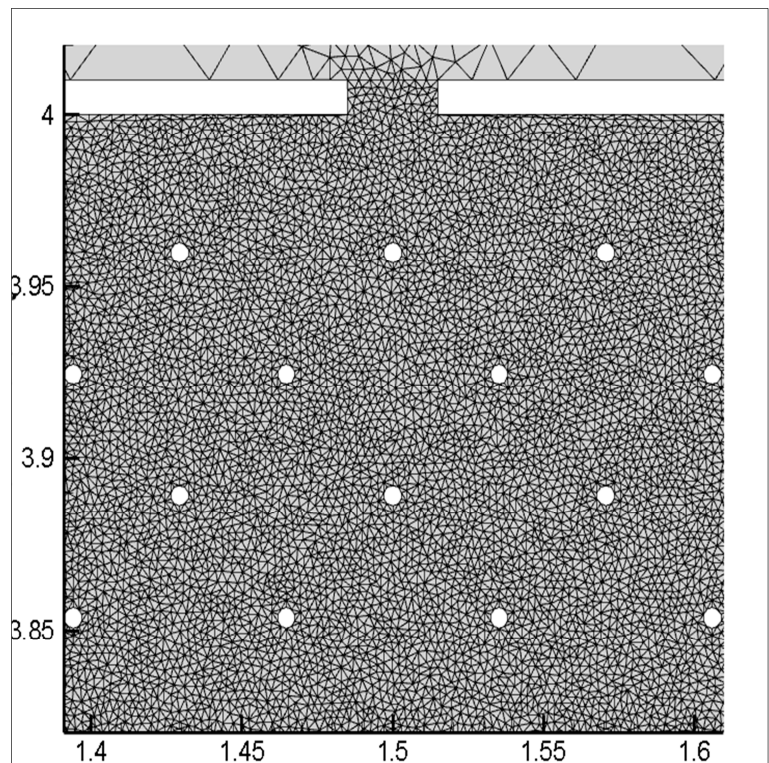


Figure 43: Zoomed view of the area close to the breach (Tecplot).

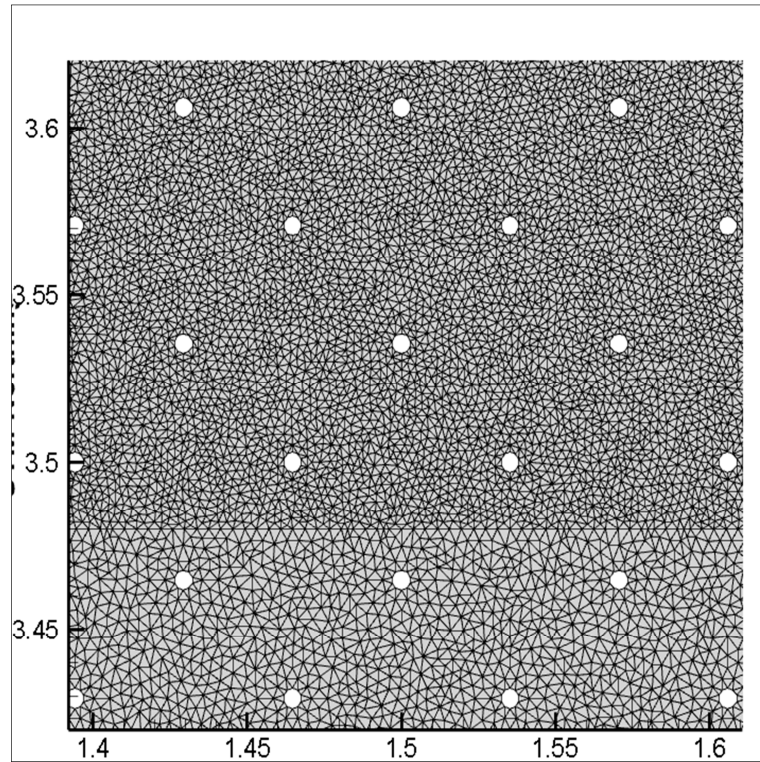


Figure 44: Zoomed view of the interface between Zone B and Zone C (Tecplot).

With this geometry and following the criterion described at point 5.1.3. , the *computational interval* is about:

$$\Delta t \cong 0.10 \times 10^{-4} \text{ seconds}$$

6. Numerical analysis with ANSYS Fluent

In this document will be described also a numerical model made with *ANSYS Fluent 18.1* in order to comprehend the influence of the vertical component in the examined situation. In particular will be discussed the comparison between the results which comes from the bi-dimensional numerical model and the model made with the CFD (Computational Fluid Dynamics) model.

6.1. Software overview [13]

ANSYS Fluent for all flows solves the conservation equations for mass and momentum. In case of flows which involve heat transfer or compressibility, an additional equation for the energy conservation is solved. Furthermore transport equations are solved when the treated flow is turbulent.

The mass conservation equation can be written as follows:

$$\frac{\partial \rho}{\partial t} + \nabla (\rho \vec{v}) = S_m \quad (6.1)$$

The equation 6.1 is the general form of the mass conservation equation and it is valid for both compressible and incompressible flows. Furthermore the source S_m represents the mass that is added to the continuous phase from the dispersed second phase.

The conservation of momentum in an inertial (non-accelerating) reference frame is:

$$\frac{\partial (\rho \vec{v})}{\partial t} + \nabla (\rho \vec{v} \vec{v}) = -\nabla p + \nabla (\bar{\tau}) + \rho \vec{g} + \vec{F} \quad (6.2)$$

Where:

- P is the static pressure;
- $\bar{\tau}$ is the stress tensor:

$$\bar{\tau} = \mu \left[(\nabla \vec{v} + \nabla \vec{v}^T) - \frac{2}{3} \nabla \vec{v} I \right] \quad (6.3)$$

Where μ represents the molecular viscosity, I is the unit tensor and at last the terms into the round brackets is the results of the volume's dilatation.

- $\rho \vec{g} + \vec{F}$ are the respectively the gravitational body forces and the external body forces.

Regarding to the flow solvers ANSYS allows the user to choose between the following two numerical methods:

- Pressure Based solver;
- Density Based solver;

Looking back to the literature about those methods, the first one was developed for low-speed incompressible flows, while the second one was used mostly for high-speed velocity flows.

Recently both methods have been improved in order to solve and work properly in a wide range of conditions.

The velocity is obtained in both methods from the momentum conservation equations, while in the density based approach the continuity equation is used with the objective to obtain the density field and the pressure field is obtained from the equation of state.

With the pressure based approach the pressure field is obtained manipulating the momentum and mass conservation equations in order to obtain a pressure correction equation.

Anyway in both cases a control-volume based system is used; this technique consists in divide the domain into a discrete control volumes trough a computational grid, integrate the governing equations for each one of those control volumes in order to build algebraic equations for the discrete dependent variables (pressure, temperature, velocities) , and the last step consists in the linearization of those discretized equations in order to obtain updated values of those variables.

This discretization process is commonly called (finite-volume).

6.2. Geometry setup

With this software only the situation related to the smooth horizontal bed-ground has been studied.

The geometry of this model is the same as described in the previous chapters, but as a input file for the geometry editor is necessary to create the three-dimensional geometry in AutoCad and save it as *.sat* format in order to make it readable by the software.

With the objective to have a detailed representation the whole domain has been divided in 13 subdomains that will depict the water and even the air into the domain.

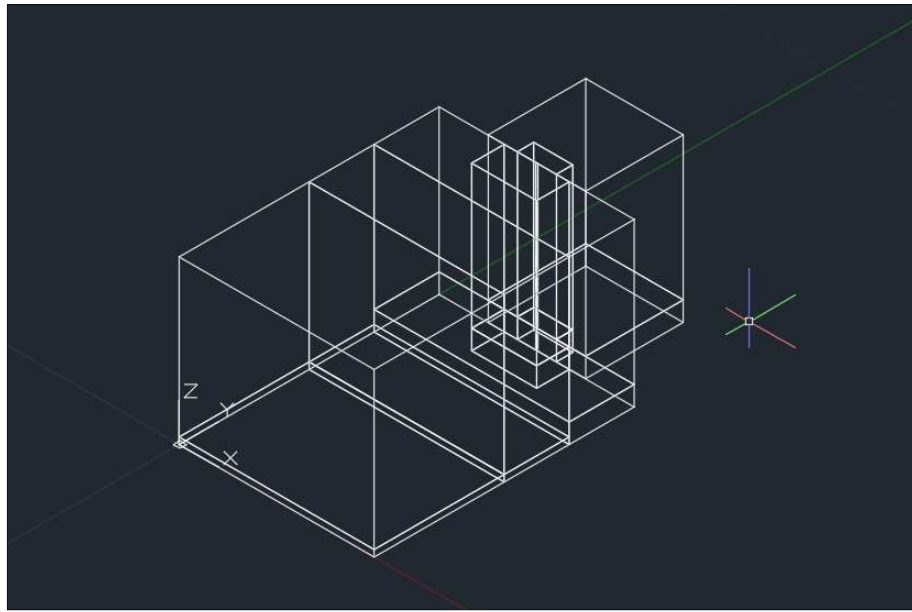


Figure 45: Geometry representation created in AutoCad.

Looking at the geometry from above are stated the names of all the subdomains:

- Into the round brackets means that the subdomain is on the top;
- Outside the round brackets means that the subdomain is on the bottom;

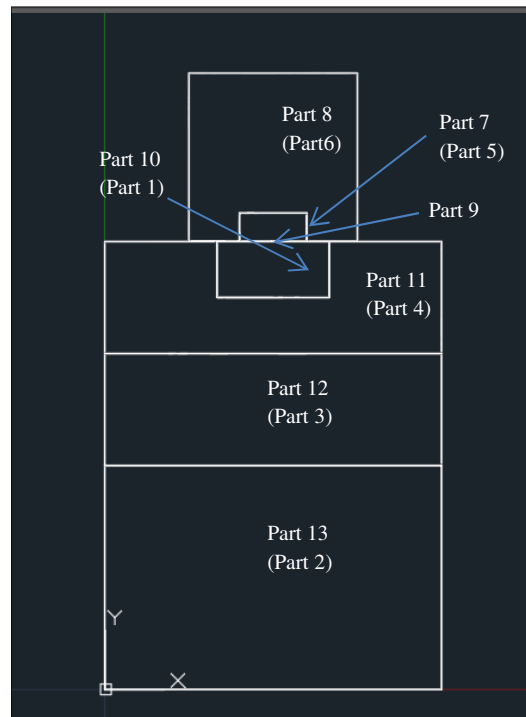


Figure 46: Division in subdomains of the whole geometry, view from above.

Just to be clearer the Part 9 is referred to a small parallelepiped that represents the breach's volume.

The total height of the domain is 3 meters while the height of those volumes is listed below:

- Part 1: 2.70 m;
- Part2: 2.70 m;
- Part 3: 2.90 m;
- Part 4: 2.70 m;
- Part 5: 2.70 m;
- Part 6: 2.70 m;
- Part 7: 30 cm;
- Part 8: 30 cm;
- Part 9: 3.00 m;
- Part 10: 30 cm;
- Part 11: 30 cm;
- Part 12: 10 cm;
- Part 13: 10 cm;

The purpose of using different height is to represent better (with a finer mesh's resolution) the domain that will be interested from the water's flow.

Importing the geometry in the Fluent's geometry editor:

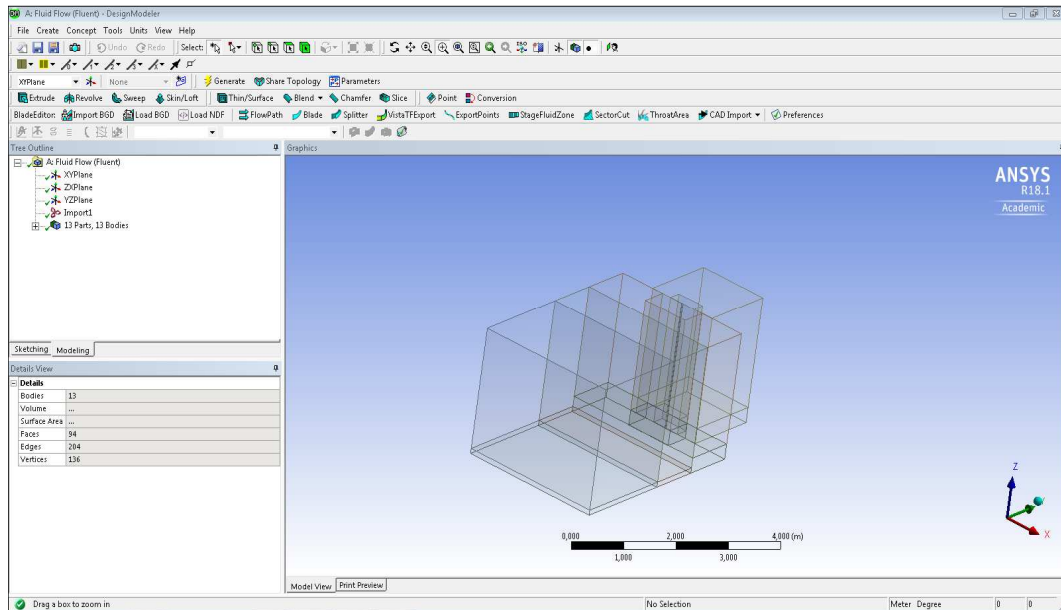


Figure 47: ANSYS Fluent Geometry editor view.

The next step consists on move to the mesh's editor of ANSYS Fluent; before to create the mesh is important to give a name to all the surfaces of the subdomains in order to know exactly which one is on the top of the model or on the bottom. This information will be useful during the boundary conditions set up.

The element of the mesh have tetrahedron shape while the mesh's sizes for the different subdomains are listed below:

- Part 1: maximum edge's length 0.10 m;
- Part2: maximum edge's length 0.10 m;
- Part 3: maximum edge's length 0.10 m;
- Part 4: maximum edge's length 0.10 m;
- Part 5: maximum edge's length 0.20 m;
- Part 6: maximum edge's length 0.20 m;
- Part 7: maximum edge's length 0.01 m;
- Part 8: maximum edge's length 0.04 m;
- Part 9: maximum edge's length 0.005 m;
- Part 10: maximum edge's length 0.01 m;
- Part 11: maximum edge's length 0.04 m;
- Part 12: maximum edge's length 0.04 m;
- Part 13: maximum edge's length 0.04 m;

The graphical representation after that the meshing was done is reported below.

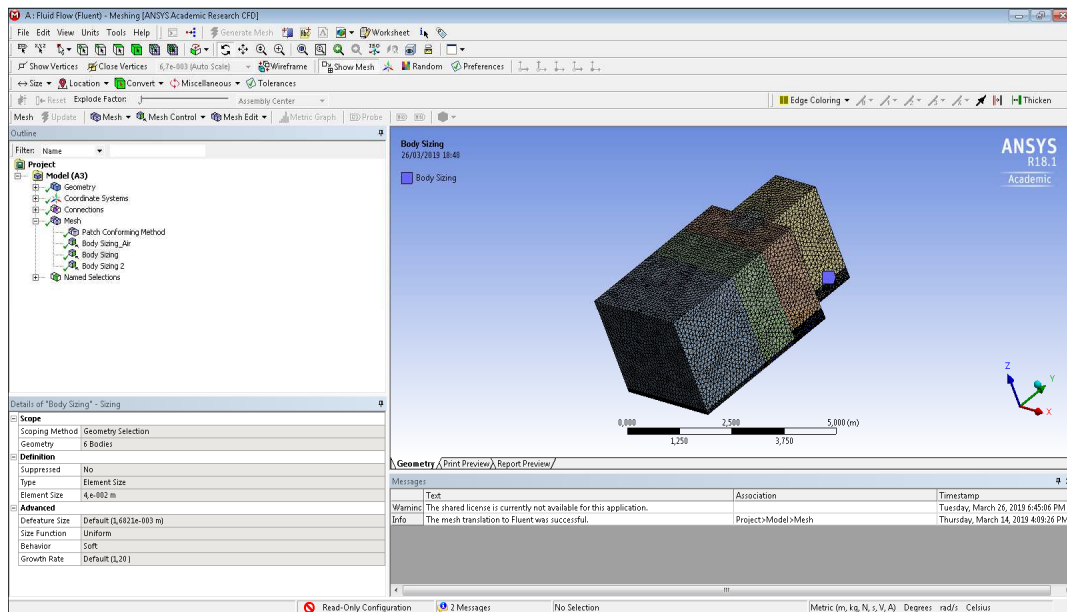


Figure 48: Geometry of the model with the mesh.

From the figure above is possible to notice some of the different mesh's sizes used to model this situation.

6.3. Computational parameters of the hydraulic model

In order to represents as better as possible the study case is necessary to set several parameters that will influence the solution and consequentially the results. All those parameters could be set up into the Setup Fluent's section.

The type of simulation that is presented in this document is a *transient* simulation, and the model is a multiphase one, where the phases are represented by the water and the air; the viscosity has been modeled with the K- ϵ model. The model adopted is a Pressure-based.

The duration of the whole simulation is about 2 seconds, while has been used a fixed computational interval equal to 0.0005 seconds. This value has been determined following the criterions showed in the ANSYS Fluent user's manual.

6.3.1. Initial Conditions

As stated regarding the BreZo's model even in this situation the initial conditions are represented by the water depth value into the tank at the beginning of the simulation; so to set up this aspect is necessary to select the parts of the geometry that are within the tank (Part 7 and 8)and set the Water Volume fraction equal to 1, while in the rest parts there is only air.

6.3.2. Boundary conditions

The boundary conditions that has been set up are:

- An atmospheric *pressure outlet* value to all the surfaces that are on the top of the model and to the exterior downstream surface of Part 13 and Part 2, where the water is free to flow away.
- A *wall* condition to all the bottoms and external surfaces of the tank; to this surfaces has been applied the *no slip* condition and a roughness value of *0.0147 millimeters*. (This value has been chosen because was the results of the analysis made with the roughness measurement instrument: Chapter 3.1.3.).

All the remaining connections between surfaces of different parts are connected with an *interface* type of connection.

7. Results and comparisons

7.1. Numerical results from *parBreZo 8.1.0*

All the input parameters and the geometry have been widely described at point 5.2.3. of this document; this chapter is dedicated to the analysis of the results of the numerical model compared with the experimental results.

For any kind of simulation made with *parBreZo* the output can be showed as a *.plt file* that can be visualized with Tecplot or as a Matlab readable format that is composed from two different files:

- *Nameoftheproject.xyz.mlab*: which is a simple text file that list the coordinates of every cell within the domain;
- *Nameoftheproject.huv.mlab*: as deductible from the name of the file this one contains the results in terms of $h = \text{water depth}$, $u = \text{velocity along the x-direction}$, $v = \text{velocity along the y-direction}$; these three variables are listed for every cell of the project's geometry.

All the simulations that were done during the time in University of California Irvine were done using the *HPC (High Performance Computing)* available for studies that need a big computational effort.

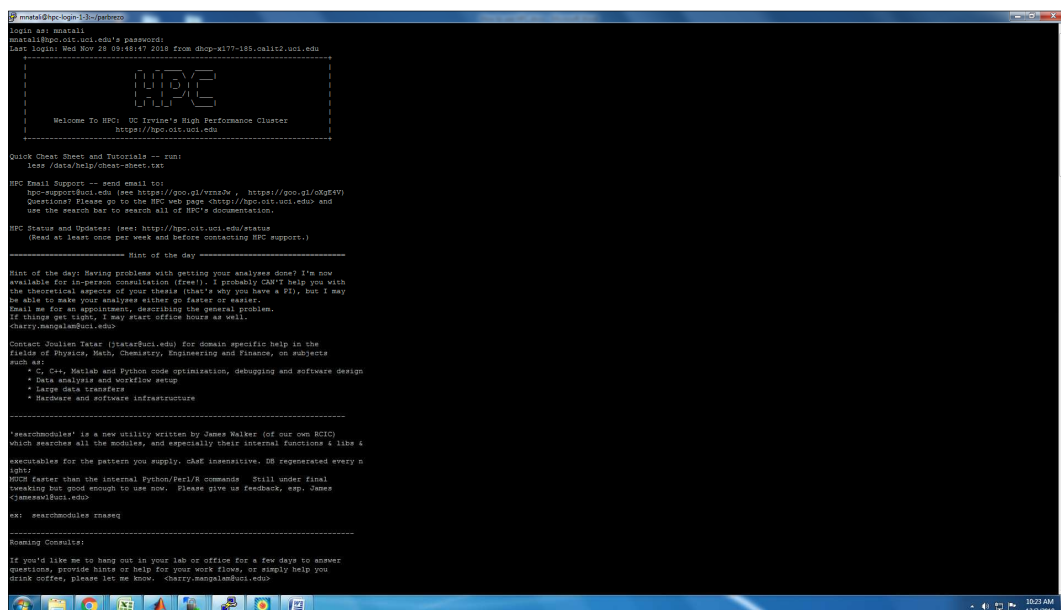


Figure 49: Sample picture of the UCI (University of California Irvine) HPC interface.

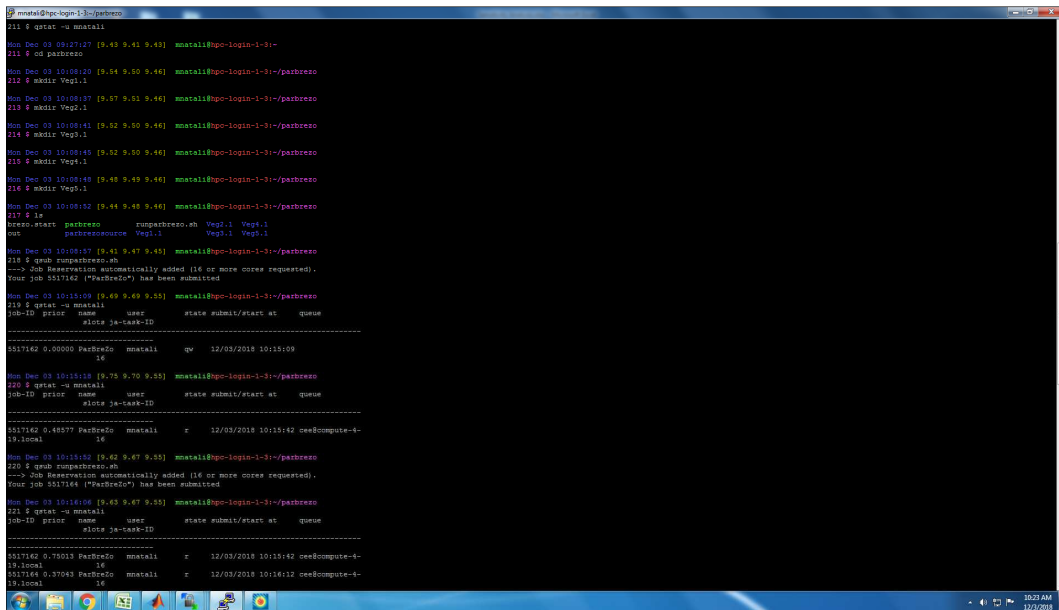


Figure 50: Sample picture of the UCI (University of California Irvine) HPC interface.

7.1.1. Smooth horizontal bed-ground

The description of how this situation has been recreated in the numerical model is being widely described at point 5.2.3.1.; as aforementioned in that subchapter the situation related to the smooth horizontal bed-ground has been modeled with two different geometries and consequently two models are being prepared:

- Model A;
- Model B;

The purpose of this choice is to understand as better as possible how the no-slip condition works into the software. Especially the most of the attention has been putted on the *u-velocity*'s pattern close to the breach; it is necessary to point out that the *u-velocity* represents the component of the velocity that is transversal in respect of the main flow direction during the efflux from the tank.

Obviously if the *u-velocity* close to the breach is too high it might cause an excessive narrowing of the fluid vein and as a consequence a lower volume that come out from the tank.

In order to have a better comprehension of this aspect those two models were developed and studied.

It was possible to analyze the *u-velocity* pattern close to the breach in both situations, Model A and Model B.

- *Model A:*

The *u-velocity* patterns have been calculated at a distance of 5 centimeters from the center of the breach.

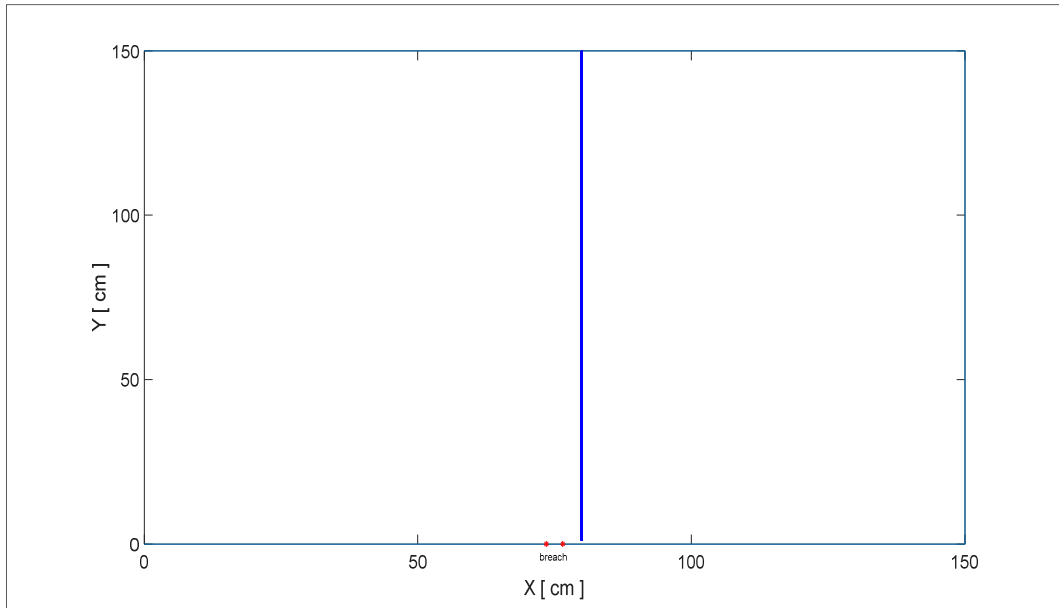


Figure 51: View from the top of the first slice into the tank where the *u-velocity* was calculated.

The velocity patterns along the slice are shown in the figure below.

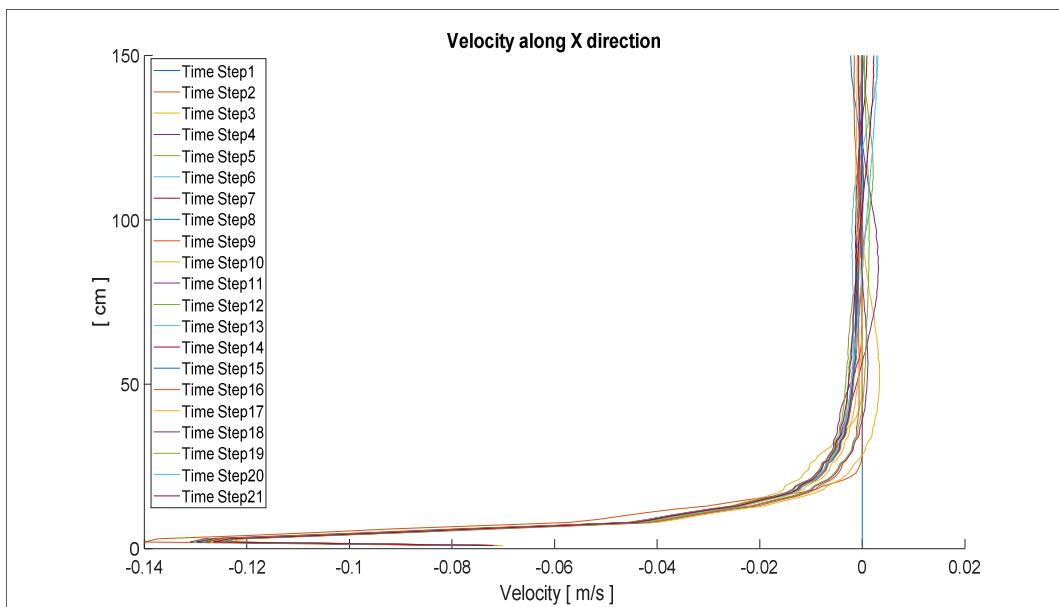


Figure 52: Velocity patterns during the whole simulation along the slice(Model A).

Looking at the velocity absolute values related to the cells closest to the walls:

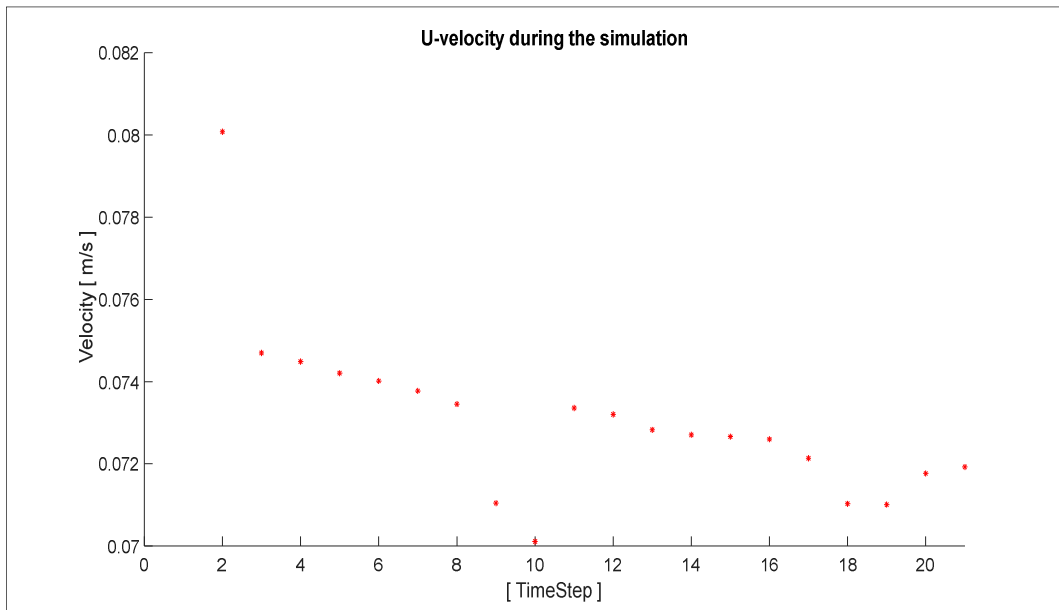


Figure 53: Absolute values of the u-velocity of the cell closest to the wall (Model A).

Numerically is possible to point out the two following values:

$$U_{x\ Max} = 0.0801 \frac{m}{s}$$

$$U_{x\ Mean} = 0.0696 \frac{m}{s}$$

- *Model B:*

Focusing the attention on the same slice showed in Figure 51 is possible to analyze the *u-velocity* calculated from Model B that, as already stated, is based on a three dimensional geometry.

Even in this case is possible to extract the velocity patterns along the slice.

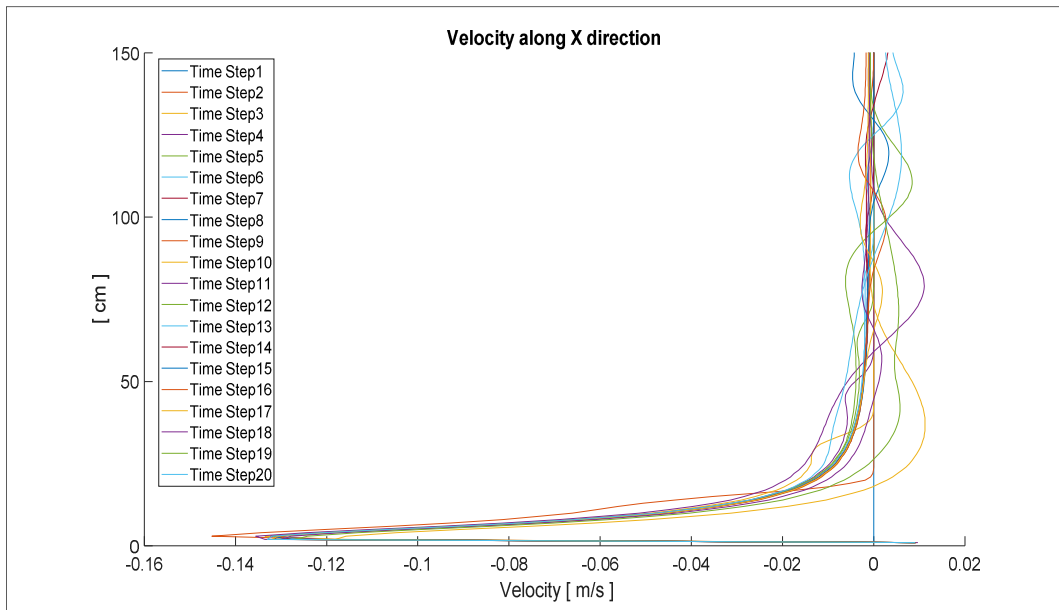


Figure 54: Velocity patterns during the whole simulation along the slice (Model B).

Looking at the closest cells to the wall is possible to observe the following pattern of the absolute values.

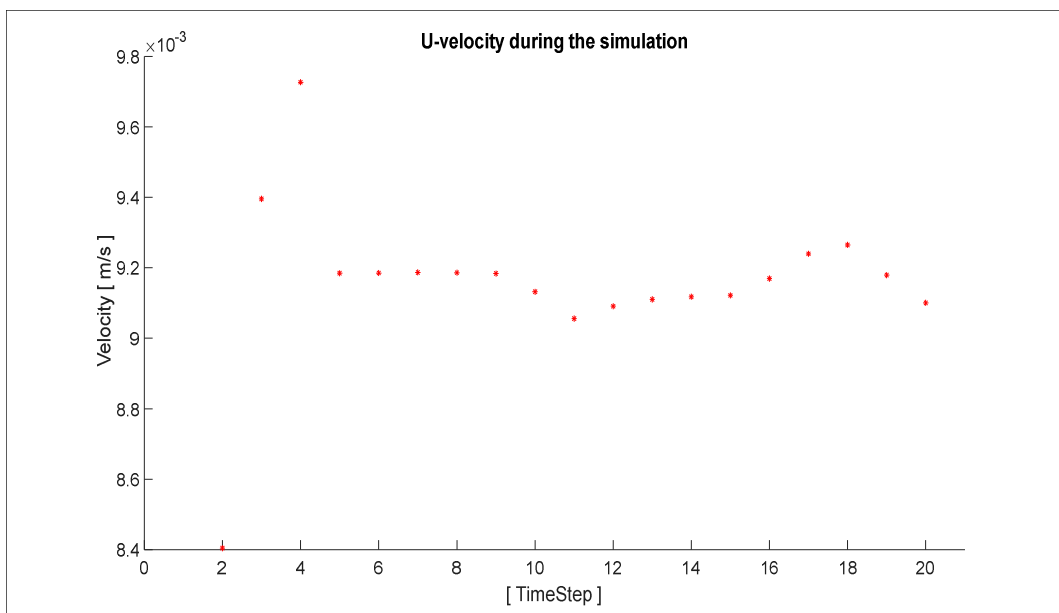


Figure 55: Absolute values of the u-velocity of the cell closest to the wall (Model B).

Even from the figure shown above is possible to notice how lower are the values of the u-velocity in this case; the numerical significant values are:

$$U_{x \text{ Max}} = 0.0097 \frac{m}{s}$$

$$U_{x \text{ Mean}} = 0.0087 \frac{m}{s}$$

As a conclusion of the comparison between the two different models is possible to claim that the best situation for the analysis is represented by the Model B.

Another way to check if this observation is true is to compare the two volume curves related to the two different models.

The Volume Curves represented herein are calculated simply calculating how much volume is on the flat surface for each time step during the simulation.

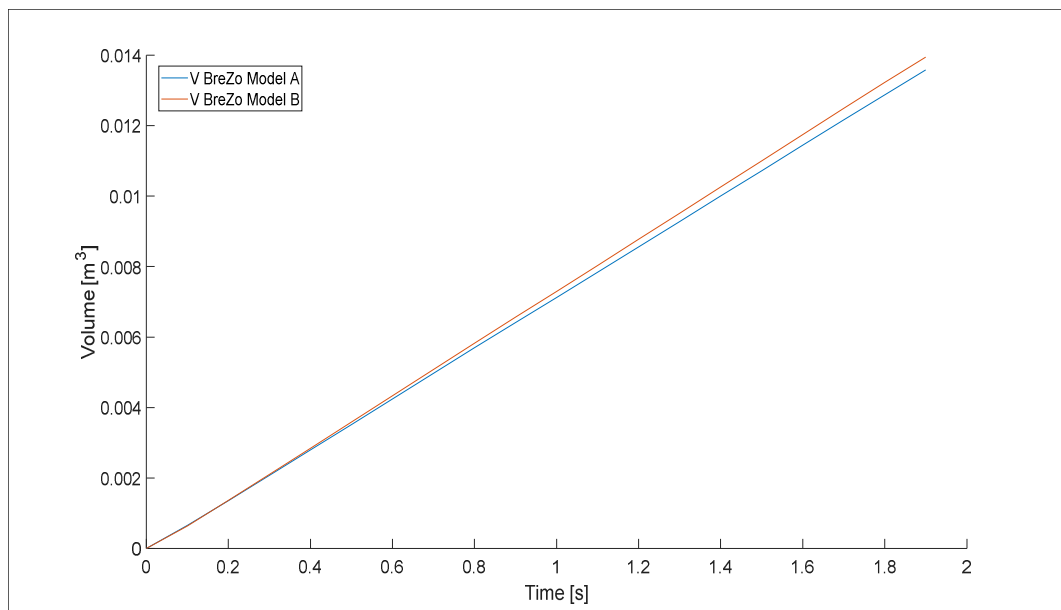


Figure 56: Comparison between the two volume curves related to Model A and B;

From the picture is possible to confirm that the Model B is the one that represents better the situation related to the *no-slip* condition into the tank. In fact having a lower value of the *u-velocity* close to the breach the narrowing of the fluid vein is limited and then the water is able to come out from the tank easily.

Model B will be used as reference to simulate this study case related to the smooth horizontal bed-ground.

Anyway the difference between the two volumes, calculated at the last instant of the simulation, is low; indeed is about the **3 %**.

The linearity of the volume curves could seem awkward at first sight; in order to investigate this aspect the Total Hydraulic Load has been calculated along the breach's direction.

The results are showed in the following figures where are shown for different times:

- The water depth calculated along a longitudinal slice in the breach's directions;
- The total hydraulic load calculated along a longitudinal slice in the breach's directions;

The following figures are referred to the first 50 centimeters close to the breach (X-axis).

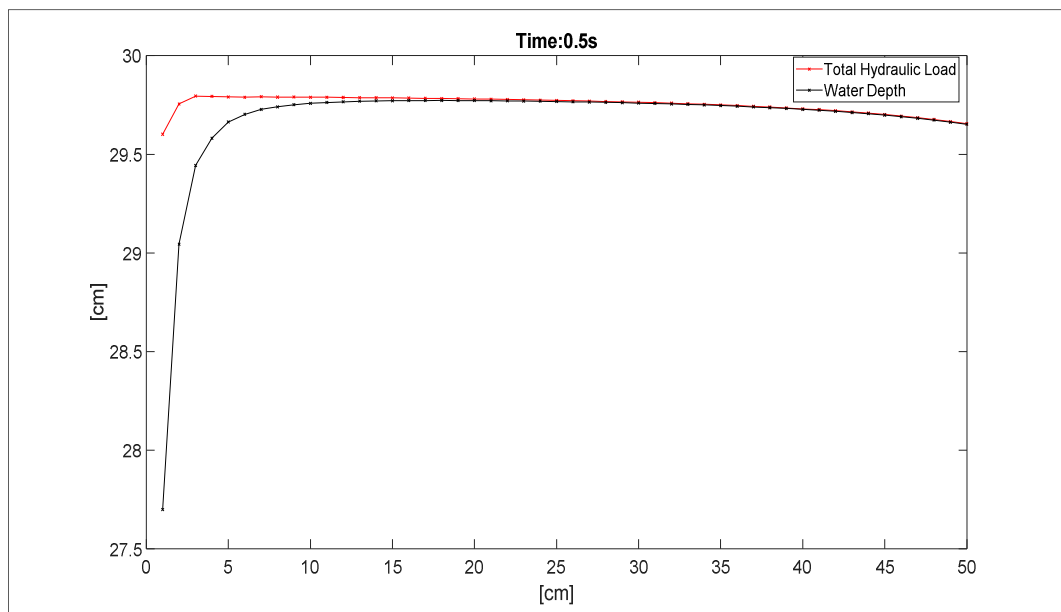


Figure 57: Water depth and Total Hydraulic Load calculated along a slice taken along the breach's direction at time= 0.5 seconds (breach on the left of the graph) (parBreZo)..

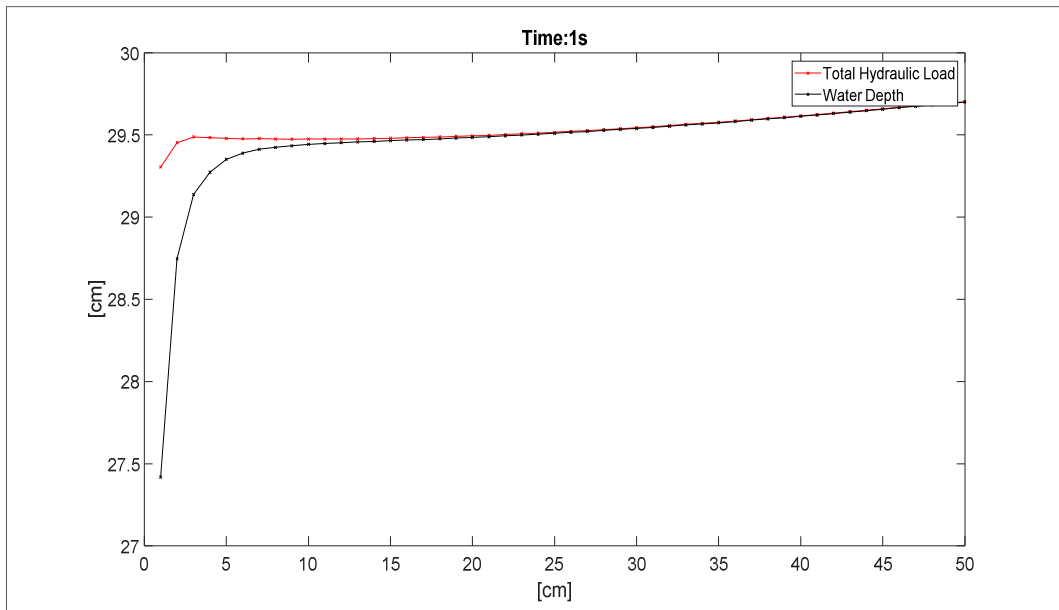


Figure 58: Water depth and Total Hydraulic Load calculated along a slice taken along the breach's direction at time= 1.0 seconds (breach on the left of the graph) (parBreZo)..

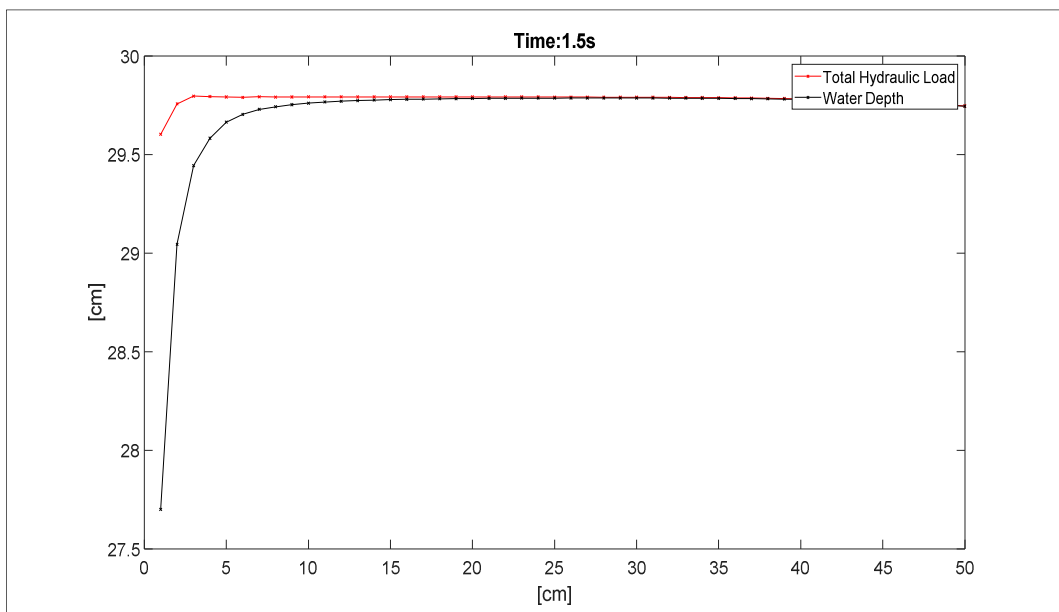


Figure 59: Water depth and Total Hydraulic Load calculated along a slice taken along the breach's direction at time= 1.5 seconds (breach on the left of the graph) (parBreZo)..

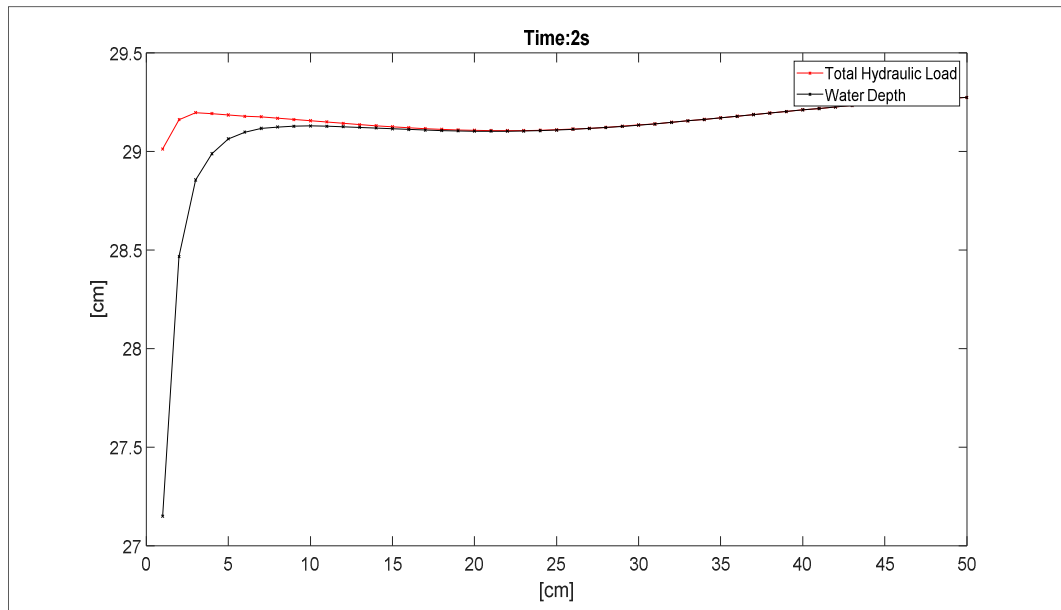


Figure 60: Water depth and Total Hydraulic Load calculated along a slice taken along the breach's direction at time= 2.0 seconds (breach on the left of the graph) (parBreZo).

Looking at the figures above is possible to notice how the total hydraulic load close to the breach is almost constant during the whole simulation; consequentially the flow that come out from the tank is almost constant during the numerical simulation.

In order to check how the fluid volume is computed in the numerical model is interesting to look at the following figure, which show the comparison between the volume curve calculated from the probes into the tank (experimental) and the volume curve calculated from the numerical simulation's results.

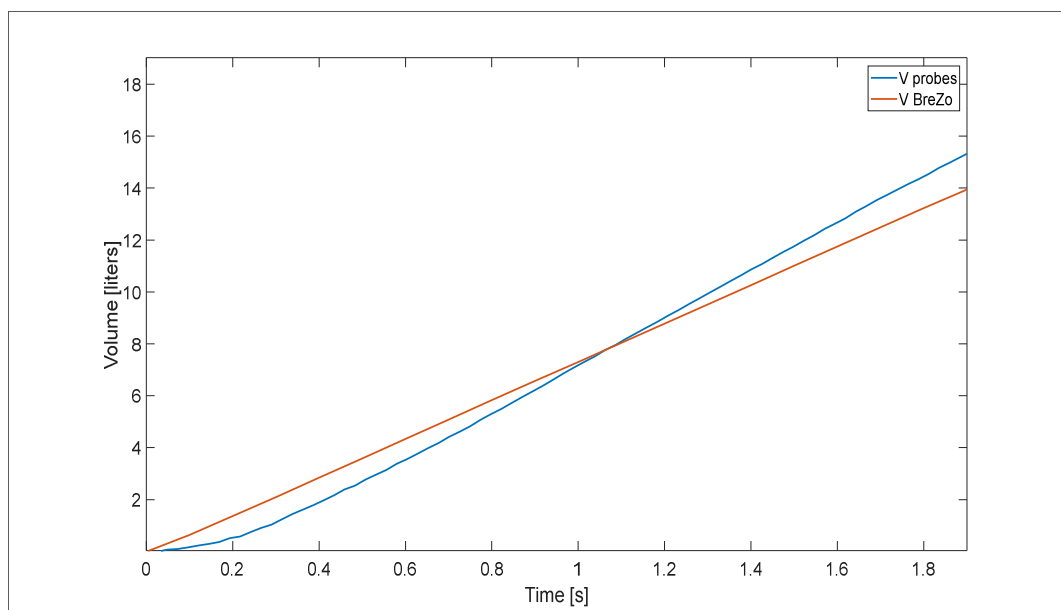


Figure 61: Comparison between the volumes calculated from the probes and the volume computed from BreZo.

In the last figure showed is possible to notice that there is an under estimation of the volume calculated from the probes during the first instants; the reason of this would be attribute to the fact that the volume into the tank is calculated like an average lowering of a flat surface that has the elevation equal to the average value of the probes' measurements. Doing this way the lowering of the water surface close to the breach is neglected.

This initial difference in the volume's computation is clearer looking at the following figure, where is easy to notice how this difference tends to lower values with the growing of the time during the simulation.

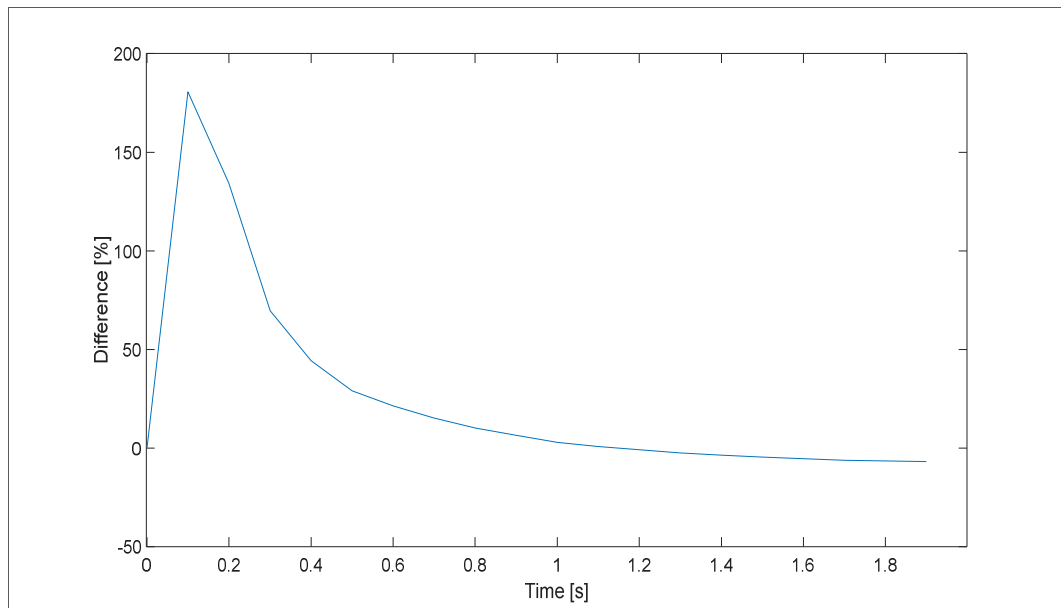


Figure 62: Percent difference between the experimental and numerical volumes during the experiment.

The differences showed in the figure above is calculated as follow:

$$Difference_{ti} = \frac{V_{Brezo_{ti}} - V_{Probes_{ti}}}{V_{Probes_{ti}}} \%$$

Where ti means the time-step i .

While in terms of volume:

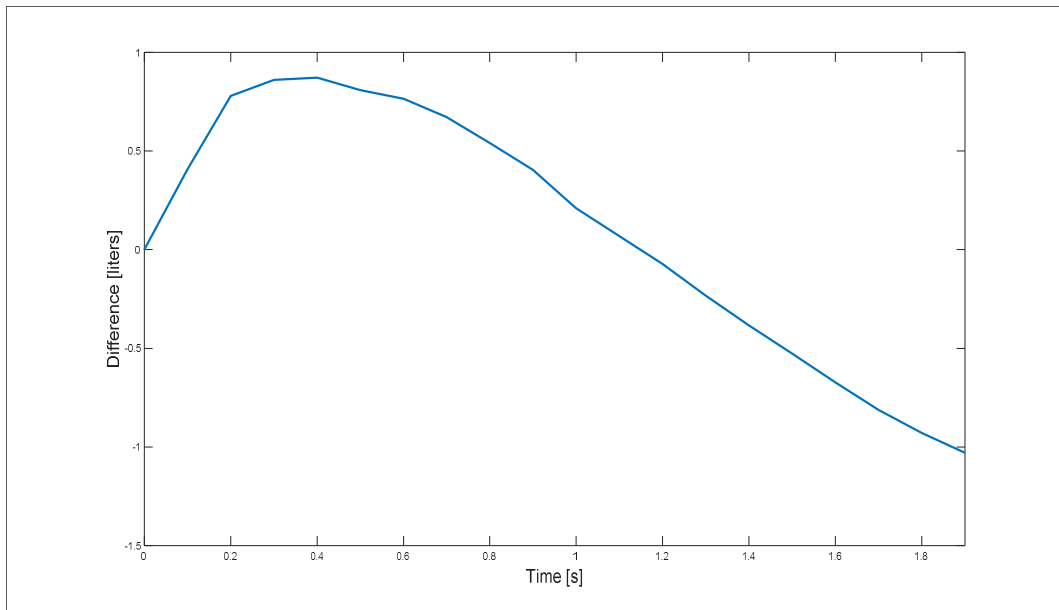


Figure 63: Difference in terms of volume between the numerical model's results and experimental results.

The maximum value of that difference is measured at the last time step, when the value is about **1.05 liters**.

7.1.1.1. Water-velocity results and comparison

The purpose of this subchapter is to show how is the matching between the results obtained from the two different approaches widely described in the previous chapters.

The comparison has been done comparing the wave-front evolution during the experiment that has been studied.

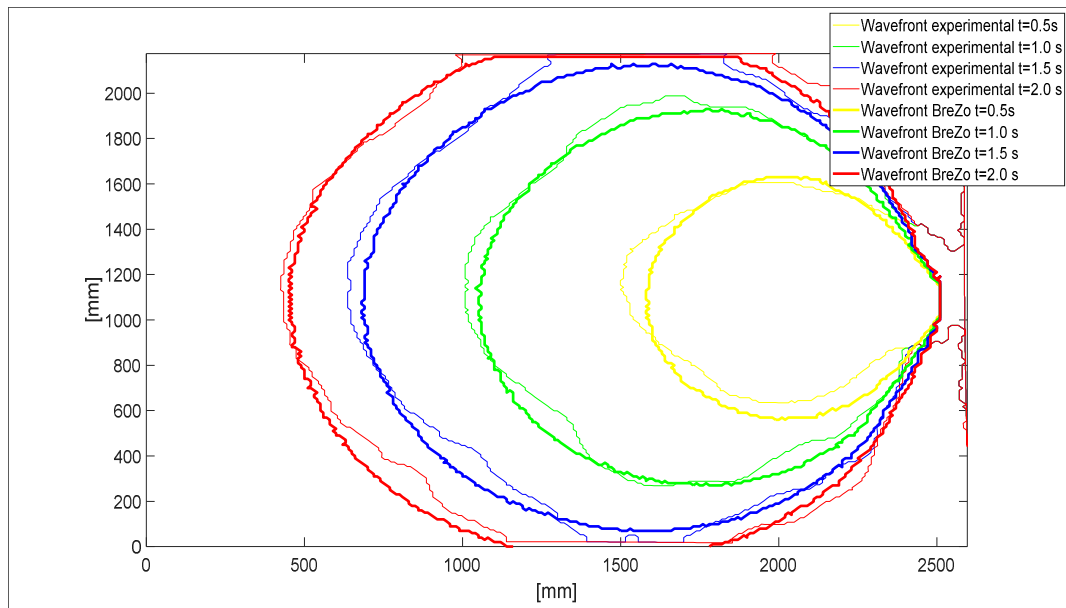


Figure 64: Wave-front evolution during the time and comparison between the two solutions.

As deductible from the figure above the average velocity of the wave is extremely similar in both the solutions presented here in this thesis.

The average wave's velocity propagation is **1.40 m/s**.

7.1.1.2. Water depth results and comparison

As already stated the water depth detection in each point of the flat surface is one of the main objectives of this analysis. In the previous chapters are being illustrated the procedures used to get the results from the experimental analysis (Chapter 4) and from the numerical model (Chapter 5).

In order to show the results related to this aspect, several slices are being analyzed and the water profiles are showed thereafter for different instants during the considered experiment.

For each instant have been considered three longitudinal slices and three transversal slices.

Transversal slices:

- 35 centimeters downstream from the breach;
- 70 centimeters downstream from the breach;
- 120 centimeters downstream from the breach;

Longitudinal slices:

- Along the breach's direction;
- 35 centimeters on the right respect the breach's direction;
- 35 centimeters on the left respect the breach's direction;

Below are reported only the wet slices for each time instant considered.

In order to be clear has been reported for every time step a global view from the top of all the slices. And the water profiles in correspondence of those slices. Only the wet slices have been reported.

- Time = 0.5 seconds :

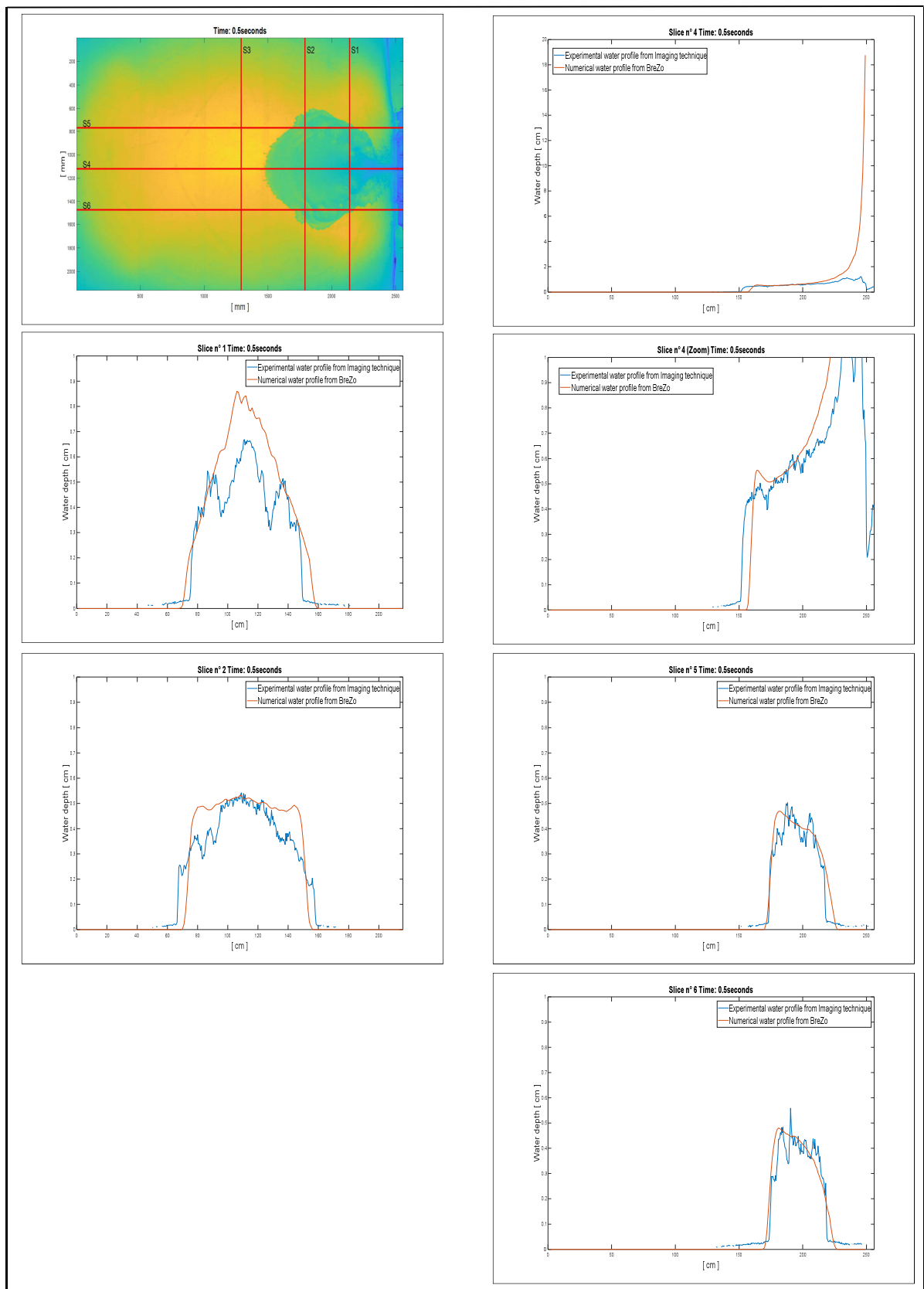


Figure 65: Comparison between experimental and numerical water profiles calculated in correspondence of the six slices showed in the first picture (Time 0.5 seconds).

Looking at the Slice 4 reported above is possible to see how the imaging technique is not able to calculate properly the water depth close to the breach. As already stated before this fact happens because the Lambert-Beer law doesn't work well if the solution thickness' value is too high.

Furthermore the method described at point 4.2. has been calibrated for lower values of water depth.

Another reason is given to the fact that in the area close to the breach the radiation is not perpendicular to the water surface and also under the water the camera sees the tank's surface that is clearly different from the flat horizontal surface.

- Time = 1.0 seconds :

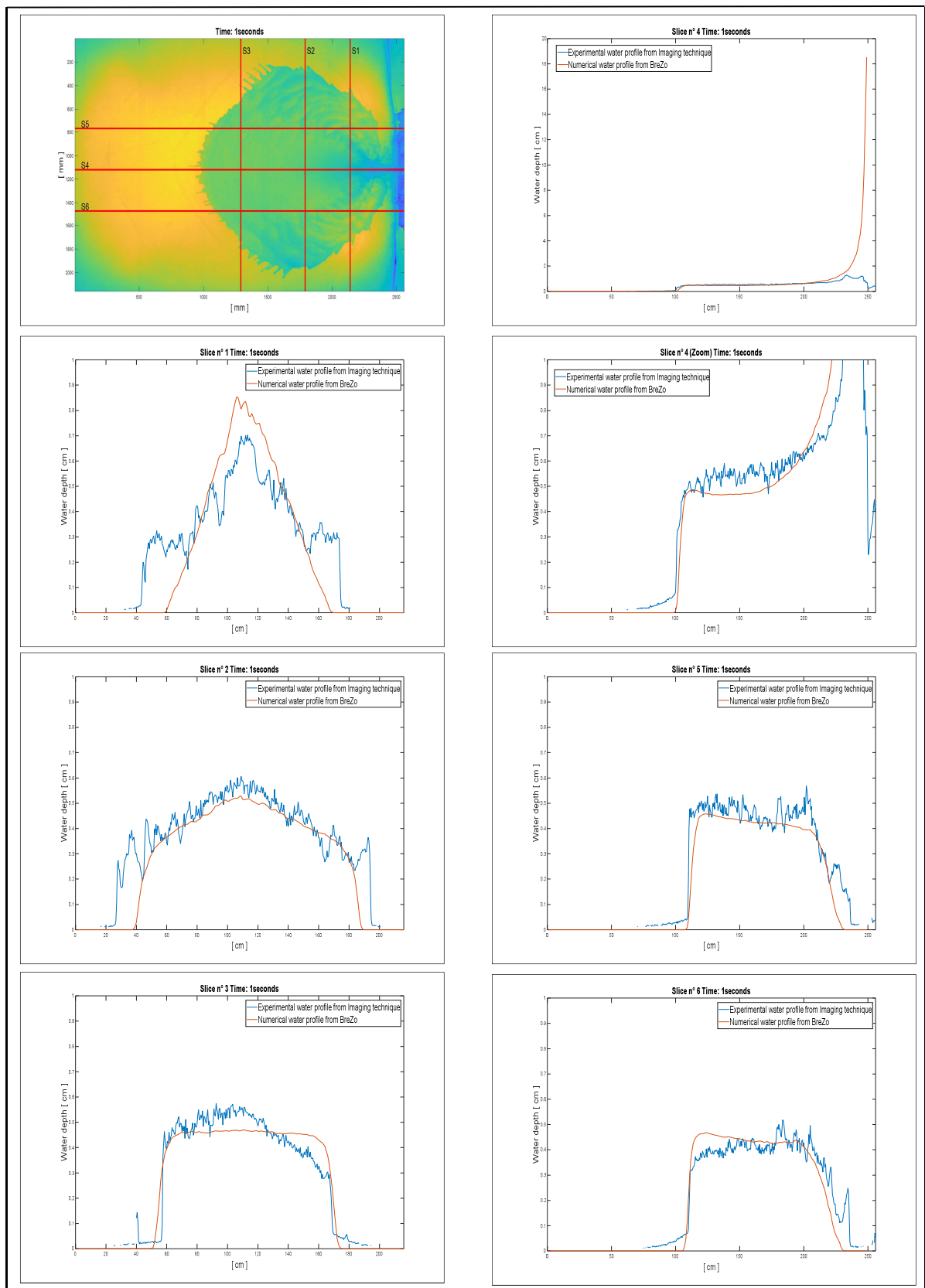


Figure 66: Comparison between experimental and numerical water profiles calculated in correspondence of the six slices showed in the first picture (Time 1.0 seconds).

- Time = 1.5 seconds :

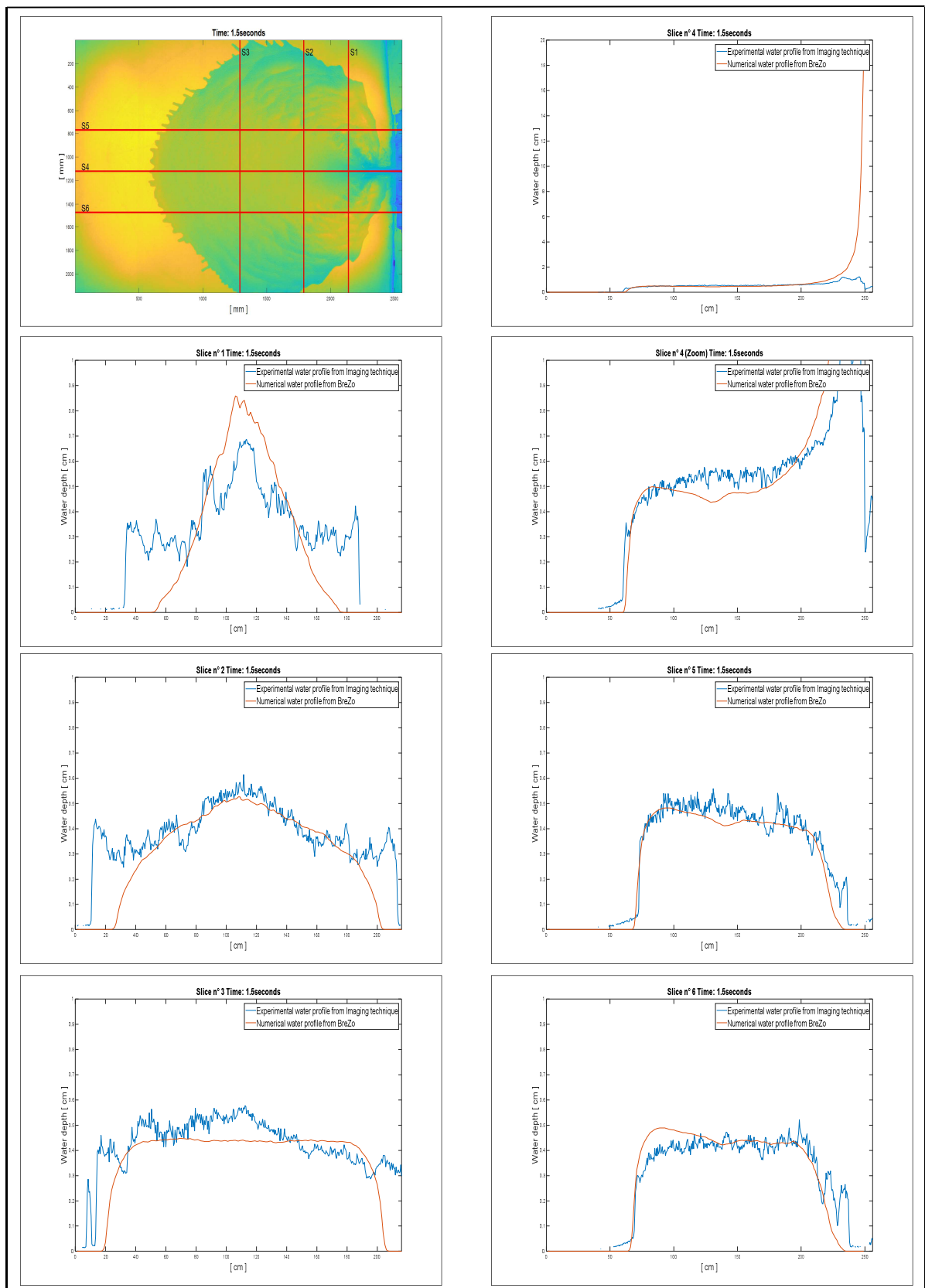


Figure 67: Comparison between experimental and numerical water profiles calculated in correspondence of the six slices showed in the first picture (Time 1.5 seconds).

7.1.2. Vegetated horizontal bed-ground

This study case has been widely described in the previous chapters.

In particular the physical model setup has been described in chapter 3.2.2. of this document while how the situation were numerically modeled is reported in chapter 5.2.3.2..

The discussion about the comparison between the volumes computed by the numerical model and from experimental measurements is exactly the same as reported at point 7.1.1. of this document. The only difference is given by the fact that for this situation just one numerical model has been prepared.

In the same way that has been done for the other study case (7.1.1.), even this time the results will be showed in terms of the water depth profiles' comparison and wave-front evolution's comparison.

7.1.2.1. Water-velocity results and comparison

In the same way how has been done for the smooth horizontal bed-ground, even for this study case was analyzed the comparison between the wave's shape.

In particular in this case is extremely interesting to see how the software is capable to catch the correct shape and the three main flow's paths.

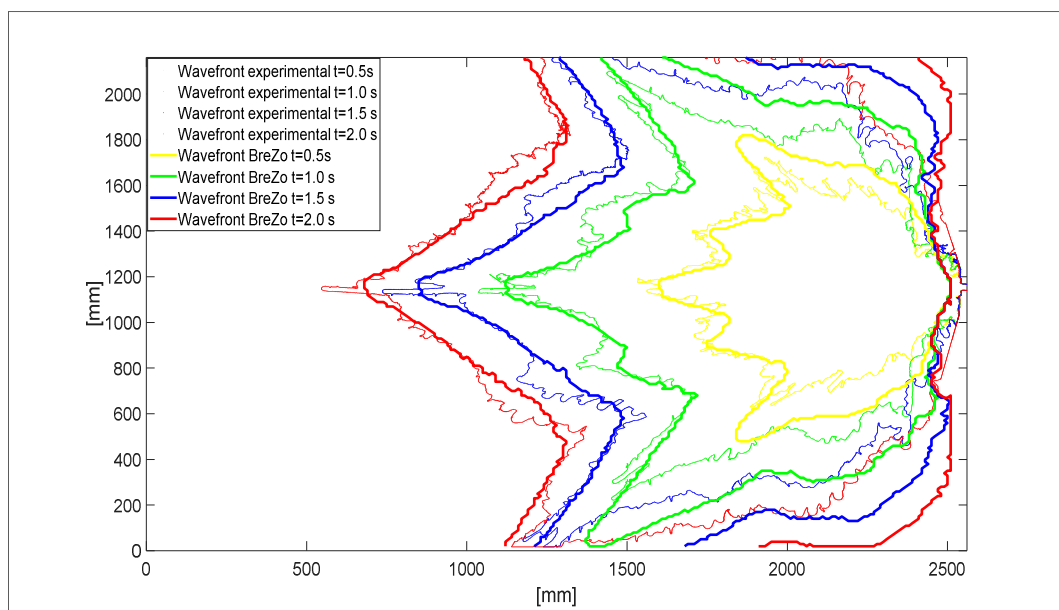


Figure 68: Wave-front evolution during the time and comparison between the two solutions.

From the picture above is possible to see that the numerical model corresponds pretty well with the physical model measurements.

The average wave's velocity propagation is **1.30 m/s**.

7.1.2.2. Water depth results and comparison

Regarded to this situation the peculiarity is that right before every rod is possible to see how the water runs up creating peaks which are clearly visible in the following pictures.

- Time = 0.5 seconds :

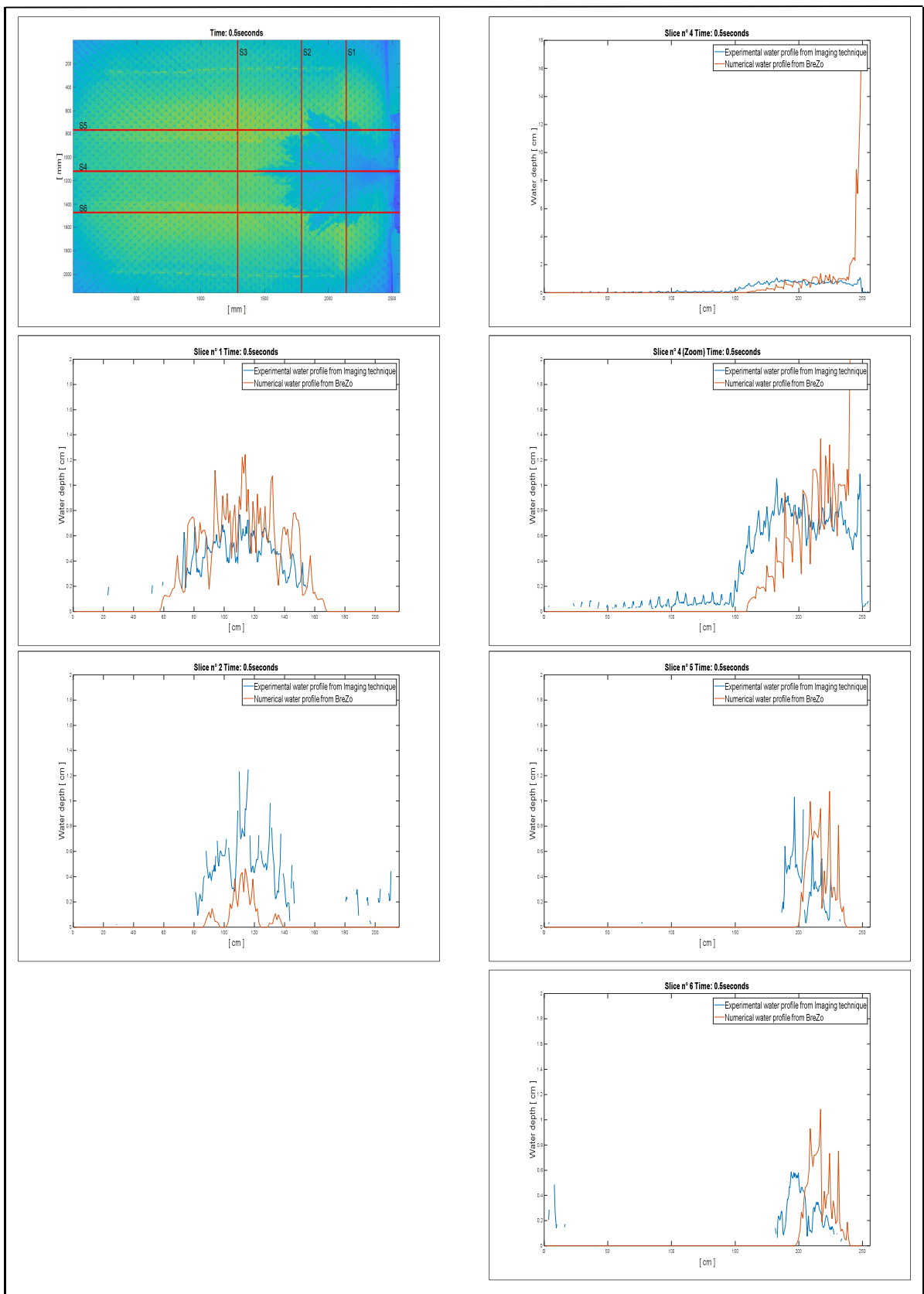


Figure 69: Comparison between experimental and numerical water profiles calculated in correspondence of the six slices showed in the first picture (Time 0.5 seconds).

- Time = 1.0 seconds :

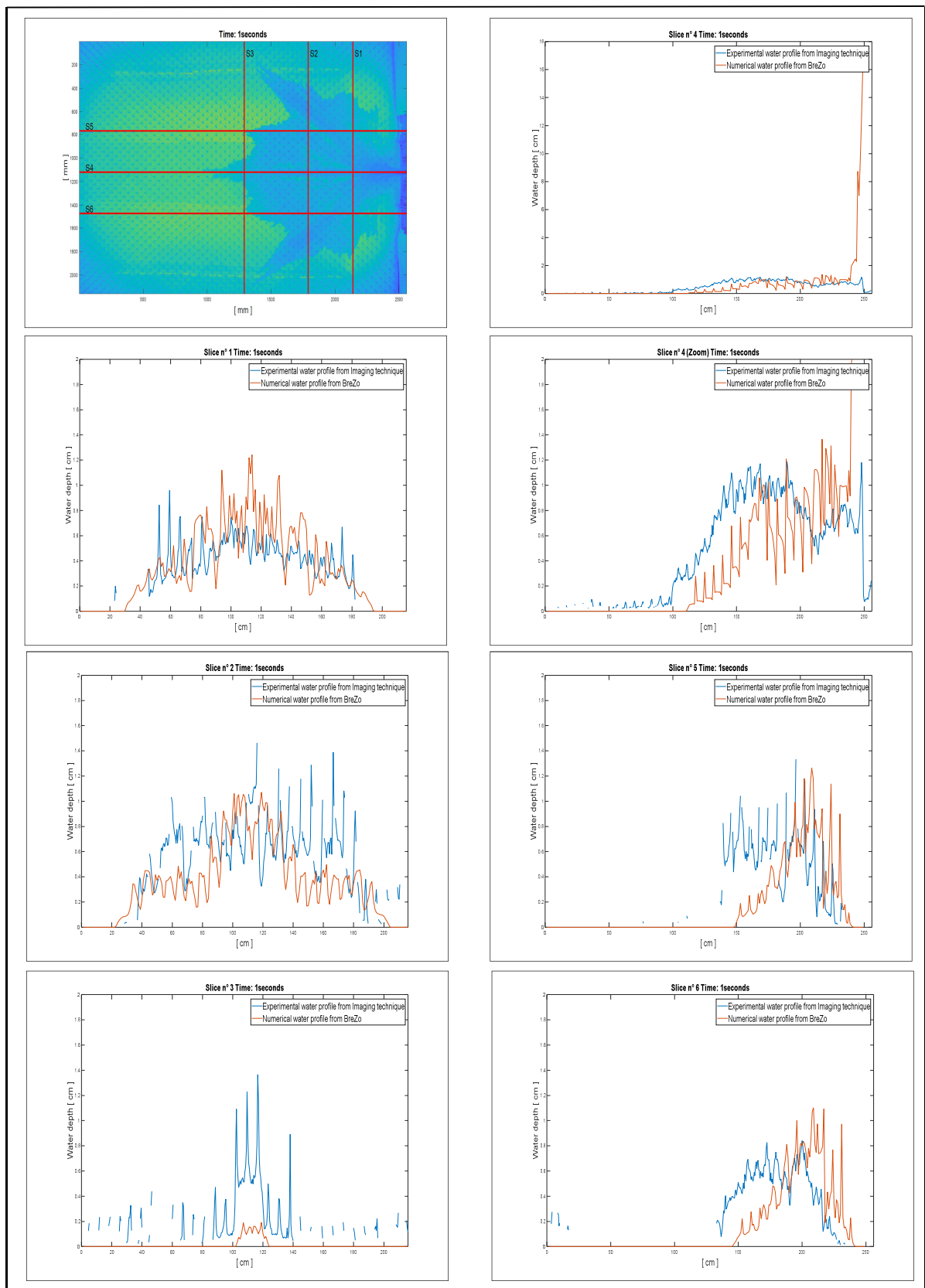


Figure 70: Comparison between experimental and numerical water profiles calculated in correspondence of the six slices showed in the first picture (Time 1.0 seconds).

- Time = 1.5 seconds :

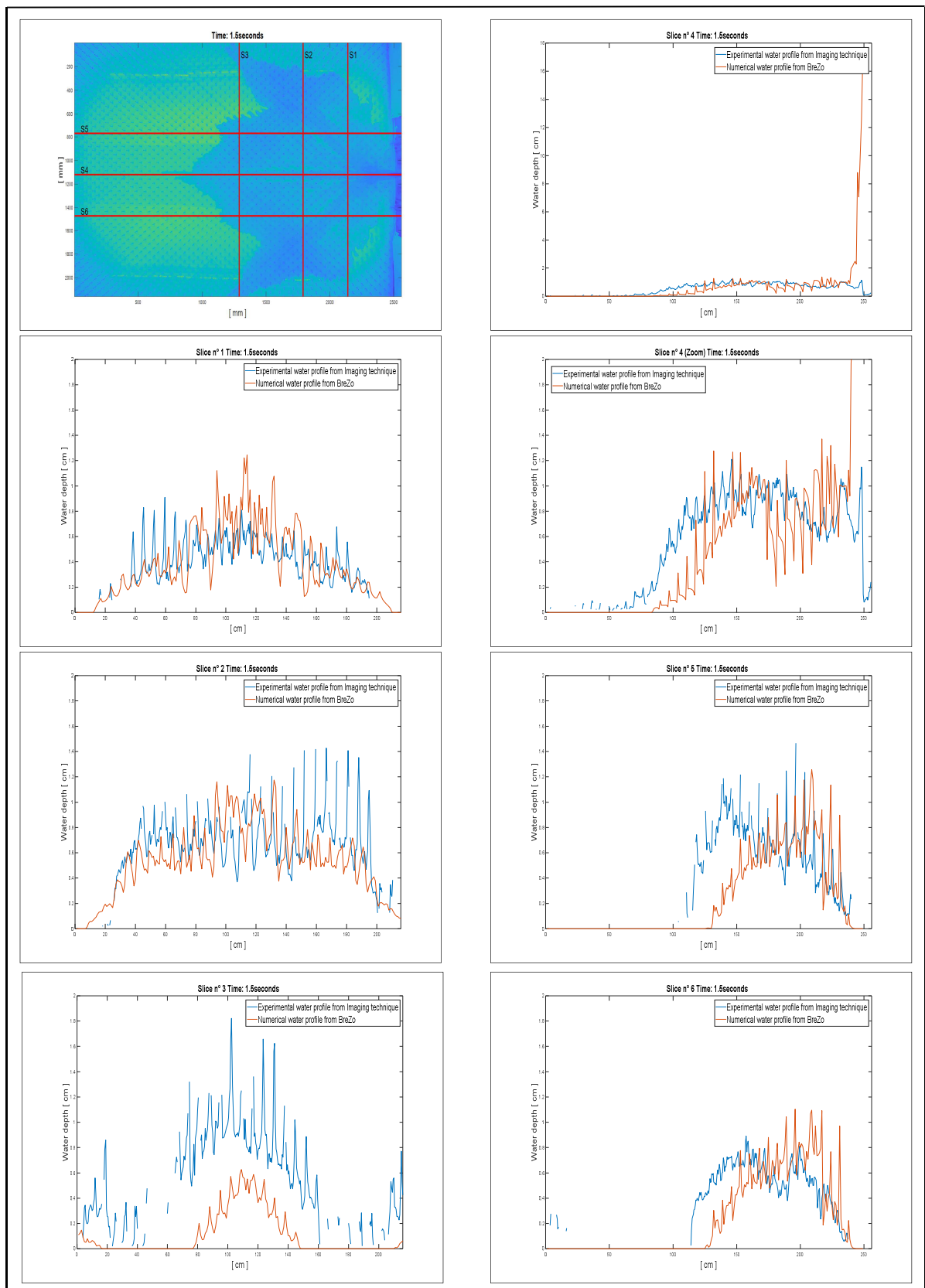


Figure 71: Comparison between experimental and numerical water profiles calculated in correspondence of the six slices showed in the first picture (Time 1.5 seconds).

7.2. Fluid vein

From the analysis reported in the previous pages of this document is possible to notice that the experimental method, based on the Lambert-Beer law, is not able to detect the fluid vein in the area close to the breach.

In order to check how is the real behavior of the water in that area, several videos have been taken from a lateral view.

From those videos was possible to detect the water profile of the fluid vein immediately outside from the tank. Further information regarding to this process are reported in the thesis of D’Oria Anna Dina (Turin Polytechnic April 2019).

Anyway this aspect is important because the parBreZo numerical model’s results are based on the *Shallow Water Equations* that consider the quantities computed making the average along the vertical direction; in that area close to the breach the vertical component is extremely important in order to have the right computation of the fluid vein.

In the following figures is shown the comparison between the experimental fluid vein measurements and the fluid vein computed by the numerical model (parBreZo).

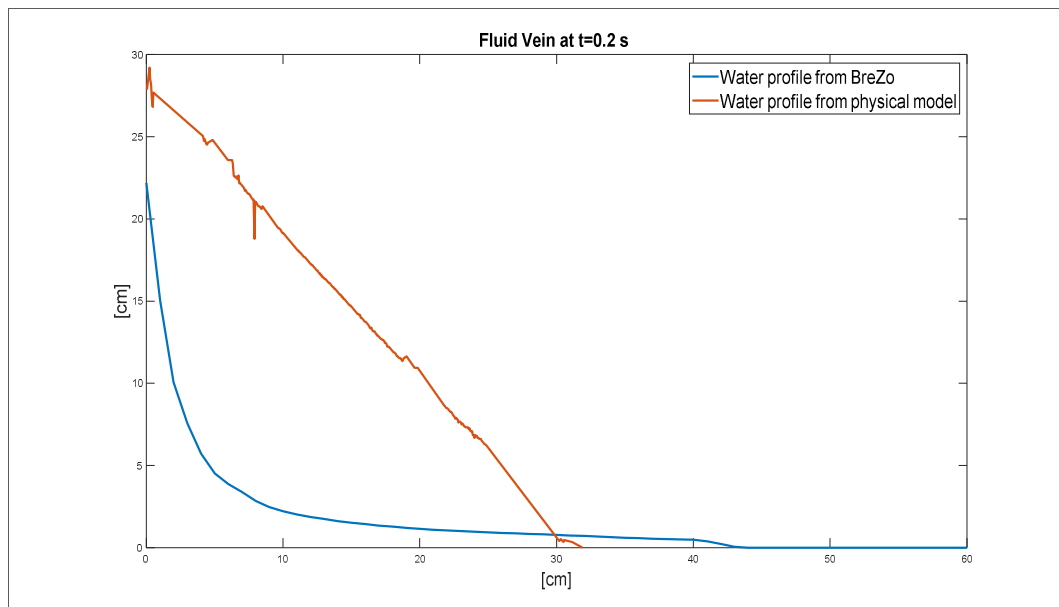


Figure 72: Fluid vein comparison between experimental measurements and numerical results (instant 0.2 seconds during the simulation).

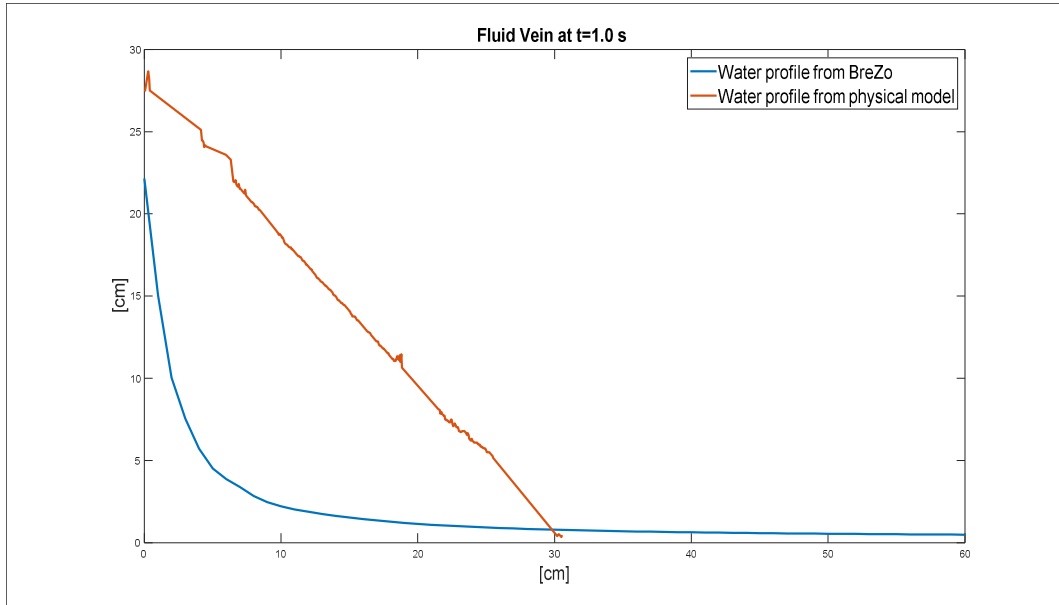


Figure 73: Fluid vein comparison between experimental measurements and numerical results (instant 1.0 seconds during the simulation).

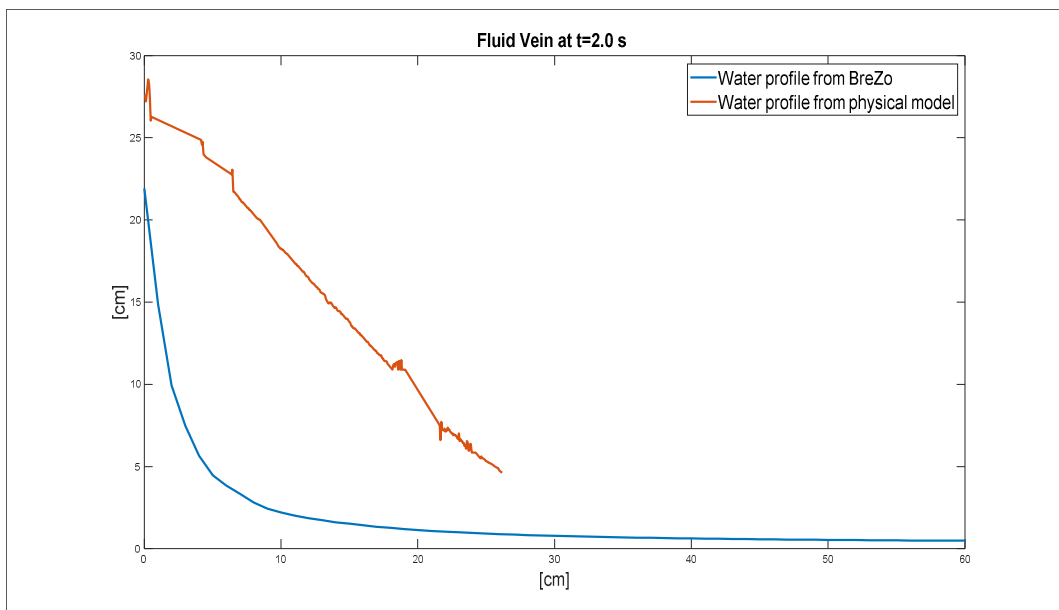


Figure 74: Fluid vein comparison between experimental measurements and numerical results (instant 2.0 seconds during the simulation).

As notable from the figures reported above the fluid vein computed by the numerical model is significantly different from what is in the reality. In fact the real fluid vein is circa a triangle with a 30 centimeters base and an height of approximately 30 centimeters as well.

Is possible to give an estimation of what this difference means in terms of volume; indeed the fluid vein volume is about:

$$V_{Fluid\ vein} = \frac{0.30 \times 0.30}{2} \times 0.03 = 1.30\ liters$$

This last volume has been calculated without consider the numerical fluid vein's volume in the same area, so this value is comparable with the simulation volume's difference stated at point 7.1.1. of this document, where the volume aspect was widely described.

7.3. Results from ANSYS Fluent and comparison

As already stated the purpose of the ANSYS Fluent numerical model is to verify how much is the error made using the Shallow Water Equations in the fluid vein's computing.

In order to check the results, the same profiles showed at point 7.2 were considered.

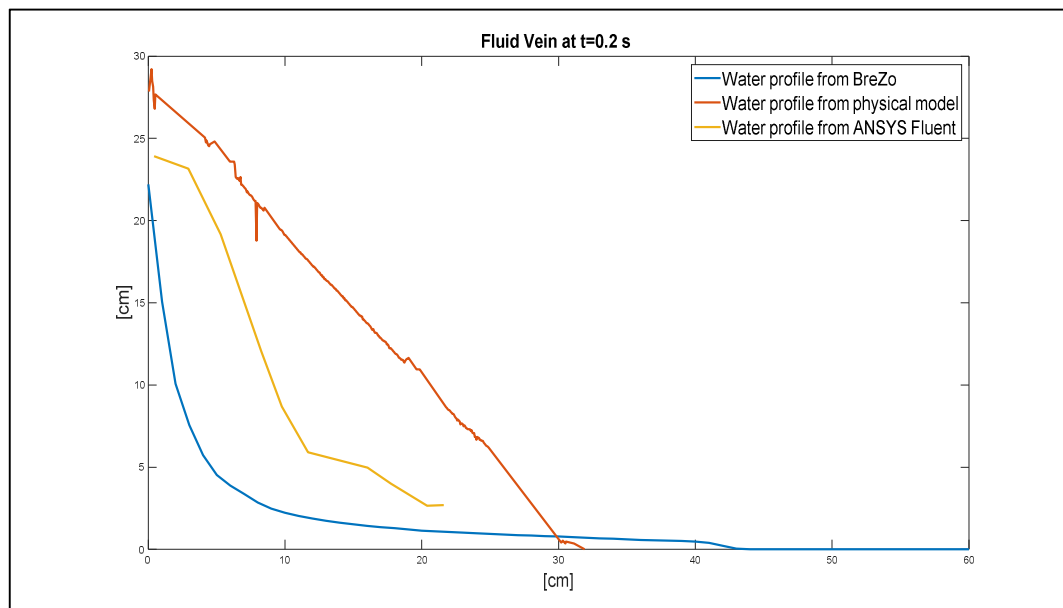


Figure 75: Comparison between the two numerical water profiles (BreZo and ANSYS Fluent) and the experimental profile (Time =0.2 seconds).

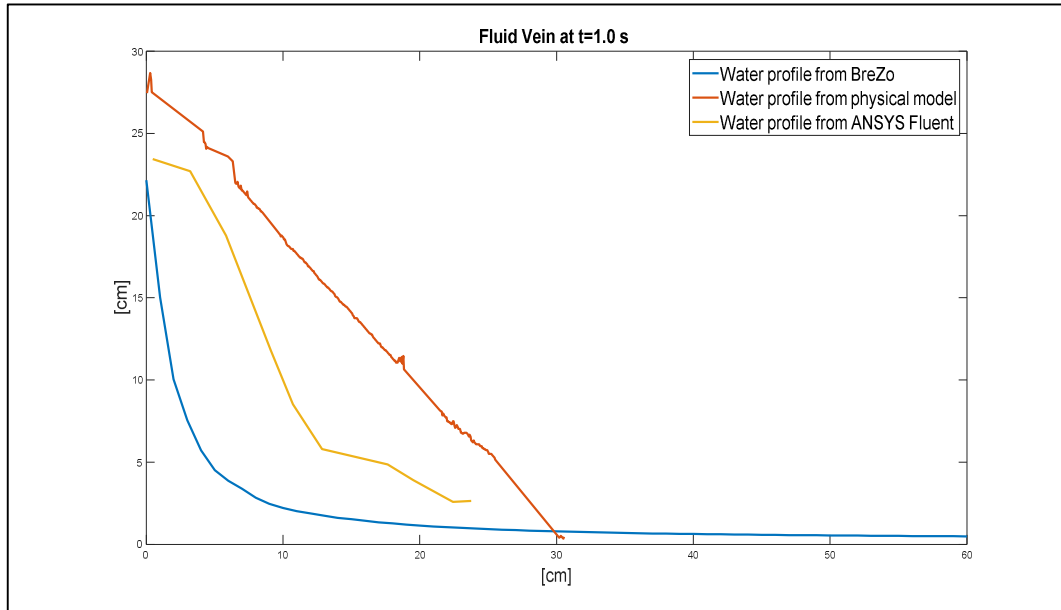


Figure 76: Comparison between the two numerical water profiles (BreZo and ANSYS Fluent) and the experimental profile (Time =1.0 seconds).

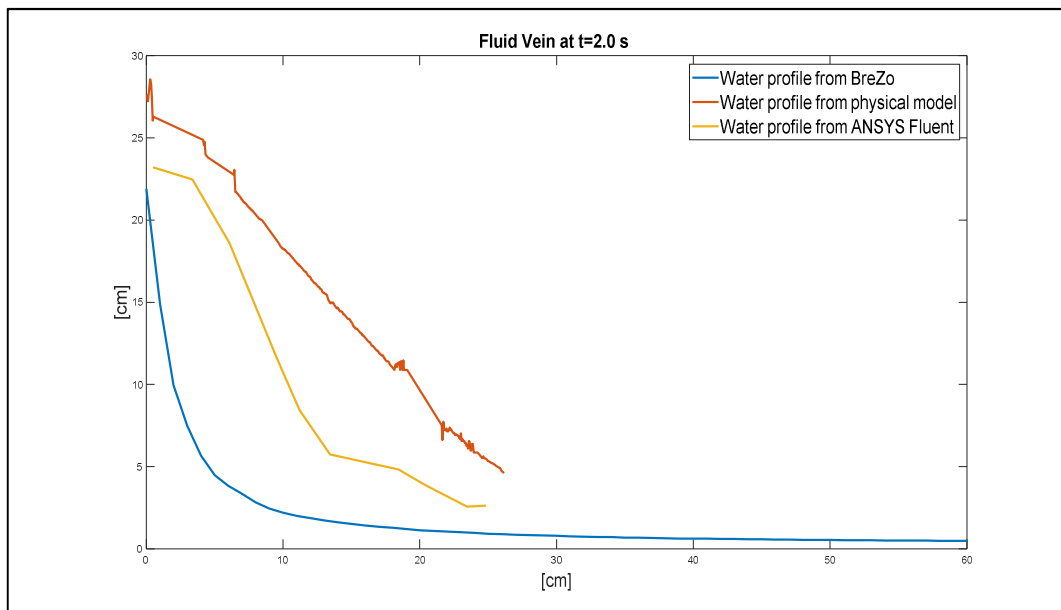


Figure 77: Comparison between the two numerical water profiles (BreZo and ANSYS Fluent) and the experimental profile (Time =2.0 seconds).

From the results given by this numerical model is possible to see how the computation of the fluid vein is significantly better than what done by the BreZo's model.

Anyway even this last results do not match exactly with the experimental profile, that is more pronounced and characterized by an almost linear pattern.

Moreover ANSYS Fluent is able to give a better representation of the fluid vein that could be helpful in order to have a better evaluation of the volumes during the experiment.

However this topic has not been studied in this thesis.

8. Future perspectives

In this chapter will be briefly listed the possibilities of improvements related to all the models analyzed in this document.

8.1. Experimental analysis

In this thesis the experimental setup that has been considered is characterized by a flat surface on the downstream; one interesting study will be to repeat the analysis giving a slope values to the surface, in fact the facility is predisposed for this eventuality. It will be interesting to study how the slope could influence the flow that will be surely faster than what observed in the situation presented in this document.

Another point of interest is given by the possibility to repeat the analysis with many different configuration of 'vegetation' and point out how is the influence in the wave's propagation.

The combination of several slopes and vegetation's configurations could represents a wide dataset useful to improve the study and the results of the whole analysis.

Furthermore another change that could be done in the physical model is to amend the breach's shape; in fact the breach considered in the analysis presented here is characterized by a rectangular shape which is not the most common geometry for the dam-break of earth dams.

In the future will be developed the analysis trying to repeat the whole analysis with triangular or trapezoidal shape.

8.2. Numerical model with parBreZo 8.1.0.

The numerical analysis with parBreZo is the biggest part of the study presented in this thesis.

One perspective of improvements related to this numerical model is to check if the model works properly even in all the different situations stated at point 8.1..

Another thing that could be tested in the future analysis is to schematize the whole geometry with the vegetation giving an elevation to each one of the rods instead of the hole's schematization presented in this document; this thing could be done amending the *makeplfile.f90* Fortran's routine in the part where the elevation is assigned to each one of the nodes of the mesh.

This fact will cause a computational effort growth because a finer mesh's resolution will be needed.

8.3. Numerical model with ANSYS Fluent

The model made with ANSYS Fluent and presented here is relative only to the smooth horizontal bed-ground, so the first thing that could be done is to try to model the study case with the vegetation. This thing would need just a bigger effort during the geometry's preparation with AutoCad inserting all the rods on the flat surface.

Another thing that was not deeply studied in this analysis is the influence of the usage of a finer mesh's resolution; it was not done here just for a matter of time.

Furthermore it could be interesting to evaluate the water's volume computed from this numerical model and compare it with the results showed at point 7.1.1. of this document.

9. Conclusions

The main objective of the whole analysis is to find a way to estimate the water depth and velocity values in order to evaluate an hazard situation correlated to a dam-break event.

In particular in this thesis what has been widely studied is the compatibility of the experimental analysis with a numerical model of the same situation.

Consequentially of the results showed in the previous chapters is possible to state that the numerical parBreZo's model is able to describe quite accurately the phenomenon; in fact the results showed at chapter 7.1. of this document demonstrate that there is a good correspondence between the experimental and numerical results. The comparison has been done looking at the water profiles and at the wave-front's velocity.

Relatively the two situations that were analyzed:

- *Smooth horizontal bed-ground:* in this case the numerical model is able to match well the water depth values, even if there is a little under-estimation of the water volume computed during the whole experiment; this aspect could be correlated to the fact that the numerical model does not reproduce well the fluid vein in the area close to the breach.
In terms of wave's propagation during the experiment the numerical results match almost perfectly with the experimental results less than local differences that are attributable to local geometry imperfections of the facility which are neglected in the numerical model.
- *Vegetated bed-ground:* in this case the modeled situation is absolutely more complicated cause the presence of the rods on the surface. However the model is able to reproduce the wave's propagation during the experiment, even if there are some differences mostly on the lateral propagation of the wave where the numerical model shows a wave that is faster that what was observed from the physical model. This aspect could be connected to the fact that in the numerical model described here, the effect of the rods' surface tension is neglected at all because all the rods are simulated as mesh's holes.
Even looking at the water depth results is possible to notice a good match; the profiles showed in this document are obviously jagged cause the rods' presence. There is a quite good correspondence of the water peaks in the proximity of each rod.

Therefore the parBreZo's numerical model could be considered a really useful support tool during the analysis referred to this facility.

As already pointed out previously the main difference between the experimental and numerical parBreZo's results is constituted from the different calculation of the fluid vein that is not faithfully reproduced. The motivation is that the parBreZo's model is based on the Shallow-Water Equations that neglect the variables computed along the vertical direction; in that area the vertical component is important in order to have a correct evaluation of the fluid vein.

With the purpose to confirm the previous statement an ANSYS Fluent's model was prepared and it showed a significant difference in the fluid vein computation in the area close to the breach. However even the representation given from this last model is not perfectly correspondent to the real observed profile but it is characterized by a more similar shape.

List of figures

Figure 1: View from above of the experimental setup (Aureli, Maranzoni, Mignosa, Ziveri)	4
Figure 2: Another view of the experimental facility (Aureli, Maranzoni, Mignosa, Ziveri).	4
Figure 3: Experimental (left) and numerical (right) water depths for Test 3 at $t=0.46$ s, $t=1.16$ s, $t=1.86$ s, $t=2.58$ s, and $t=4.77$ s (Aureli, Maranzoni, Mignosa, Ziveri).	6
Figure 4: Experimental facility geometry (S.Soares-Fra ζ ao & Y.Zech).	7
Figure 5: Experimental facility cross-sections: (a) Channel, (b) Gate (S.Soares-Fra ζ ao & Y.Zech).	8
Figure 6: Results from the imaging techniques during different time steps (S.Soares-Fra ζ ao & Y.Zech).	9
Figure 7: Geometry overview of the whole facility that has been set up at the Giorgio Bidone Laboratory at Turin Polytechnic (dimensions are stated in centimeters).	11
Figure 8: Picture took from upstream of the physical model.	12
Figure 9: Picture took from upstream of the physical model.	12
Figure 10: System of ultrasonic probes set on a metallic frame that was placed above the tank.	13
Figure 11: Extract from the ultrasonic probes' manual (Balluff).	14
Figure 12: Image of the working station that was used for the monitoring of the probes' measurements with LabVIEW	15
Figure 13: Three-dimensional reconstruction of the water surface into the tank in a sample time step during the experiment.	16
Figure 14: Three-dimensional reconstruction of the water surface into the tank in a sample time step during the experiment.	17
Figure 15: View of the two cameras that are placed above of the flat horizontal surface...	19
Figure 16: Picture extracted from the Zyla sCMOS manual.	20
Figure 17: Sample picture taken with Zyla from where the camera is placed; in this figure the surface is	21
Figure 18: Sample slideshow taken from the Zyla camera during an experiment with smooth and horizontal surface.	22
Figure 19: Sample slideshow taken from the Zyla camera during an experiment with vegetated surface.	23
Figure 20: Example of a spectrum measured by the spectrometer.	26
Figure 21: Relationship between the constant K and the water depth values (Aquarium).	27
Figure 22: Relationship between the constant K and the water depth values (Aquarium and Model's surface).	27
Figure 23: Relationship between I/I0 and water depth for the three different situations that were analyzed.	29

Figure 27: Reconstruction of the water depth’s field associated to the frame. The water depth value is known in every pixel of the image. 30

Figure 27: Sample frame taken by Zyla during an experiment with smooth horizontal surface..... 30

Figure 27: Reconstruction of the water depth’s field associated to the frame. The water depth value is known in every pixel of the image. 30

Figure 27: Sample frame taken by Zyla during an experiment with smooth horizontal surface..... 30

Figure 29: Wave’s edges representation..... 31

Figure 29: Sample frame taken by Zyla during an experiment with smooth horizontal surface..... 31

Figure 31: Sample frame taken by Zyla during an experiment with vegetated horizontal surface..... 31

Figure 31: Wave’s edges representation..... 31

Figure 32: Example of computational cells and relatives parameters. 33

Figure 33: Volume into the computational cell; (a) $z1 < \eta \leq z2$ (b) $z2 < \eta \leq z3$ (c) $z3 < \eta$ 35

Figure 34: Subdivision of the whole geometry in three different..... 44

Figure 35: Representation of some of the decagonal holes (image from Tecplot)..... 45

Figure 36: Zoomed view of the three different mesh’s zones resolution(Tecplot). 48

Figure 37: Zoomed view of mesh in the area close to the breach(Tecplot)..... 48

Figure 38: Zoomed view of the mesh interface between Zone B and C (Tecplot)..... 49

Figure 39: Three-dimensional view of the model from downstream(Tecplot). 51

Figure 40: Three-dimensional view of the model from upstream(Tecplot). 51

Figure 41: Three-dimensional detail of the tank and the breach(Tecplot). 52

Figure 42: Detail of the rod schematization as a decagonal hole and the mesh around it (Tecplot)..... 54

Figure 43: Zoomed view of the area close to the breach (Tecplot). 54

Figure 44: Zoomed view of the interface between Zone B and Zone C (Tecplot)..... 55

Figure 45: Geometry representation created in AutoCad. 58

Figure 46: Division in subdomains of the whole geometry, view from above..... 59

Figure 47: ANSYS Fluent Geometry editor view. 60

Figure 48: Geometry of the model with the mesh. 61

Figure 49: Sample picture of the UCI (University of California Irvine) HPC interface. . 63

Figure 50: Sample picture of the UCI (University of California Irvine) HPC interface. . 64

Figure 51: View from the top of the first slice into the tank where the u-velocity was calculated. 65

Figure 52: Velocity patterns during the whole simulation along the slice(Model A). 65

Figure 53: Absolute values of the u-velocity of the cell closest to the wall (Model A). 66

Figure 54: Velocity patterns during the whole simulation along the slice (Model B)..... 67

Figure 55: Absolute values of the u-velocity of the cell closest to the wall (Model B). 67

Figure 56: Comparison between the two volume curves related to Model A and B;..... 68

Figure 57: Water depth and Total Hydraulic Load calculated along a slice taken along the breach's direction at time= 0.5 seconds (breach on the left of the graph) (parBreZo).....69

Figure 58: Water depth and Total Hydraulic Load calculated along a slice taken along the breach's direction at time= 1.0 seconds (breach on the left of the graph) (parBreZo)..... 70

Figure 59: Water depth and Total Hydraulic Load calculated along a slice taken along the breach's direction at time= 1.5 seconds (breach on the left of the graph) (parBreZo)..... 70

Figure 60: Water depth and Total Hydraulic Load calculated along a slice taken along the breach's direction at time= 2.0 seconds (breach on the left of the graph) (parBreZo)..... 71

Figure 61: Comparison between the volumes calculated from the probes and the volume computed from BreZo.....71

Figure 62: Percent difference between the experimental and numerical volumes during the experiment.72

Figure 63: Difference in terms of volume between the numerical model's results and experimental results.73

Figure 64: Wave-front evolution during the time and comparison between the two solutions.74

Figure 65: Comparison between experimental and numerical water profiles calculated in correspondence of the six slices showed in the first picture (Time 0.5 seconds).76

Figure 66: Comparison between experimental and numerical water profiles calculated in correspondence of the six slices showed in the first picture (Time 1.0 seconds).78

Figure 67: Comparison between experimental and numerical water profiles calculated in correspondence of the six slices showed in the first picture (Time 1.5 seconds).79

Figure 68: Wave-front evolution during the time and comparison between the two solutions.80

Figure 69: Comparison between experimental and numerical water profiles calculated in correspondence of the six slices showed in the first picture (Time 0.5 seconds).82

Figure 70: Comparison between experimental and numerical water profiles calculated in correspondence of the six slices showed in the first picture (Time 1.0 seconds).83

Figure 71: Comparison between experimental and numerical water profiles calculated in correspondence of the six slices showed in the first picture (Time 1.5 seconds).84

Figure 72: Fluid vein comparison between experimental measurements and numerical results (instant 0.2 seconds during the simulation).85

Figure 73: Fluid vein comparison between experimental measurements and numerical results (instant 1.0 seconds during the simulation).86

Figure 74: Fluid vein comparison between experimental measurements and numerical results (instant 2.0 seconds during the simulation).86

Figure 75: Comparison between the two numerical water profiles (BreZo and ANSYS Fluent) and the experimental profile (Time =0.2 seconds).87

Figure 76: Comparison between the two numerical water profiles (BreZo and ANSYS Fluent) and the experimental profile (Time =1.0 seconds).88

Figure 77: Comparison between the two numerical water profiles (BreZo and ANSYS Fluent) and the experimental profile (Time =2.0 seconds).88

Bibliography

- [1] John D Pisaniello. A comparative review of environmental protection policies and laws involving hazardous private dams: Appropriate practice models for safe catchments. *Wm. & Mary Envtl. L. & Pol'y Rev.*, 35:515, 2010.
- [2] LM Zhang, Y Xu, and JS Jia. Analysis of earth dam failures: A database approach. *Georisk*, 3(3):184–189, 2009.
- [3] Francesca Aureli, Andrea Maranzoni, Paolo Mignosa, Chiara Ziveri. Dam-Break Flows: Acquisition of Experimental Data Through an Imaging Technique and 2D Numerical Modeling. *Journal of Hydraulic Engineering* 2008.134:1089-1101.
- [4] S. Soares-Frazão, Y.Zech. Experimental study of dam-break flow against an isolated obstacle. *Journal of Hydraulic Research* Vol. 45 Extra Issue (2007), pp. 27–36
- [5] Brett F.Sanders, Lorenzo Begnudelli: A hydrodynamic flood simulation algorithm by Brett F. Sanders and Lorenzo Begnudelli <http://sanders.eng.uci.edu/brezo.html>.
- [6] Cordero Silvia, Davide Poggi, Stefania Grimaldi. Modellazione numerica della propagazione di onde di dam-break, caso studio: gli sbarramenti in terra.
- [7] Scott F.Bradford, Brett F.Sanders. Finite-Volume Model for Shallow Water Flooding of arbitrary Topography (2002).
- [8] J.E.Schubert, B.F.Sanders, M.J.Smith, N.G.Wright (2008). “Unstructured mesh generation and landcover-based resistance for hydrodynamic modeling of urban flooding”. *Advances in Water Resources* (31, 1603-1621).
- [9] L.Begnudelli, S.Bradford, B.F.Sanders (2008). “Adaptive Godunov-Based Model for Flood Simulation.” *Journal of Hydraulic Engineering* (Vol 134, No 6, 714-724).
- [10] L.Begnudelli, B.F.Sanders (2006). “Unstructured Grid Finite-Volume Algorithm for Shallow Water Flow and Scalar Transport with Wetting and Drying”. *Journal of Hydraulic Engineering* (Vol 132, No 4, 371-384).
- [11] R.Courant, K.O.Friedrich, H.Lewy (1967). “On the partial differential equation of mathematical physics”. *Advances in Water Resources*.
- [12] Jonathan Richard Shewchuk, Triangle A Two-Dimensional Quality Mesh Generator and Delaunay Triangulator. <http://www.cs.cmu.edu/afs/cs/Web/People/quake/triangle.html>

Experimental and numerical analysis of dam-break wave propagation on vegetated slopes.

[13] ANSYS Fluent Manual

<http://www.afs.enea.it/project/neptunius/docs/fluent/html/th/node11.htm>

[14] CIGB ICOLD, Commission internationale des grands barrages, International Commission on Large Dams.

https://www.icold-cigb.org/GB/dams/definition_of_a_large_dam.asp

Acknowledgements

È doveroso da parte mia esprimere un pensiero di ringraziamento per tutti coloro che mi hanno accompagnato durante questa mia esperienza Universitaria.

Ringrazio sentitamente il Professor Davide Poggi, relatore di questa tesi, per gli insegnamenti, il supporto e per l'avermi concesso l'opportunità di affrontare un'esperienza unica ed indimenticabile durante il periodo trascorso in California.

Durante quei mesi ho avuto il piacere di conoscere e collaborare con il Professor Brett Sanders, il quale non smetterò mai di ringraziare per tutto ciò che mi ha trasmesso in termini di conoscenza ed a livello umano. Ringrazio lui, ed allo stesso tempo tutti gli amici e colleghi conosciuti alla UCI; tutti loro per me hanno rappresentato una guida ed un supporto costante e decisivo per ogni aspetto della mia esperienza negli Stati Uniti.

Ringrazio l'Ing. Silvia Cordero e tutti i colleghi con i quali ho avuto il piacere di collaborare durante questo percorso.

Ringrazio ovviamente tutti i miei Amici, da quelli di sempre fino alle più recenti conoscenze. Grazie a voi l'intero percorso è stato senza dubbio più piacevole e leggero.

Ma il mio più grande ringraziamento è doveroso che vada a tutta la mia Famiglia. Loro sono stati, sono oggi, e sempre saranno il mio più grande punto di forza.

In particolare dico grazie al mio Fratellone ed ai miei fantastici Genitori che anche durante le difficoltà non hanno mai dubitato di me, senza farmi mancare mai nulla: vi sarò infinitamente grato per tutto ciò che mi avete dato, siete indubbiamente i migliori MAESTRI DI VITA che potessi desiderare.

Tutti voi, compreso anche chi purtroppo oggi mi guarda dall'alto con il sorriso, avete avuto un ruolo fondamentale fin dal primo giorno in modo che mi potessi realizzare come studente e come uomo.

Sono consapevole che questo traguardo debba rappresentare per me un nuovo punto di partenza, difatti non vedo l'ora di condividere con voi nuovi momenti di gioia.

GRAZIE

